Seismic analysis of concrete gravity dams using a novel time domain spectral finite element method

Avirup Sarkar

A Thesis

In the Department

of

Building, Civil and Environmental Engineering

Presented in Partial Fulfillment of the requirements for the degree of

Doctor of Philosophy (Civil Engineering) at

Concordia University

Montreal, Québec, Canada

May 2024

CONCORDIA UNIVERSITY

SCHOOL OF GRADUATE STUDIES

This is to certify that the thesis prepared

By: Avirup Sarkar

Entitled: Seismic analysis of concrete gravity dams using a novel time domain spectral finite element method

and submitted in partial fulfillment of the requirements for the degree of

Doctor Of Philosophy (Civil Engineering)

complies with the regulations of the University and meets the accepted standards with respect to originality and quality.

Signed by the final examining committee:

---------- Chair

Dr. Andrea Schiffauerova

---------- External Examiner

Dr. David Lau

---------- External to Program

Dr. Mehdi Hojjati

---------- Examiner

Dr. Anjan Bhowmik

---------- Examiner

Dr. Emre Erkmen

---------- Thesis Supervisor

Dr. Ashutosh Bagchi

Approved by ----------

Dr. Mazdak Nik-Bakht, Graduate Program Director

Friday, May 17, 2024

Dr. Mourad Debbabi, Dean

Gina Cody School of Engineering and Computer Science

ABSTRACT

Seismic analysis of concrete gravity dams using a novel time domain spectral finite element method

Avirup Sarkar, Ph.D.

Concordia University, 2024

This thesis introduces a two-dimensional spectral finite element formulation tailored for the dynamic analysis of concrete gravity dams. While the Finite Element Method (FEM) is widely utilized for dynamic structural analysis, its application to large structures often demands substantial computational resources and time. To address this challenge, alternative modelling techniques known as Spectral Finite Element Methods (SFEMs) have been developed over the past decades to enhance computational efficiency.

The objective of this thesis is to develop a computationally efficient analysis procedure for dynamic analysis of large structures like concrete gravity dams and then apply the developed procedure for assessing the behaviour of dams subjected to seismic ground motions as well as deterioration effects like alkali-aggregate reactions.

The Time Domain-based SFEM (TDSFEM) was chosen for dynamic time history analysis of concrete gravity dams due to its advantages over the Frequency Domain-based SFEM (FDSFEM). TDSFEM is particularly effective in handling irregular geometries and finite domains, making it a better choice for complex structural analyses. Sensitivity analyses and convergence studies were conducted using both 4-noded and 9-noded elements, revealing TDSFEM's superior computational efficiency, especially when higher-order elements are employed.

Comparative studies between TDSFEM and conventional FEM highlighted TDSFEM's advantage in reducing computational time while maintaining accuracy in large-scale dynamic analyses.

Modal analysis and time history analysis indicated that TDSFEM, when used with higher-order elements, could be a practical alternative to conventional FEM, offering substantial time savings without sacrificing precision.

The study also investigated damage detection methods based on modal parameters, including displacement, curvature, and strain energy. Among these, modal strain energy emerged as the most effective and reliable indicator for identifying and localizing damage. Additionally, TDSFEM was applied to model the behaviour and failure modes of FRP-reinforced concrete deep beams, with results closely matching experimental data, further demonstrating its efficiency.

Moreover, the thesis introduced a simplified thermo-mechanical approach for modelling deterioration effects, such as alkali-aggregate reactions (AAR), providing a novel alternative to existing chemical reaction-based models. TDSFEM is thus presented as a viable, efficient method for analysing large structures, offering significant time savings and effective applications in damage detection and deterioration modelling.

Keywords: Concrete gravity dams, Spectral Finite Element methods (SFEMs), Time Domain Based Spectral Finite Element method (TDSFEM), Numerical efficiency, Infinite Elements, Modal Strain Energy, FRP, concrete deep beams, Alkali-Aggregate Reaction (AAR).

Acknowledgements

I would like to thank my doctoral supervisor Dr. Ashutosh Bagchi for his continued support and encouragement during my doctoral studies. I am thankful to him for first of all considering me worthy of pursuing a doctoral degree program and accepting me in his research laboratory. His teaching and guidance have always been inspirational to me, and I cannot thank him enough for always showing me the direction whenever I was stuck at a problem for which I could not find a solution. Furthermore, I wish to sincerely express my gratefulness to Dr. Bagchi for inspiring me to achieve more than my potential and work hard with honesty in that respect. I shall always remember his words that one must try to solve a tough or complex problem as once it is solved; the sense of achievement brings a lot of joy. Other than the technical aspect, I have learnt a lot of life lessons from him like honesty, humility and staying calm in tough situations. Overall, this journey would not have been possible without his kind support and supervision.

I wish to express my sincere gratitude to my thesis committee: Dr. David Lau, Dr. Anjan Bhowmick, Dr. Emre Erkmen and Dr. Mehdi Hojjati for their careful inspection of the thesis and providing their valuable insights and feedback which have gone a long way in improving my thesis.

I would like to especially thank Dr. Emre Erkmen for his continuous help and support during my years at Concordia University. I first came to know him through the finite element course taught by him and his teaching thoroughly inspired me and established my keen interest in the subject. During the course of my doctoral studies, I have interacted with him a lot of times with many doubts and questions, and he has always been patient and kind enough to help me with his knowledge and resources. Dr. Erkmen will always remain an inspiration to me.

I would like to thank faculty members of the BCEE Department: Dr. Khaled Galal, Dr. Lucia Tirca, Dr. Lan Lin, Dr. Jassim Hassan, Dr. Ghazanfarah Hafeez and others for their help and support during my doctoral studies.

I sincerely thank the BCEE Department staff and executives Ms. Jenny Drapeau, Ms. Caroline Durand, Mr. Tiberiu Aldea, Ms. Elena Castigliano, Mr. Roberto Perez and others for their kind help and support.

I would like to take this opportunity to thank my lab colleagues Mr. Amit Chandra, Dr. Timir Baran Roy, Mr. Bikram Patra, Mr. Saikat Bagchi and Mr. Amal Pradeep for their continuous help and support and inspiring me in my journey.

In my life and during my doctoral studies, friends have played a huge role as a support system. I would like to take this opportunity to thank all my friends for always believing in me, helping me and keeping me sane. My special thanks to Mr. Aakash Khatri, Mr. Subhasish Sarkar, Dr. Girish Narayan Prajapati, Mr. Balla Taraka Malleswara Rao, Ms. Srimoyee Bhattacharya, Mrs. Sananda Mitra, Mr. Anish Sinha Roy, Mr. Sumedh Dey, Dr. Devdeep Basu, Mr. Manas Ranjan Pal, Mr. Abhishek Pal, Mr. Arjun Sengupta, Mr. Amardip Kumar Singh, Ms. Jhelum Paul for being amazing friends and keeping me happy through tough stages of my life.

In my years in Montreal, I had a small family all of whom will be etched in my memory forever. This cricket team named “Montreal Mavericks” has been a parallel journey for me along with my Doctoral studies and to some extent played a huge role in keeping me healthy, happy and active which enabled me to continue my studies without disruption. I would like to specially mention Mr. Harshil Dokania and Mr. Nimesh Gautam for being amazing human beings. I would also like to thank my roommate in Montreal Mr. Deekshith Moolayil.

I would like to express my sincere gratitude to Dr. Yogendra Singh (Professor at IIT Roorkee) for mentoring me during my Masters dissertation and instilling in me the interest for earthquake engineering and structural dynamics which led me to pursue my doctoral studies in this domain.

I would like to thank my wife Mrs. Ahelee Sarkar for being an amazing support for all these years. I could not have pursued this journey without her immense mental and emotional support throughout the years. Also, thanks to my in-laws Mr. Subrata Sarkar and Mrs. Chandana Sarkar for believing in me and for their encouragement.

Finally, I would like to thank my parents Mrs. Madhumita Sarkar and Mr. Sanjoy Sarkar and my elder brother Mr. Avishek Sarkar. Their constant support and encouragement in each of my life’s endeavors has enabled me to reach this stage in my life. I cannot thank my mother enough for her numerous sacrifices and always motivating me to pursue my doctoral studies.

Table of Contents

List of Figures

List Of Tables

CHAPTER 1: INTRODUCTION

I. Background

In recent years, there have been major changes in the philosophy of design of structures. With the introduction of concepts of capacity-based design and performance-based engineering design of structures, bulky and heavy weight structures are being replaced by light weight and sleek structural components. This makes the need for monitoring the state of the structure inevitable, continuously or at periodic intervals. The process of assessing the structural performance, detecting the damage (if any) and predicting the future life of the structure started out as Non-destructive testing and evaluation and finally led to the branch of engineering called Structural Health Monitoring (SHM). SHM has evolved as a multi-disciplinary research domain with widespread applications in the field of aerospace, civil, mechanical, and naval structures. SHM requires deep understanding and knowledge of different branches of science like signal processing, sensors and electronics, material science, etc. Along with these, numerical simulation and modeling plays an important part of any SHM and damage detection framework. In the field of SHM, modeling has two basic parts: flaw modeling and damage detection algorithm. The type of flaw modelling depends on the type of structure to be investigated. In the case of steel structures, flaw is generally in the form of vertical, horizontal, inclined cracks or corrosion cracks, while in composites, delamination is the main type of flaw that needs to be modeled. The cracks due to creep, shrinkage, etc. need attention while modelling flaws in concrete structures. An efficient damage detection strategy demands that all these types of flaw modeling be incorporated in its numerical simulation scheme. Another requirement for an efficient damage detection technique to work properly is that it should blend well with the chosen mathematical model and work effectively in case of incomplete or noise pollution data. The earliest methods of damage detection are based on changes in modal parameters of structures. Damage in a structure leads to a reduction in the stiffness which in turn leads to changes in natural frequencies of the structure. This global nature has led to the development of many damage detection techniques based on changes of modal parameters. The starting point of damage detection based on changes in modal parameter was based only on changes in the natural frequencies of the structure (Cawley et al, 1979). At a later stage, damage detection methods based on changes in flexibility of the structure were proposed

(Chopra & Chakrabarti, 1973). By this method, damage in a structure could be easily detected and localized based on the first few modes of vibration of the structure. However, the problem with the aforementioned techniques is that they are insensitive to small damages. An advancement over these methods was made by a damage detection method based on changes in mode shape curvature (Chróścielewski, 2009). This method can effectively detect damage even of small dimensions. However, this method requires a large number of sensors to obtain the spatial resolution required to fully characterize the modes and compute the curvatures. A detailed review of the advantages and disadvantages of modal parameter based, or vibration-based damage detection based are present in literature (Pandey et al, 1991, Doebling at al, 1998). The major takeaway from the study of vibration-based damage detection methods is that they rely on low frequency characteristics of structures and return large errors for higher frequencies. Also, these methods require a large number of sensors if the method involves signal processing, which results in higher overall cost of the method. A solution to all the above-mentioned shortcomings is provided by methods of damage detection based on wave propagation. An efficient damage detection method also requires a suitable mathematical tool for proper handling of the problem at hand. The most common analysis tool applied in mathematical modeling of problems of structural dynamics is the finite element method. The Finite element method is a robust analysis method and provides solutions to large variety of problems of structural analysis. The matrix methodology adopted in this framework is also suitable for computer implementation. This is an important reason behind the popularity of the finite element method in solving most present-day engineering problems. But there are some inherent problems in the finite element methodology which needs to be addressed before applying it to solving problems of structural dynamics and damage detection. The starting point in solving a problem of structural dynamics by the finite element method is writing the dynamic equation of motion and formulation of the stiffness and mass matrices. The two types of mass matrices used are: lumped mass matrix and the consistent mass matrix. In the lumped mass matrix, the total mass of the element is equally distributed in the two nodes leading to a diagonal mass matrix. In the consistent mass matrix formulation, the entries of the mass matrix are calculated by computing the partial derivatives of the kinetic energy of the element with respect to the nodal velocity components. In both the formulations, if the nodes are far apart, many elements must be used to model the mass distribution correctly. Thus, even for a uniform rod with constant parameters, many elements must be used, and this leads to increased size of the problem, use of more computer

space and memory, high computational time and cost. This inherent problem of finite element method needs use of an analysis tool free from these shortcomings. The spectral element method is a comparatively new analysis tool developed on the principles of wave propagation, free from the problems of finite element method and leads to much less computation time and use of much less computation space. The details of the method are discussed in detail in the next chapter. The main objective of this study is to develop an efficient damage detection technique based on the principles of wave propagation of structures using spectral finite element method as an analysis tool.

Finite Element Method (FEM) is one of the most extensively used analysis tools in varied engineering applications. The ease of implementation due to adopted matrix methodology in FEM formulations makes it highly compatible with modern day digital computation facility. This has led to the versatile use of FEM in almost all engineering applications over a considerable period of time. In dynamic analysis, accurately capturing the higher vibration modes of a structure is crucial for understanding its behavior for a significant level of precision. This is particularly relevant, where the response of structures to seismic excitation is of great importance. Conventional FEM often requires very fine mesh sizes to capture these high-frequency modes. The required mesh size should be comparable to the wavelength of the high frequency modes. It results in huge computational problems for large and complex structures like concrete gravity dams. In such cases, dynamic analysis using the conventional FEM requires significant computational time, space, and cost and this could impact the accuracy of the solution. It could be particularly challenging for vibration-based model updating and damage detection using finite element models (Bagchi et al., (2007)) where the conventional FEM has been used in dynamic analysis of structures. Damage or anomaly detected in dams using data driven models could mitigate the computational issues as they do not require an FEM model (Garabedian et al. 2006 a, b). However, they may have limited applicability.

The shape functions used in conventional FEM are static and frequency independent. Over the past few decades, alternative analysis techniques have been developed with the objective of solving dynamic problems using less computational time and cost. The starting idea of these methods was to use shape functions which are dynamic or frequency dependent. One of the early methods developed in this direction is the Dynamic Stiffness Method (DSM) (Kolousek (1941),

Przemieniecki (1968)). In this method, frequency-dependent shape functions are used. These frequency-dependent interpolation functions can adequately represent the higher modes of the structure with high level of precision. Also, there is no need to perform mesh refinement for higher accuracy. Another method developed with a similar idea which works in the frequency domain is the Spectral Analysis Method (SAM) (Newland (1993), Ginsberg (2001) and Humar (2001)). In the aforementioned method, the Fast Fourier Transform (FFT) is employed to efficiently compute the frequency dependent components of as many high frequency modes as deemed necessary for the problem. The key features of conventional FEM, DSM and SAM combined to the development of Spectral Finite Element Method (SFEM) (Beskos (1978)) which is frequency based (or FFT based) and sometimes also referred to as Frequency Domain based Spectral Finite element method (FDSFEM) (Doyle (1997) and Lee (2009)).

Another class of finite element method was developed with the view to achieve computational efficiency over the conventional FEM, which is now referred to as the Time Domain Based Spectral Finite Element Method (TDSFEM) (Patera (1984)) which operates in a totally different methodology than the above mentioned FDSFEM. While the TDSFEM is labeled as a 'spectral' method, it operates in the time domain with spatial discretization. The term 'spectral' in this context refers to the incorporation of higher-order polynomials as interpolating functions, uses Gauss-Lobatto-Legendre (GLL) integration technique, allowing for efficient computation. Although the method does not directly provide frequency domain information, it offers computational advantages over conventional FEM. The historical development of these methods, advantages and disadvantages are discussed in detail in the next few sections. The main objective of this research is to develop a TDSFEM-based method for the dynamic time history analysis of concrete gravity dams, and demonstrate the computational efficiency of the proposed TDSFEM-based method over conventional FEM. By applying TDSFEM to dynamic time history analysis, it was aimed to quantify the computational advantages of the method over conventional FEM. Such studies are not available in the available literature. The present research mainly focuses on investigating the computational time savings achieved by TDSFEM, particularly in case of complex geometries and large practical structures (like concrete gravity dam). For that purpose, TDSFEM elements were developed with linear and higher order interpolation functions. Also, infinite elements for TDSFEM were developed to model the foundation. The uniqueness of the present work comes from the development and practical application of the higher order TDSFEM elements and the

infinite elements. In terms of analysis of concrete gravity dams, another important aspect which needs to be looked at is the damage caused by alkali-aggregate reaction (AAR). In concrete structures, this is a typical problem due to the chemical ingredients of concrete. AAR is a chemical process which sets in concrete structures at a certain age and then structural degradation happens. AAR causes volumetric expansion, and the structures get affected by cracks. Depending on the amount of AAR, the cracks in the structure could be local or the damage could be high, needing severe retrofitting and repair measures to be adopted for the proper functioning of the structure. In many concrete gravity or arch dams, AAR has been observed to cause severe issues related to structural health. However, modeling of AAR and its effects on a dam is a challenging aspect as it requires rigorous chemical modeling followed by the standard mechanical analysis procedures to be implemented. In this thesis, a simplified thermo-mechanical approach has been adopted to model the effects of AAR on dams.

II. Motivations for the study

A. The available methods of damage detection based on changes in vibration characteristics of structures have many shortcomings, are insensitive to small damage and require a high number of sensors to be deployed for accurate damage detection.
B. Finite element method, the most commonly used mathematical modeling tool for problems in structural dynamics and damage detection also has many inherent problems. For accurate modeling of inertial properties, it requires fine meshing leading to high computational space, time and cost. Thus, to develop an alternative computationally efficient analysis technique for analysis of large structures like concrete gravity dams.
C. There is no considerable work done in the literature on damage detection of large structures like concrete gravity dams incorporating the above-mentioned points.
D. To showcase the application and efficiency of developed numerical analysis procedures for structures other than dams but requiring heavy computational effort like pseudo-static or dynamic analysis considering material nonlinear behavior.
E. To develop a simplified numerical algorithm for modeling deterioration effects in concrete structures like alkali-aggregate reactions (AAR).

III. Objectives of the study

The objectives of the present research are as follows:

A. To formulate an efficient analysis tool using spectral element method to save computational space, time, and cost, then apply it to two-dimensional problems.
B. To develop a damage detection method capable of detecting and locating damage in concrete gravity dams based on modal parameters.
C. To develop a TDSFEM-based method for seismic analysis of concrete gravity dams considering the effect of dam-reservoir-foundation interaction and application of above-mentioned damage detection tools for dams.
D. To demonstrate the efficiency of the developed procedure for other structures than concrete gravity dams but requiring heavy computational efforts like pseudo-static analysis considering the effect of material nonlinear behavior.
E. To develop a simplified numerical algorithm for the modeling of deterioration effects in concrete structures like alkali-aggregate reactions (AAR).

IV. Outline of the thesis

The report starts with the basic introduction to the research topic of structural health monitoring and damage detection, leading to the discussions on shortcomings of prevalent damage detection methods and analysis tools. The introductory chapter ends with discussing the ideas that could be explored for overcoming the mentioned problems and mentions the overall motivations of the research work and objectives of the study. Chapter 2 is a background literature review on the available spectral finite element methods discussing their advantages and disadvantages and applicability in the context of dynamic analysis of large structures like concrete gravity dams. The chapter also presents the literature review on vibration-based damage detection methods and the deterioration effects of alkali-aggregate reactions on large structures like concrete gravity dams. Chapter 3 presents the methodology adopted in the thesis for the analysis performed using the time domain based spectral finite element method. Chapter 4 presents a detailed verification study of the developed TDSFEM based programs for the linear static, linear dynamic, non-linear static and non-linear dynamic problems solved in the thesis. Chapter 5 is on the application of the time domain based spectral finite element method in the linear dynamic analysis of concrete gravity

dams and damage localization based on modal parameters. In Chapter 6, nonlinear analysis of the concrete gravity dams is showcased considering the effect of reservoir and semi-infinite foundation. In Chapter 7, the modeling of alkali-aggregate reaction (AAR) in concrete gravity dams using a simplified thermos-mechanical model is shown. The final chapter is based on the overall summary and conclusions of the thesis.

CHAPTER 2: LITERATURE REVIEW

I. Alternative modeling techniques

As discussed in the previous section, the need for alternate methods to conventional FEM emerged from the fact that it requires very fine mesh to accurately capture the higher vibration modes of a structure while performing dynamic analysis. The size of the mesh required is comparable to the wavelength of the highest required vibration mode of the structure. This results in a huge size of the problem to be solved which needs high computational time, space and cost.

In order to circumvent the problem of mesh refinement, researchers came up with the concept of dynamic shape functions which are frequency dependent in the method named Dynamic Stiffness Method (DSM). The idea was to use exact wave solutions of the governing differential equations. This enables accurate representation of the higher vibration modes without increasing the computational burden. The governing differential equation in the time domain is first transformed to frequency domain. This leads to dynamic stiffness matrix which is frequency dependent, and it accurately captures the inertial properties of the dynamics of the structure like mass distribution, stiffness distribution and damping. So, for a part of the structure with no material or structural discontinuity, a single element is sufficient and meshing it into finite elements is no longer needed. Consequently, the total number of degrees of freedom to be considered in the structure for dynamic analysis is much less compared to conventional FEM which means reduction in computational time as the problem to be solved is much less in size owing to reduced number of degree of freedoms. Development of the accurate dynamic stiffness matrix of a Euler-Bernoulli beam can be traced back to the work by Kolousek (1941). Similar frequency dependent dynamic stiffness matrices were developed for both beam and bar elements by Przemieniecki (1968). However, the problem in this method is that the eigen value problem posed by DSM is not a linear eigen value problem as is seen is case of conventional FEM. DSM leads to eigen value problems which are transcendental in nature and solving it to calculate all the natural frequencies of a structure posed major computational challenges. This issue was solved by Wittrick and Williams (1971) with their development of the well-known Wittrick-Williams algorithm to calculate the undamped natural frequencies of a structure for transcendental eigen value problems. Following the development of the Wittrick-Williams algorithm, the applicability of DSM increased manifold. Leung (1993)

provided a comprehensive literature review of the varied applications of DSM in the field of structural dynamics. Around the same time, Fourier transform based Spectral Analysis Method (SAM) was developed in which the solution to the governing differential equation is presented as the superposition of a large number of wave modes of different frequencies. Detailed description, explanations and review of literature on the DFT/FFT based SAM have been provided by Newland (1993), Ginsberg (2001) and Humar (2001). Combining the concept of DSM and using the FFT algorithm like SAM, Beskos (1978) developed the Spectral Element Method (SEM) for the dynamic analysis of beams. However, the term "Spectral Element Method" was later coined by Doyle (1988).

Extended research has been carried out using the frequency domain based SFEM (FDSFEM) and a detailed review of the literature on it can be found in Doyle (1997) and Lee (2009). Other frequency domain-based methods were also developed to solve soil-structure interaction problems (Humar et al., 1998). FDSFEM provides high accuracy in frequency domain problems such as calculating eigen-frequencies even for the higher modes of vibration. However, they do not address the issue of application to structures with complicated geometry or the computational aspect of dynamic analysis of practical structures.

The motivation for researchers to develop efficient computational techniques for the dynamic analysis of structures led to the development of other spectral element methods. Patera (1984) developed one such spectral element method to be applied in the field of fluid dynamics named the time domain based spectral finite element method (TDSFEM). In that method, the structure of the conventional FEM was efficiently combined with the accuracy of the spectral techniques to solve the relevant governing differential equation i.e., the Navier-Stokes equation. The unknown field variable was approximated using Lagrange interpolation functions. Unlike the FDSFEM, TDSFEM does not provide any frequency domain or "spectral" information directly, as the framework is similar to conventional FEM. Thus, the inclusion of the term "spectral" in the TDSFEM can be questioned. The established procedure leads to computational efficiency over the conventional FEM. Later on, researchers applied this technique for solving problems of dynamics in the domain of structural engineering. The computational efficiency over conventional FEM being attributed to the applied numerical integration scheme.

While the available literature shows extensive work on FDSFEM and TDSFEM, their application was limited to structures with simpler geometries. While there is a difficulty in applying FDSFEM in 2D or 3D structures with irregular geometries, TDSFEM are amenable to such applications. Here, the application of TDSFEM is explored for 2D planer structures such as dams. While TDSFEM formulations for 2D plane-stress/plane-strain problems are available in the literature, their application to dynamic analysis was limited to modal analysis. Also, for a problem like dam-foundation-reservoir system, their semi-infinite foundation required an infinite element that is not developed in TDSFEM yet. Also, there is no study available for dynamic time history analysis to 2D plane structures using TDSFEM. The objective of the present study is close the above research gaps by adapting the 2D TDSFEM to modeling concrete gravity dam-foundation systems, developing the necessary formulations for an infinite element in TDSFEM to model the semi-infinite foundation boundaries, and implementing a linear dynamic time-history analysis method for such systems.

II. Frequency domain-based spectral finite element method (FDSFEM)

The frequency domain based spectral finite element method (FDSFEM) works with exact solutions to the governing differential equations and thus the dynamic properties of the system are modeled with the highest accuracy. This method leads to the requirement of a single element for modeling a part of a structure with no material or geometric continuity, thus significantly reducing the size of matrices to be solved. As the method works in the frequency domain, the response is calculated by superposition of responses over a number of frequencies using the FFT and Inverse FFT algorithms. The computational efficiency of the FDSFEM has been demonstrated for simple Euler-Bernoulli beams first by Doyle (1990) in his work on flexural wave propagation in beams. His research team extended the earlier work for application to Timoshenko beam theory (Gopalakrishnan et at, (1992)). To showcase the computational accuracy and efficiency of the FDSFEM, a comparison of modal analysis of Euler-Bernoulli beams using conventional FEM and FDSFEM has been performed (Lee & Lee, (1996)). Frequency domain based SFEM formulations for lattice structures have been developed by Lee (2000). In this work also, the necessity of much smaller number of elements and degrees of freedom for performing dynamic analysis of structures using FDSFEM with respect to conventional FEM has been demonstrated. Sarvestan et al (2017) performed vibration analysis of multi-story portal frame using both conventional FEM and FDSFEM, demonstrating that the former required almost 40 times the number of degrees of

freedom as required by the latter for reaching same accuracy in results. The application of FDSFEM can be extensively found in the domain in structural health monitoring and damage detection. Detection of additional mass in rods using the FDSFEM and experimental validation of the same has been done by Palacz et al (2005). Damage detection using iterative search techniques have also been performed where the FDSFEM has been used for modeling by Krawczuk (2002) and Palacz & Krawczuk (2002). The problem of damage detection using FDSFEM has also been solved by converting it into an optimization problem and henceforth also calculating the associated uncertainties by Ng et al. (2009). Some other varied applications of FDSFEM can be found in Park & Lee (2012), Wu (2013), Jin et al (2017), Kim & Lee (2017), Boudaa et al (2019), Caglar & Safak (2019) and Hamioud (2021). From the above-mentioned literature, some of the distinct advantages of the FDSFEM that can be pointed out are decrease in the number of degrees of freedom, number of equations to be solved, thus reducing computational time and high accuracy in the frequency domain problems like calculation of eigen frequencies.

However, there are certain restrictions involved with the application of FDSFEM to structural engineering problems. FDSFEM requires the exact solutions of governing equations of wave propagation which are not available for structures with irregular geometry. Equations (1) and (2) depict the two-dimensional wave propagation equations for which the exact solutions only exist for regular geometries and not for irregular geometries like concrete gravity dams.

$$\mu\nabla^2 u + (\lambda + \mu)\left[\frac{\partial^2 u}{\partial x^2} + \frac{\partial^2 \omega}{\partial x \partial z}\right] = \rho \frac{\partial^2 u}{\partial t^2} \qquad (1)$$

$$\mu\nabla^2 w + (\lambda + \mu)\left[\frac{\partial^2 w}{\partial z^2} + \frac{\partial^2 u}{\partial x \partial z}\right] = \rho \frac{\partial^2 w}{\partial t^2} \qquad (2)$$

Also, the FDSFEM formulation uses throw-off elements at the boundary which are one-noded semi-infinite elements simulating the flow of energy out of the structure. The throw-off elements to be modeled at the element boundary restrict the application of FDSFEM to structures with complex geometries which are applicable to most real-life practical structures. The necessity for the element at the boundary to be infinitely long in FDSFEM formulation makes it impractical to be used in real life structures with complex geometry (He and Ng, (2017)). The use of FFT in FDSFEM causes wrap-around problem for forces with short duration, i.e., the response does not die down with the chosen time window irrespective of the type of damping adopted and this leads to distorted response (Mitra and Gopalakrishnan, (2005)). These limitations in the application of

FDSFEM highlight the need for further research and find alternatives or alternatives in SFEMs to overcome these challenges and expand their applicability.

III. Time-domain based spectral finite element method (TDSFEM)

The spectral element method developed by Patera (1984) later came to be known as the time domain based spectral finite element method (TDSFEM) provides an alternative. It needs to be pointed out here that in TDSFEM, the discretization is in the spatial domain. The difference between TDSFEM and the conventional FEM is the use of higher order polynomial as interpolating functions and the integrating points being connected to the element nodes, rather than in the element domain. This results in a diagonal mass matrix and thus it requires less computation time as compared to conventional FEM, saving computational cost. Applications of TDSFEM in the field of seismology and seismic wave propagation can be found in Smith (1975), Komatitsch (1999), Komatitsch & Tromp (2002), Tromp et al. (2008), Kudela & Ostachowicz (2009), Komatitsch et al. (2010). Semblat & Brioist (2000) pointed out the efficiency gained by use of higher order polynomials in finite element formulations. Kudela et al (2007) demonstrated that TDSFEM can be effectively used in modeling wave propagation in structures. Rucka (2009) has performed experimental and numerical studies of damage detection in rods with structural discontinuities using the TDSFEM formulation. Different rod theories and their behavior were modeled using TDSFEM by Zak and Krawczuk (2010). Witkowski et al. (2009) formulated TDSFEM for Timoshenko beam elements and carried out damage detection in frames. Chróścielewski et al. (2009) carried out a similar work for steel truss structures. Application of TDSFEM can be widely seen in 2D structures as the method is free from the problems faced in FDSFEM. Zak (2009) proposed a novel TDSFEM formulation for isotropic plates. Rucka (2011) used TDSFEM formulation for modeling in-plane wave propagation in plates and damage detection. Witkowski (2012) formulated 2D time domain based spectral finite elements for wave propagation analysis using plane stress elements. A comprehensive guide for wave propagation analysis in structures using time domain based spectral finite elements is provided by Ostachowicz et al (2012). Wang (2022) presented the vibration characteristics of simply supported beams, cantilever beams and a four-edged rectangular plate using the TDSFEM.

From the above literature review, it is evident that the FDSFEM has higher computational efficiency over the TDSFEM as it requires only a single element to model the dynamic properties

of a structural part with no material or geometric discontinuity. However, the necessity of modeling a throw-off element in FDSFEM formulation limits its use in two-dimensional problems or in structures with complex or irregular geometry. Also, the solution of governing differential equations for wave propagation needed in FDSFEM formulation is not available for irregular geometries. The TDSFEM formulation adopts an integration scheme different from the Gauss Quadrature used in the conventional FEM, and thereby gains significant computational efficiency over the conventional FEM. Detailed comparison of the FDSFEM and TDSFEM has been provided by Palacz (2018) and Hafeez & Krawczuk (2023). It is thus imperative that for application to two-dimensional practical structures with complicated geometry, the TDSFEM is a more appropriate approach for modeling. Incidentally, there has been no major research performed on modeling large civil engineering structures (which have irregular geometries) like concrete gravity dams using alternative techniques like TDSFEM. Concrete gravity dams being enormous in size require huge computational time, space and cost when conventional FEM is used, especially when a finer mesh needs to be used to capture the stress variation in certain critical locations of a dam.

IV. Modal parameter-based damage detection

There are not many applications of the TDSFEM in the case of large structures like concrete gravity dams. The computational efficiency in terms of the time achieved in TDSFEM will be more beneficial in the case of large structures like dams. This thesis applies the concept and methodology of TDSFEM in the case of concrete gravity dams. The application is made in terms of dynamic analysis, damage detection, and localization which is a challenging task considering the enormity of the structure. Vibration-based methods in damage detection employ modal parameters like frequency, displacement mode shape, curvature mode shape, etc. to detect the presence of damage as well as for the localization and quantification of the same. However, these parameters, though can identify the presence of damage, cannot always efficiently detect the location of the damage. While vibration-based damage identification techniques are well established, it has many challenges as identified in Humar et al. (2006). Among many such methods, matrix update method and strain energy-based was observed to be comparatively more effective in damage localization Humar et al. (2006). Strain energy-based damage detection method was demonstrated for a concrete gravity dam by (Bagchi et al., 2019).

V. Alkali-aggregate reaction (AAR) and its severe impact on structures

The durability and structural integrity of concrete structures can be significantly impacted by the alkali-aggregate reaction (AAR), especially in concrete gravity dams. This chemical reaction occurs when alkali hydroxides in Portland cement react with reactive silica in aggregates, resulting in the formation of an expansive gel that causes cracking and structural damage over time (ACI, 2001). The impact of this phenomenon is particularly alarming for the numerous large dams across the globe, which play a vital role in water supply, irrigation, flood control, and hydroelectric power generation. With more than 58,000 large dams in operation worldwide currently (ICOLD, 2023), the potential consequences of AAR on these critical infrastructures are a matter of global concern. To ensure the proper handling of AAR in dam structures, a comprehensive approach is required. This approach should include the use of suitable construction materials, continuous monitoring, and timely remedial actions. AAR can have a significant impact on the static and dynamic behaviors of dams, weakening their load-bearing capacity and making them less resistant to seismic events (ACI, 2001 and Thomas & Folliard, 2007).

Highlighting the global scale of the AAR challenge, various dams worldwide have suffered significant impacts due to this phenomenon. In the United States, both the Gene Wash and Copper Basin dams have encountered stress-related issues attributed to AAR (Wood, 2001). The Mactaquac Dam, situated on Canada's St. John River, has been grappling with AAR-related expansion and leakage issues since the mid-1970s, manifesting through its construction joints (Holman, 2024). The Kariba Dam, straddling the Zambia/Zimbabwe border, exemplifies the complexities involved in managing AAR within essential hydroelectric infrastructure (World Bank, 2024). In Portugal, the Alto Ceira and Santa Luzia dams are among several structures that have faced structural challenges due to AAR (Wood, 2001), while in France, approximately thirty dams, including the Salanfe Dam, have reported swelling and cracking problems as a result of AAR (de Larrard & Duprat, 2015), (Droz et al, 2013). Additionally, the Fontana Dam in the USA stands as a notable example in the annals of dam engineering, suffering from AAR-induced cracking (Pan et al, 2012). These instances underscore AAR's significant risk to the operational safety and effectiveness of large dam infrastructures globally. Combating this issue demands an integrated approach, leveraging the latest in material science, engineering methodologies, and ongoing maintenance practices to preserve the structural health and reliability of these vital structures.

The objective of this study is to evaluate the impact of alkali-aggregate reaction (AAR) on the static and dynamic behaviors of the Koyna dam by comparing scenarios with and without AAR effects. Utilizing a simplified thermo-mechanical approach, this research model AAR effects as equivalent thermal strains, introducing a pseudo-temperature method to account for mechanical expansion similar to thermal expansion. This novel approach allows for the assessment of AAR's impact on dam safety and integrity without the need for complex, rigorous experimental setups that attempt to replicate field conditions. Through static and dynamic analysis, the study aims to demonstrate how AAR significantly compromises the structural integrity of dams, potentially leading to failure. Also, the computationally efficient time domain spectral finite element method has been used for all the analysis performed in this study. For large structures like concrete gravity dams, as computational time is huge, saving in computational time is beneficial. The research highlights the severity of AAR effects, suggesting the potential for further detailed investigations that could include stepwise analysis to observe AAR progression over time and non-linear analysis to predict dam behavior more accurately under AAR conditions.

VI. Summary

From the above literature review, it is evident that the need for alternative computationally efficient analysis techniques need to be adopted for dynamic analysis of large structures like concrete gravity dams. From the literature review, it was found that the Spectral Finite Element Method (SFEM) provides an efficient alternative to the conventional Finite Element Method (FEM). Two different families of SFEM are available in the literature, Frequency Domain SFEM (FDSFEM) and Time Domain SFEM (TDSFEM). While FDSFEM is formulation requires regular geometry, TDSFEM could work for irregular geometry as the domain can be discretized in the same manner as in conventional FEM. While there has been extensive development in TDSFEM in recent years, its application to two-dimensional stress analysis is limited. There is a need for further development in that area, particularly for the analysis of large structures like concrete gravity dams where foundation domain could extend to infinity. Also, there is a need for further development to formulate TDSFEM to account for material nonlinearity, dynamic effects, and thermal stress. As mass concrete structures such as concrete gravity dams could be affected by Alkali-Aggregate Reaction (AAR), there is a need for developing an appropriate method to account for the AAR effect in TDSFEM-based analysis of dams. Based on the analysis, a simplified damage detection and localization methodology could be useful to assess the structural condition of such structures.

CHAPTER 3: METHODOLOGY

I. Time domain spectral finite element formulation for two-dimensional plane stress element

The plane stress element formulation comes directly from the fundamentals of solid mechanics mentioned in the following discussion. Here, we consider a two-dimensional elastic body B where u_α, $\dot{u}_\alpha$, $\ddot{u}_\alpha$, $\varepsilon_{\alpha\beta}$, $\sigma_{\alpha\beta}$, b_α, C denote the displacement vector, the velocity vector, the acceleration vector, infinitesimal strain tensor, the Cauchy stress tensor, the body force and the positive definite elasticity tensor (Hughes, 2000). The domain ∂B of B consists of two non-empty parts ∂B_d and ∂B_f which are disjoint. In this chapter, indicial notation is used throughout where the Greek subscripts take the value of the integers 1 and 2. For the two-dimensional homogenous and isotropic conditions, the field equations for the initial-boundary value problem are given in equations as below.

$$\varepsilon_{\alpha\beta} = \frac{1}{2}(u_{\alpha,\beta} + u_{\beta,\alpha}) \equiv u_{(\alpha,\beta)} \tag{3}$$

$$\sigma_{\alpha\beta,\beta} + b_\alpha = \rho \ddot{u}_\alpha \tag{4}$$

$$\sigma_{\alpha\beta} = C_{\alpha\beta\gamma\pi} u_{(\gamma,\pi)} \tag{5}$$

$$C_{\alpha\beta\gamma\pi} = \bar{\lambda}\, \delta_{\alpha\beta}\delta_{\gamma\pi} + \mu(\delta_{\alpha\gamma}\delta_{\beta\pi} + \delta_{\alpha\pi}\delta_{\beta\gamma}) \tag{6}$$

Here, ρ is the mass density and λ, υ are the material constants. The energy equilibrium equation of the system can be written below.

$$U(t) + K(t) - G_{ext}(t) = 0 \tag{7}$$

In the above equation, U(t) is the internal elastic energy density, K(t) is the kinetic energy density and G(t) is the work done by the external forces. The above equation can be written in the weak form as follows.

$$\int_B \rho w_\alpha \ddot{u}_\alpha \, dV + \int_B C_{\alpha\beta\gamma\pi} w_{(\alpha,\beta)} u_{(\gamma,\pi)} dV = \int_B w_\alpha b_\alpha dV + \int_{\partial B_f} w_\alpha f_\alpha dS \tag{8}$$

In the above equation, u denotes the set of kinematically admissible displacement functions, w represents the set of kinematically admissible displacement functions satisfying homogenous boundary conditions. By applying the finite element formulation on the above equation, the overall domain B is subdivided into small parts and is approximated as a summation of the smaller "finite" elements as shown in Equation 9.

$$B \approx \cup_{e \in N_e} B_{(e)} \tag{9}$$

Here, Ne is the number of finite elements into which the whole domain is divided. As per the conventional of the finite element method, $B_{(e)}$ for a typical element is a smooth image of the standard element $\pi_{(e)}$. The standard element in case of two-dimensional problems is $\pi_{(e)}$ = [-1,1] x [-1,1], also called the element in the natural or parent domain $\xi = (\xi^1, \xi^2)$. The number of nodes considered in the ξ^1 direction is m^1 and the number of nodes considered in the ξ^2 direction is m^2, thus having a total $N=m^1.m^2$ number of nodes. Lagrange type interpolation functions are used as shape functions for the displacement field considered in the problem. Considering C^0 interpolating functions, the matrix of shape functions for the node 'a' and an element with N nodes are as mentioned in equations below.

$$L_{a_{(2x2)}}(\xi) = L_a(\xi) I_{(2x2)} \tag{10}$$

$$L_{(e)}(\xi) = [L_1(\xi), L_2(\xi), ..., L_N(\xi)] \tag{11}$$

For the displacement field in general, the interpolation scheme can be represented as shown in equation below.

$$u(\xi, t) = L_{(e)}(\xi) u_{(e)}(t) \tag{12}$$

$$u_{(e)}(t) = \{u_1(t), u_2(t), ..., u_N(t)\}^T \tag{13}$$

$$u_a(t) = \{u_1(t), u_2(t)\}_a^T \qquad \text{where a=1 to N} \tag{14}$$

Ignoring the time dependency, the strain tensor and its virtual counterpart can be written in vector notation as follows

$$\varepsilon \rightarrow \varepsilon = \{\varepsilon_{11}, \varepsilon_{22}, 2\varepsilon_{12}\}^T = Du \tag{15}$$

$$\delta\varepsilon \rightarrow \delta\varepsilon = \{\delta\varepsilon_{11}, \delta\varepsilon_{22}, \delta 2\varepsilon_{12}\}^T = Dw \tag{16}$$

$$D = \begin{bmatrix} (.)_{,1} & 0 \\ 0 & (.)_{,2} \\ (.)_{,2} & (.)_{,1} \end{bmatrix} \quad (17)$$

In abridged form, the displacement-strain relations can be written in equation form as below.

$$\varepsilon(\xi,t) = DL_{(e)}(\xi)u_{(e)}(t) = B_{(e)}(\xi)u_{(e)}(t) \quad (18)$$

$$\delta\varepsilon(\xi) = DL_{(e)}(\xi)w_{(e)} = B_{(e)}(\xi)w_{(e)} \quad (19)$$

$$B_{(e)}(\xi) = DL_{(e)}(\xi) \quad (20)$$

Finally, the constitutive relationship for the plane-stress condition relating stress and strain can be written as follows.

$$\begin{bmatrix} \sigma_{11} \\ \sigma_{22} \\ \sigma_{12} \end{bmatrix} = \frac{E}{1-\gamma^2} \begin{bmatrix} 1 & \gamma & 0 \\ \gamma & 1 & 0 \\ 0 & 0 & 0.5(1-\gamma) \end{bmatrix} \begin{bmatrix} \varepsilon_{11} \\ \varepsilon_{22} \\ 2\varepsilon_{12} \end{bmatrix} \quad (21)$$

II. Formulation of element mass, stiffness and force matrices

The section above describes the two-dimensional plane stress formulation from the background of solid mechanics. The present section presents in detail the two-dimensional plane stress formulation in the context of TDSFEM and how it deviates from the conventional FEM. The stiffness and mass matrices and the load vector can be written in the general form below. Four-noded rectangular elements with two degrees of freedom at each node (as shown in Figure 1) are considered for both conventional FEM and TDSFEM formulations.

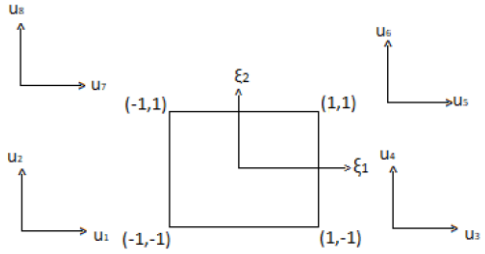

Figure 1: A typical two-dimensional 4-noded rectangular element with 8 degrees of freedom

$$\int_B C_{\alpha\beta\gamma\pi} w_{(\alpha,\beta)} u_{(\gamma,\pi)} dV \rightarrow K_{(e)} = h_0 \int_B B^T_{(e)}(\xi) E B_{(e)}(\xi) dx_1 dx_2 \quad (22)$$

$$\int_B \rho w_\alpha \ddot{u}_\alpha \, dV \rightarrow M_{(e)} = \rho h_0 \int_B L^T_{(e)}(\xi) L_{(e)}(\xi) dx_1 dx_2 \quad (23)$$

$$\int_B w_\alpha b_\alpha dV + \int_{\partial B_f} w_\alpha f_\alpha dS \rightarrow f_{(e)}^{ext} = h_0 \int_B L_{(e)}^T(\xi) b dx_1 dx_2 + \int_{\partial B_f} L_{(e)}^T(\xi) f dS \quad (24)$$

For transformation from the parent element to the mapped element, the Jacobian determinant needs to be used which takes the form:

$$j(\xi) = \frac{\partial x_1}{\partial \xi^1}\frac{\partial x_2}{\partial \xi^2} - \frac{\partial x_1}{\partial \xi^2}\frac{\partial x_2}{\partial \xi^1} \quad (25)$$

$$dV = h_0 j(\xi) \partial\xi^1 \partial\xi^2 = h_0 dx_1 dx_2 \quad (26)$$

For the total element load vector, the external load vector is added to the nodal load vector as below.

$$f_{(e)} = f_{(e)}^{ext} + f_{(e)}^{node} \quad (27)$$

$$f_{(e)}^{node} = \{P_1, P_2, ..., P_N\}^T \quad (28)$$

$$P_a = \{P_{x1}, P_{x2}\}_a^T \quad (29)$$

Here, the vector Pa represents the nodal loads applied to the node ‘a’ of an element in the global co-ordinate system.

However, to obtain the element matrices, numerical integration needs to be performed.

$$K_{(e)} = \int_{-1}^{1} B_{(e)}^T(\xi) E B_{(e)}(\xi) j(\xi) d\xi \approx \sum_{p=1}^{n_p} w_p B_{(e)}^T(\xi_p) E B_{(e)}(\xi_p) j(\xi_p) \quad (30)$$

$$M_{(e)} = \int_{-1}^{1} N_{(e)}^T(\xi) \mu N_{(e)}(\xi) j(\xi) d\xi \approx \sum_{p=1}^{n_p} w_p N_{(e)}^T(\xi_p) \mu N_{(e)}(\xi_p) j(\xi_p) \quad (31)$$

$$f_{(e)} = \int_{-1}^{1} N_{(e)}^T(\xi) f_{(e)}(\xi) j(\xi) d\xi \approx \sum_{p=1}^{n_p} w_p N_{(e)}^T(\xi_p) f_{(e)}(\xi_p) j(\xi_p) \quad (32)$$

In the above equations, n_p represents the number of integration points, ε_p indicates the co-ordinates of the integration points and wp are the associated weights of numerical integration. The departure of the TDSFEM from the conventional FEM in the numerical integration scheme is that it uses Gauss-Lobatto-Legendre (GLL) quadrature rule instead of the Gauss-Legendre quadrature rule used in the conventional FEM. In the GLL quadrature rule (Hilderbrandt, (1956)), the co-ordinates of the integration points and the associated weights are expressed as given in the equations below.

$$(1-\xi^2)\frac{dP^{M-1}(\xi)}{d\xi}=0, M \leftarrow m_1, m_2 \quad (33)$$

$$w=\frac{2}{M(M-1)(P^{M-1}(\xi))^2}, M \leftarrow m_1, m_2 \quad (34)$$

Here, PM denotes the Legendre polynomial of the M-th order given by the equation below.

$$P^M(\xi)=\frac{1}{2^M M!}\frac{d^M}{d\xi^M}[(\xi^2-1)^M], \xi \leftarrow \xi^1, \xi^2 \quad (35)$$

The essential feature of the GLL quadrature rule is that the co-ordinates of the integration point coincide with the element nodes. Due to the nature of the interpolating polynomials used and the integration being carried out over the GLL nodes, the element mass matrix calculated by TDSFEM becomes a diagonal matrix. The global matrices are constructed from the element matrices by standard aggregation procedure as followed in conventional FEM. The accuracy achieved by TDSFEM and its computational efficiency over the conventional FEM has been studied and demonstrated in the next few chapters.

III. Formulation for inelastic analysis

Concrete is a brittle material and like other brittle and quasi-brittle materials, it follows the non-associative plasticity in which the yield function and the plastic flow function are not the same. In the present work, the Concrete Damage Plasticity (CDP) model for concrete as suggested by Lee and Fenves (1998), which is a modified version of the one suggested by Lubiner et al (1989), has been considered. In this approach, the tensile and compressive damage are considered using separate variables which is a realistic way of modeling the behavior of concrete undergoing both tensile and compressive stresses. The yield functions and the plastic flow potential function considered are mentioned in the following equations.

$$\sigma = (1-d)D_0^{el}:(\varepsilon-\varepsilon^{pl}) \quad (36)$$

$$\varepsilon = \varepsilon^{el}+\varepsilon^{pl} \quad (37)$$

$$F(\bar{\sigma},\tilde{\varepsilon}^{pl})=\frac{1}{1-\alpha}(\bar{q}-3\alpha\bar{p}+\beta(\tilde{\varepsilon}^{pl})(\hat{\bar{\sigma}}_{max})-\gamma(-\hat{\bar{\sigma}}_{max}))-\bar{\sigma}_c(\tilde{\varepsilon}_c^{pl})\leq 0 \quad (38)$$

$$\dot{\varepsilon}^{pl}=\dot{\lambda}\frac{\partial G(\bar{\sigma})}{\partial\bar{\sigma}} \quad (39)$$

$$G=\sqrt{(\epsilon\sigma_{t0}\,tan\,\psi)^2+\bar{q}^2}-\bar{p}\,tan\,\psi \quad (40)$$

In recent years, other researchers have developed modified concrete damage plasticity models for specific applications like Grassl (2009), Unger et al. (2011). For the return mapping algorithm, an elastic predictor-plastic corrector methodology is adopted along with the Newton-Raphson method for solving the set of non-linear equations as suggested by Simo and Taylor (1986).

IV. Dynamic analysis

In this thesis, dynamic analysis has been performed to evaluate the performance and computational efficiency of TDSFEM and also to evaluate the structural behavior of concrete gravity dams subjected to seismic ground motions. Few types of dynamic analysis have been performed- modal analysis, linear dynamic analysis, and non-linear dynamic analysis. Modal analysis has been performed for simply supported beams and concrete gravity dams in the verification stages of the developed TDSFEM algorithms in the study. Linear dynamic analysis has been performed for a concrete gravity dam for four node and nine node elements considering multiple ground motions of varying intensity, magnitude, and duration. For solving the set of linear matrix equations in linear dynamic analysis, Newmark's method has been adopted in this thesis. Time history analysis of the concrete gravity dam considering the effect of material non-linear behavior has been performed for better prediction of the structural behavior subjected to seismic ground motion. In the verification chapter for establishing the TDSFEM algorithms, pseudo-static analysis of the concrete deep beams has been performed and the load-deflection as well as the failure mechanisms have been compared to the experimental behavior of the concrete deep beams. For the pseudo-static analysis of the concrete deep beams, monotonic increasing load has been applied at a very slow rate till the failure of the beams. The slow rate of load application ensures that no inertial forces are generated.

The basic structure of the developed algorithms is shown in Figure 2. The types of analysis performed are provided in Figure 3.

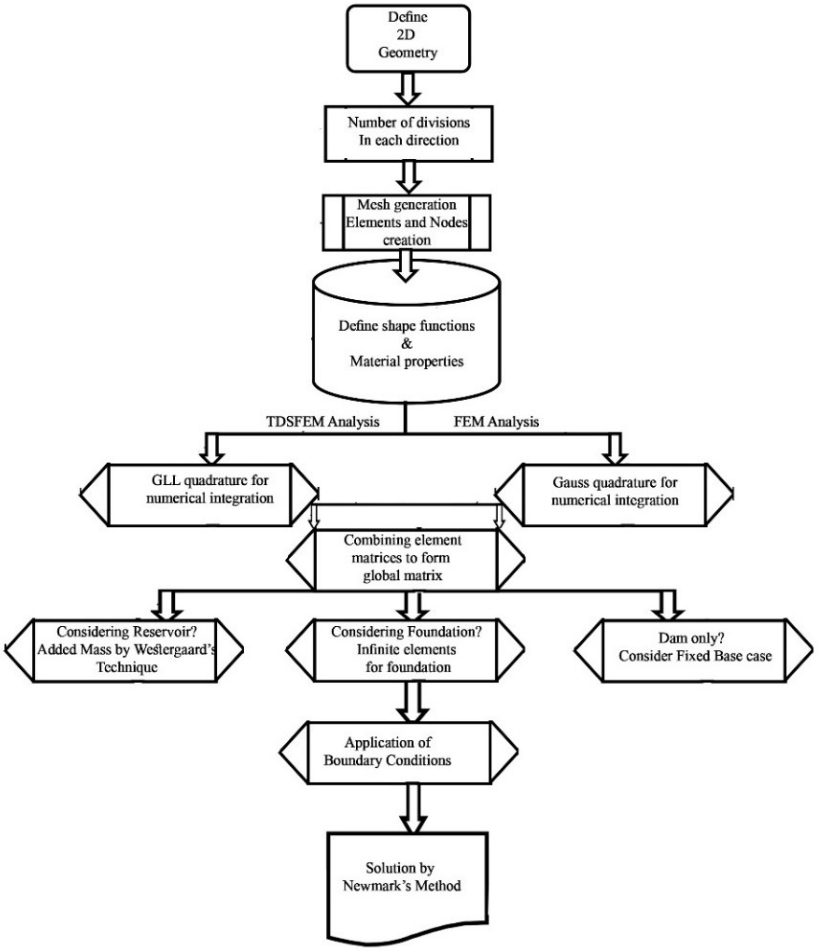

Figure 2: Flowchart of developed algorithm for linear dynamic analysis

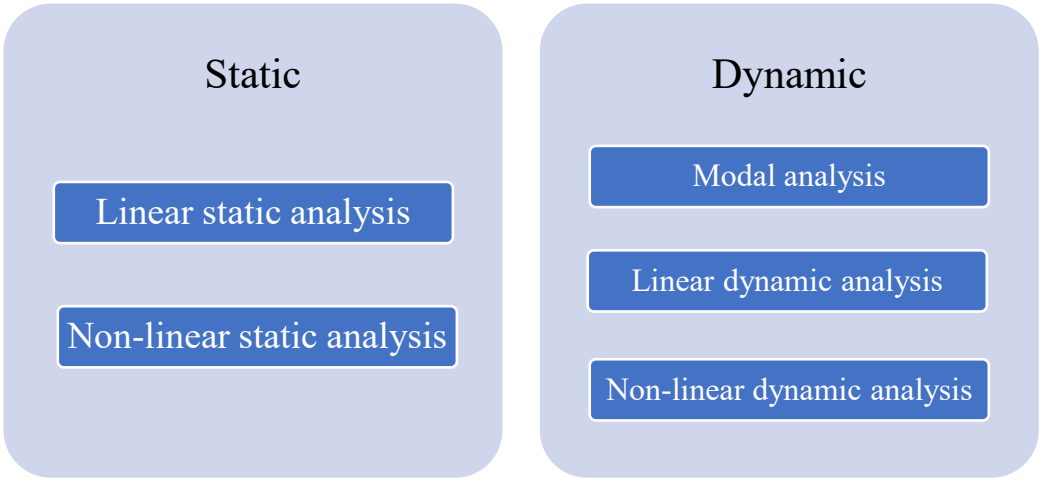

Figure 3: Types of analysis performed (check)

V. Vibration-based Damage Detection

Damage in a structure causes change in the modal parameters of the structure. In this thesis, the change in modal parameters have been considered as indicator for presence and location of damage in a structure. The modal parameters considered for this purpose are frequency, modal displacements, modal curvatures, and modal strain energy. For identification and location of damage, a backward method has been adopted, i.e., damage has first been introduced in the structure and then the above-mentioned parameters are calculated for the damaged structure. Damage index for each modal parameter for a particular mode has been defined as the change in the parameter value in the damaged structure relative to the parameter value in the original undamaged structure divided by the parameter value in the original undamaged structure, corresponding to the mode number considered. Higher value of damage index determines the location of the damage. A particular modal parameter is considered accurate in determining the location of damage if it has higher value of damage index corresponding to the location where the damage is introduced in the structural model. In this study, damage in the structure in terms of reduction of material modulus. It needs to be pointed here that very small damage does not affect the lower modes of vibration but only causes change in the higher vibration modes. Thus, at the onset of structural deterioration, change could only be noticed in the higher vibration modes. From this, it could be stated that the modal parameter which sees higher magnitude of change in the higher vibration modes for same level of damage could be considered a better damage identifier. A flowchart of the procedure for detecting damage based on changes in the modal parameter is shown in Figure 4.

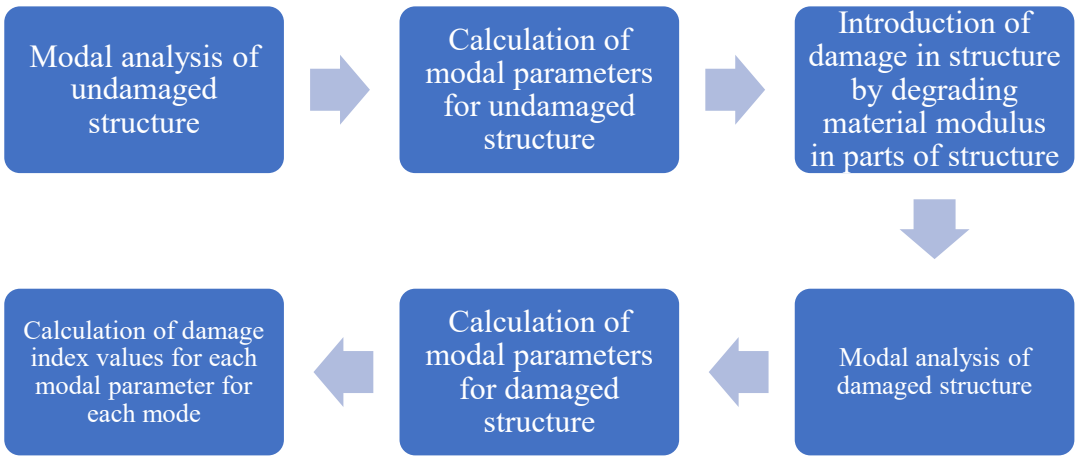

Figure 4: Flowchart showing the modal parameter-based damage detection process

The calculation of damage index for the modal parameters is as shown below.

$$ddi_i = \frac{d_{di-}\, d_{ui}}{d_{ui}} \qquad (41)$$

Where, $(d_{di})_i$ is the displacement damage index for mode i, d_{di} is the modal displacement for the damaged structure for mode i and d_{ui} is the modal displacement of the undamaged structure for mode *i*.

$$\varphi di_i = \frac{\varphi_{di} - \varphi_{ui}}{\varphi_{ui}} \qquad (42)$$

Where, $(\varphi_{di})_i$ is the curvature damage index for mode *i*, φ_{di} is the modal curvature for the damaged structure for mode *i* and φ_{ui} is the modal curvature for the undamaged structure for mode *i*.

$$sdi_i = \frac{s_{di} - s_{ui}}{s_{ui}} \qquad (43)$$

Where, $(s_{di})_i$ is the strain energy damage index for the i-th mode, s_{di} is the strain energy of the damaged structure for the *i*-th mode and s_{ui} is the strain energy of the undamaged structure for the *i*-th mode.

VI. Alkali Aggregate Reaction (AAR)

Alkali Aggregate reaction (AAR) is a chemical process which causes differential expansion in the structure and causes large cracks which needs retrofitting measures to be carried out. While AAR is a complex phenomenon and several chemical models are available based on laboratory tests conducted to simulate the effects of AAR on structures, this thesis presents a simplified thermo-mechanical approach to model the structural behavior affected by AAR. Considering the fact that AAR causes expansion, a pseudo-temperature is calculated to produce the AAR strain. This pseudo-temperature is applied on the structure and the mechanical stresses produced by the same are evaluated along with the stresses produced by the other loads acting on the structure. Two stages are considered- one where the structure is not impacted by AAR and another where the structure is impacted by full AAR effects. Static and dynamic analysis are performed for both these stages. Figure 5 provides a flowchart of the methodology adopted for the AAR analysis.

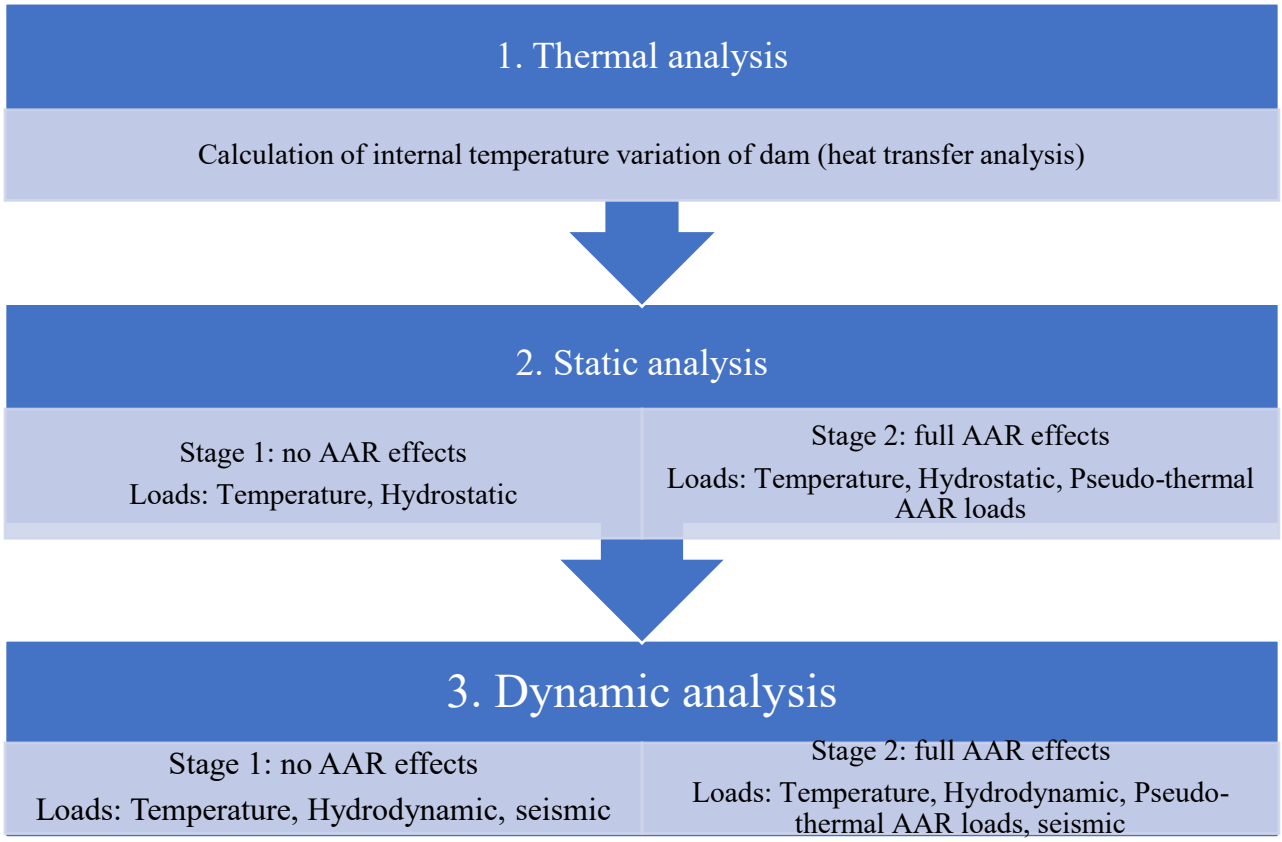

Figure 5: Procedure adopted for AAR analysis

For the calculation of the internal temperature variation of the dam, a thermal gradient is considered along the external surfaces of the dam and a thermal/ heat transfer analysis is performed in ABAQUS. This provides the internal temperature across the internal nodes of the dam body. Once the nodal temperatures are obtained, these are used to calculate the thermal loads on the structure and calculate the corresponding displacements and mechanical stresses produced as a result of temperature. Next is to calculate the pseudo-temperature to be applied for the AAR strain simulation. In order to do that, the AAR strain needs to be calculated.

The calculations of AAR strains (Saouma & Perrotti, 2006) are elaborated as follows.

$$\xi(t,T) = \frac{1-e^{-\frac{t}{\tau_c(T)}}}{1+e^{-\frac{t-\tau_L(T)}{\tau_c(T)}}} \quad (44)$$

$$\tau_c(T) = \tau_c(T_0)e^{U_c\left(\frac{1}{T}-\frac{1}{T_0}\right)} \quad (45)$$

$$\tau_L(T) = \tau_L(T_0)e^{U_L\left(\frac{1}{T}-\frac{1}{T_0}\right)} \quad (46)$$

$$U_c = 5400 \pm 500K \quad (47)$$

$$U_L = 9400 \pm 500K \quad (48)$$

$$\frac{E}{E_0} = \frac{B}{\varepsilon_A + B} \quad (49)$$

Once the AAR strain is calculated, the pseudo-temperature for the calculation of the AAR strain is done as follows.

$$\alpha\delta T_{pseudo} = \text{AAR strain} \quad (50)$$

Once the pseudo-temperature to simulate the AAR strain is calculated, static and dynamic analysis is performed for the cases considering no AAR strain and full AAR strain for comparison of the effects caused by AAR along with the other applied loads- thermal, seismic and water.

VII. Implementation in MATLAB

In this thesis, all the analysis performed are using developed algorithms in MATLAB. Different modules have been created in MATLAB for i) geometry creation of two-dimensional structures, ii) meshing of the two-dimensional geometry, iii) material property definition, iv) creation of element matrices: mass, stiffness, load, etc., v) assembly of element matrices to form global matrices, vi) application of loads: hydrostatic, hydrodynamic, thermal, seismic ground motions, etc., vii) application of boundary conditions, vii) modal analysis and extraction of modal parameters: direct- modal displacement, indirect- curvature mode shapes, modal strain energy, viii) linear dynamic time history analysis, ix) non-linear pseudo-static analysis, x) non-linear dynamic analysis considering material non-linearity only, no geometric and contact nonlinearity considered, xi) calculation of principal stress components, etc. The algorithms are developed for both TDSFEM and conventional FEM for comparison of computation time in both the procedures, thus the structure of algorithms is kept same in both cases. The difference between the two cases is in the shape functions and numerical integration scheme as described in detail in the first subsection of this chapter. The details of some of the algorithms are presented in Appendix 2 of the thesis.

VIII. Summary

In this chapter, the basics of the adopted methodology in the thesis have been presented. The chapter starts with the formulation of the TDSFEM procedure in two dimensional problems, following which the details of the matrix formulations are described. While the basic formulation of TDSFEM for linear stress analysis of planer structures is available in the literature, the present thesis develops the formulation to account for material nonlinearity and semi-infinite domain of foundation for static and dynamic analysis. For dynamic analysis, step-by-step time history analysis based on Newmark's method has been implemented here. To account for material nonlinearity in concrete, the Concrete Damage Plasticity (CDP) method has been utilized. For solving the nonlinear equations following the peak response, and displacement control algorithm has been implemented at that stage to resolve any numerical instability. While the TDSFEM formulations remain the same and have been followed throughout the thesis, each chapter follows the development of a particular method specific to the analysis performed in that chapter which have been briefly presented in this chapter like the procedure followed for nonlinear analysis, dynamic analysis, vibration-based damage localization, simulation of AAR, etc. As the TDSFEM formulations are not available in the commercially available software packages, all the programs developed in this thesis have been developed in MATLAB and specific modules have been written for each particular type of analysis performed in this analysis. This chapter also discusses the MATLAB implementation briefly. The detailed methodology and problem statement for all the analysis performed in this thesis have been discussed in detail in the specific chapters of the thesis.

CHAPTER 4: VERIFICATION OF THE TDSFEM-BASED METHOD

I. Introduction

This chapter presents a detailed verification study of the developed TDSFEM-based method. The method has been applied to some of the benchmark problems including the modal analysis of a 2D concrete beam and a concrete gravity dam for which numerical results are available in literature. Additionally, nonlinear static analysis was performed for a set of FRP-reinforced concrete deep beams results of which were compared with available experimental results.

One of the objectives of the thesis is to demonstrate the application of TDSFEM in 2D plane structures and highlight the computational efficiency of the method. The other objective is to apply the TDFSEM to the dynamic time history analysis of concrete gravity dams subjected to seismic ground motions. For that purpose, a set of MATLAB-based programs has been developed for dynamic analysis using the TDSFEM, and also the conventional finite element method. In order to verify the developed TDSFEM programs, a set of problems available in literature are first solved using the codes and the results verified against the available results. For the purpose of studying the computational efficiency of TDSFEM, the order of polynomials for shape functions and degrees of freedom used in case of both conventional FEM and TDSFEM are kept same. The computational efficiency of TDSFEM arises from the following two aspects: i) the shape functions and the integration scheme chosen in SFEM leads to diagonal mass matrix; and ii) the Gauss quadrature integration scheme used in conventional FEM uses irrational co-ordinates is avoided in TDSFEM by choosing integration points at the element nodes.

First, the developed program has been validated by performing modal analysis of a simply supported beam and verifying the numerical results with analytical results. Also, modal analysis of a concrete gravity dam (Pine Flat Dam) has been performed and the results have been verified with those reported in literature. Next, the developed program has been used to non-linear pseudo-static analysis of FRP reinforced concrete deep beams and the results are validated against experimental results.

II. Modal Analysis of a 2D-beam

A simply supported beam used in Witkowski (2012) is considered with dimensions as shown in Table 1. Figure 6 shows the mesh details used here based on the benchmark problem reported in Witkowski (2012), and it is used for both conventional FEM and TDSFEM programs for comparison.

Table 1: Properties of simply supported beam

Simply Supported Beam Details					
Length (m)	Width (m)	Depth (m)	E (GPa)	Poisson's Ratio	Density (kg/m^3)
1	0.05	0.125	200	0	7850

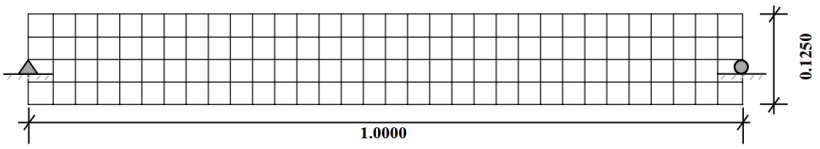

Figure 6: Mesh refinement details of beam (same followed in both FEM and SFEM) (Witkowski (2012))

Table 2: Modal Frequencies

Comparison of Frequencies (Hz)				
Mode Number	Analytical (Euler-Bernoulli)	FEM	SFEM	SFEM (Witkowski, 2012-Table 2)
1	285.96	283.71	306.92	308.17
2	1143.82	1118.82	1156.80	1154.9
3	2573.60	2207.23	2334.46	2377.6

The modal frequencies obtained from conventional FEM and the TDSFEM are shown in Table 2. The modal frequencies of the beam are comparable to those reported by Witkowski (2012) considering both conventional FEM and TDSFEM. Thus, the developed MATLAB programs for TDSFEM and conventional FEM are validated by the above analysis.

II. Modal Analysis of a Concrete Gravity Dam

For further validation of the developed programs in case of concrete gravity dams, the well-researched Pine Flat Dam has been considered. Pine Flat dam is situated in California, United States of America and was constructed in 1954. The geometric and material property details of the

dam can be found in various literature (Rea et al (1972), Chopra and Chakrabarti (1980), Feltrin et al. (1992), Salamon et al. (2021)). The modal analysis of the dam (considering fixed base and empty reservoir condition) has been performed using the developed FEM and TDSFEM programs. The reported frequency of the first mode in literature (Chopra and Chakrabarti (1980)) is 3.155 Hz with matches closely with the obtained frequency values in the present study (as shown in Figure 7). The percentage difference in modal frequency estimation (values presented in Figure 7) between FEM and TDSFEM are 1.1 %, 0.3 % and 0.74 % for modes 1, 2 and 3 respectively.

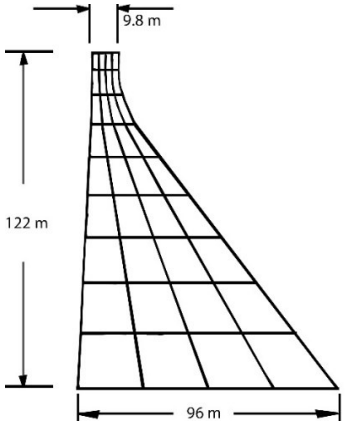

Elastic Modulus = 22407 MPa
Density = 2482 kg/m³
Poisson's ratio = 0.2

Frequency values in Hz

Mode Number	Present study (SFEM)	Present study (FEM)
1	3.086	3.053
2	7.781	7.764
3	9.688	9.617

Figure 7: A typical meshing of the Pine Flat Dam, material properties and frequency values

III. Nonlinear Static Analysis of FRP reinforced concrete deep beams

Ongoing research is dedicated to the evaluation of the performance of concrete structural elements, such as beams and columns, reinforced with fiber-reinforced polymer (FRP). In recent years, numerous international design standards have incorporated relevant provisions for the design of structural elements reinforced with FRP in concrete. Notably, the behavior of deep beams deviates significantly from beams governed by flexural behavior, yet design provisions specifically addressing FRP concrete deep beams are limited. This limitation may be attributed to the insufficient volume of research on the behavior of FRP concrete deep beams.

This study focuses on two key aspects related to FRP-reinforced concrete deep beams. Firstly, it presents the findings of an experimental investigation conducted on an FRP-reinforced concrete deep beam. Secondly, an alternative modeling approach is introduced to simulate the beam's behavior. The rationale for adopting this alternative modeling technique is elaborated upon in the subsequent paragraph.

Since its inception, Finite Element Method (FEM) has been extensively used by researchers and practitioners for a varied range of engineering analysis. This can be attributed to various factors, such as, (i) it is the one of the most well researched analysis techniques, (ii) it has the capacity to model complex multi-physics problems and even used for different type of analysis like static, quasi-static, dynamic, etc. (iii) the ease of application in various engineering problems due to its matrix methodology and integration of FEM in commercial software packages. Despite the above stated reasons, there are certain challenges in the application of FEM. One of the challenges is the computational time required for quasi-static or dynamic analysis. Thus, there has been ongoing research in the past few decades to come up with computationally more efficient analysis techniques. Some of the developed computationally efficient techniques are known as "spectral finite element methods". In the present work, some of the spectral element methods available in literature and their applicability in the present context of work is discussed. Finally, the time domain based spectral finite element method (TDSFEM) is used for predicting the behavior of the deep beam. The authors also discuss the saving in computation time achieved by the applied methodology over the conventional FEM. This kind of application of the TDSFEM in the context of modelling the behavior of fiber-reinforced concrete beam is a novelty and adds significantly to the body of existing research in the domain.

Various research studies have extensively presented the behavior and performance of fiber-reinforced polymer (FRP) strengthened reinforced concrete columns (Nayak et al (2014), Rao et al (2021), Rao et al (2023)). The performance of FRP-reinforced concrete beams is also well-documented in the literature (Prajapati et al (2017)). However, there is limited available literature on the performance of FRP-reinforced concrete deep beams. An effort to assess the performance of such deep beams was undertaken by Latosh (2014). Latosh (2014) conducted both experimental and numerical analyses using the Finite Element Method (FEM) to investigate the behavior of FRP-reinforced concrete deep beams. Latosh et al (2019) also performed extensive numerical studies using the conventional FEM to simulate the behavior of the FRP reinforced concrete deep beams.

In all the above-mentioned literature, the used analysis tool has been the finite element method (FEM). However, the need for the use of other computationally more efficient analysis techniques stems from the fact that FEM can sometimes consume huge computation time depending on the

nature of the problem to be solved. In case of problems where iterative techniques need to be applied to solve the equilibrium equations like the application of Newton-Raphson procedure in solving the non-linear equation of motion, the solution procedure becomes quite cumbersome. This is due to the fact the matrix equations need to be solved iteratively to reach convergence for a particular equilibrium stage. In situations where this process needs to be repeated for multiple stages like quasi-static or dynamic problems, the computation time becomes huge in the conventional FEM. This leads to the need for other computationally efficient techniques where the computation time needed to solve the above-mentioned problems could be reduced.

Incidentally, there has been no major research performed on modeling the failure mechanisms or behavior of FRP-reinforced concrete deep beams considering material non-linearity. The objective of this paper is to apply the efficient TDSFEM for quasi-static analysis of FRP-reinforced concrete deep beams under monotonic loadings, compare the failure mechanisms with observed experimental results and quantify the computational efficiency achieved over conventional FEM in terms of the computational time saved using TDSFEM. In this study, the order of the polynomials of shape functions and degrees of freedom used for both FEM and TDSFEM simulations is considered the same to study the comparative performance of the two methods.

To evaluate the performance of the FRP reinforced concrete deep beams, extensive experimental studies are performed by Latosh (2014). A total of 9 samples of concrete deep beams are cast which are divided into 3 groups with varying slenderness ratio and percentage of longitudinal and transverse reinforcement. All the beams are simply supported and tested under monotonically increasing loading at the mid-point of the beams till the failure of the beams. The details of the beam specimens are presented in Table 1. In the nomenclature, the first letter represents the group name, followed by a number which represents the a/d ratio and another number which represents the ratio of percentage of nominal web reinforcement. The total length of all the beams is 1.8 meters and the width of all beams are also the same, 230 mm. The properties of the FRP bars are presented in Table 12. A typical experimental setup of the beams is shown in Figure 8.

Table 3: Details of all deep beam specimens

Specimen No	f'_c (MPa)	b (mm)	d (mm)	L_e (mm)	a/d	Main reinforcement	f_{fu} (MPa)	ε_{fu}	ρ (%)	ρ_v (%)
A1/100	49.8	230	621	1240	1	6 # 6(19 mm)	656	0.0153	1.197	0.141
A1/75	52.2	230	621	1240	1	6 # 6(19 mm)	656	0.0153	1.197	0.095
A1/50	52.5	230	621	1240	1	6 # 6(19 mm)	656	0.0153	1.197	0.061
A1/00	52.7	230	621	1240	1	6 # 6(19 mm)	656	0.0153	1.197	N/A
B1.5/100	51.8	230	447	1340	1.5	3 # 6(19 mm) 3# 4 (13 mm)	656 708	0.0153 0.0170	1.201	0.145
C2/100	50.8	230	328	1310	2	6 # 4(13 mm)	708	0.0170	1	0.158
C2/75	51.0	230	328	1310	2	6 # 4(13 mm)	708	0.0170	1	0.095
C2/50	51.3	230	328	1310	2	6 # 4(13 mm)	708	0.0170	1	0.061
C2/00	51.3	230	328	1310	2	6 # 4(13 mm)	708	0.0170	1	N/A

Table 4: Details of FRP bars

Soft Metric Size	Diameter (mm)	Area (mm^2)	Tensile Modulus of Elasticity E_t (GPa)	Ultimate Tensile Strength f_u (MPa)	Ultimate Strain in Tension ε_{Fu} (%)	Poisson's Ratio μ
# 6	6.350	31.7	46.1	874	1.90	0.25
#10	9.525	71.3	45.4	856	1.89	0.21
#13	12.700	126.7	46.3	708	1.70	0.26
#19	19.050	285	47.6	656	1.53	0.25

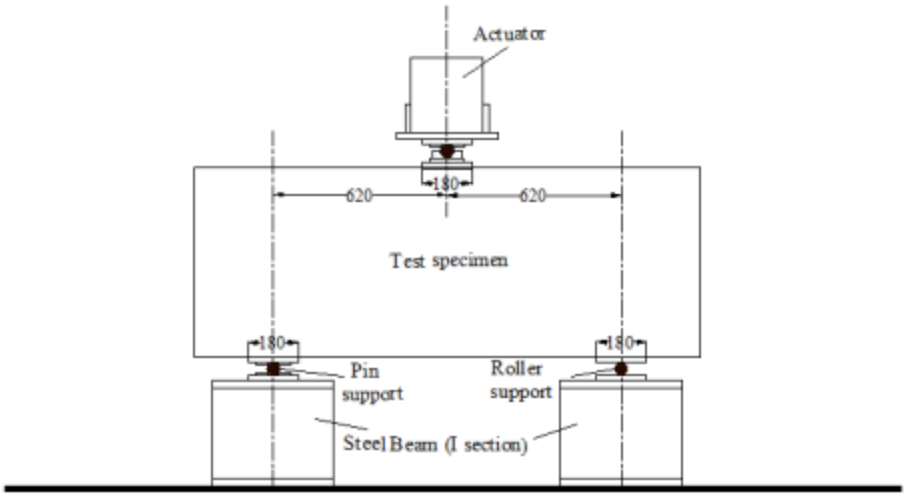

Figure 8: A typical experimental setup of the deep beams

Concrete is a brittle material and like other brittle and quasi-brittle materials, it follows the non-associative plasticity in which the yield function and the plastic flow function are not the same. In the present work, the concrete damage plasticity model for concrete as suggested by Lee and Fenves (1998), which is a modified version of the one suggested by Lubiner et al (1989), has been considered. In this approach, the tensile and compressive damage are considered using separate variables which is a realistic way of modeling the behavior of concrete undergoing both tensile and compressive stresses. The yield functions and the plastic flow potential function considered are mentioned in the methodology section.

In recent years, other researchers have developed modified concrete damage plasticity models for specific applications like Grassl (2009), Unger et al. (2011). For the return mapping algorithm, an elastic predictor-plastic corrector methodology is adopted along with the Newton-Raphson method for solving the set of non-linear equations as suggested by Simo and Taylor (1986).

IV. Results of failure analysis of FRP reinforced concrete deep beams

The results of the applied load versus the mid-point deflection of all the beams are presented next as observed in the experiments and the numerical simulations.

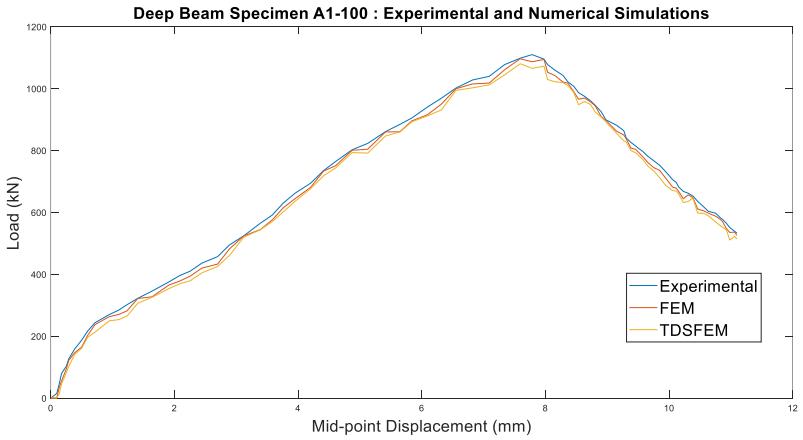

Figure 9: Load v/s mid-point deflection for A1-100

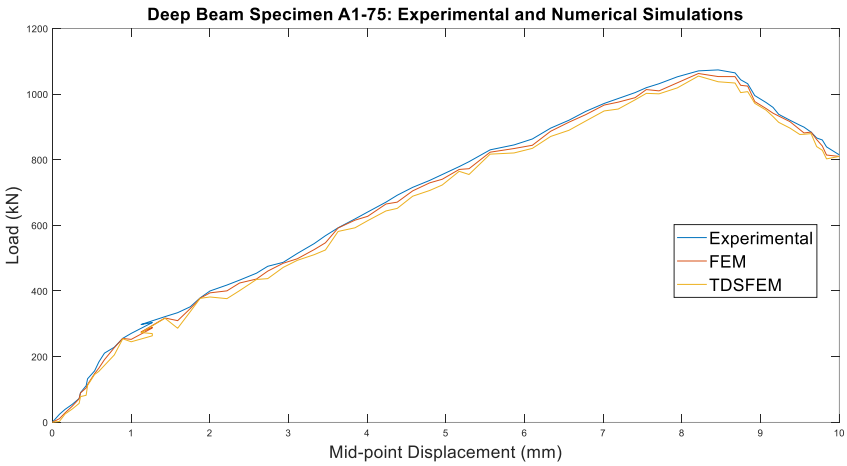

Figure 10: Load v/s mid-point deflection for A1-75

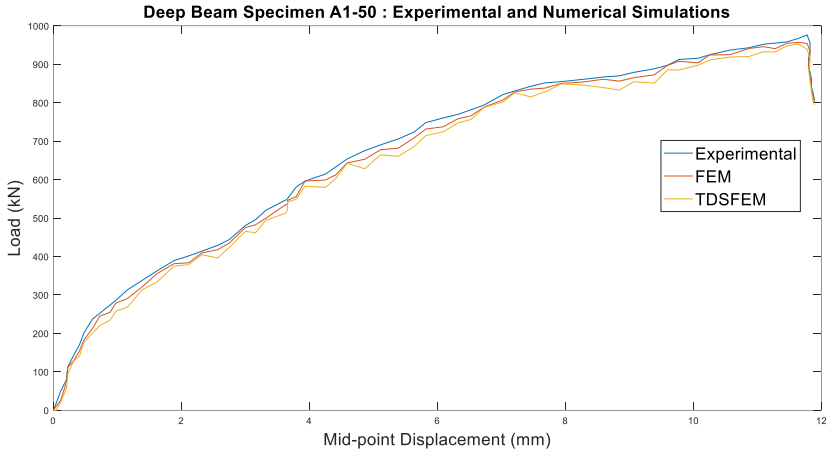

Figure 11: Load v/s mid-point deflection for A1-50

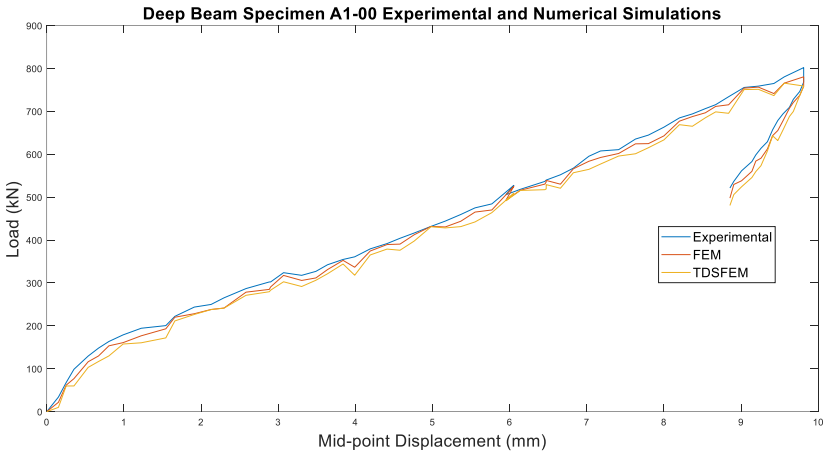

Figure 12: Load v/s mid-point deflection for A1-00

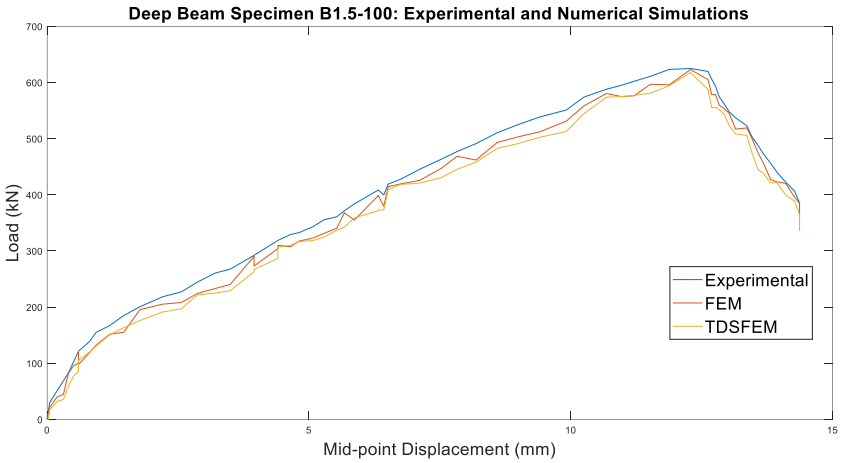

Figure 13: Load v/s mid-point deflection for B1.5-100

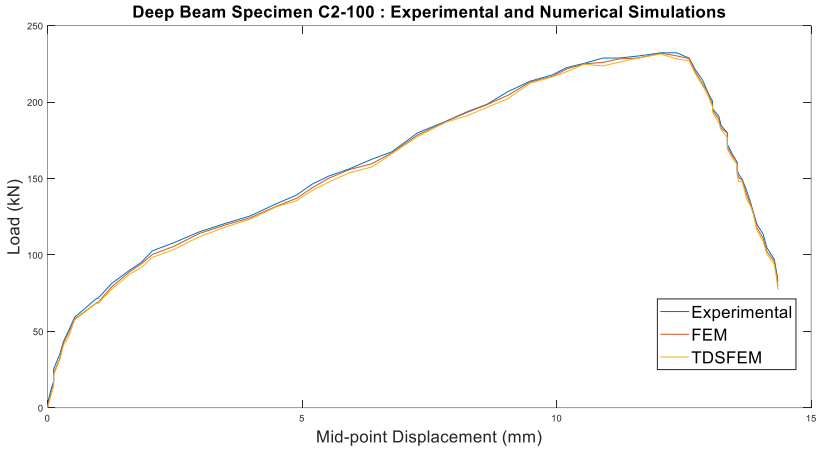

Figure 14: Load v/s mid-point deflection for C2-100

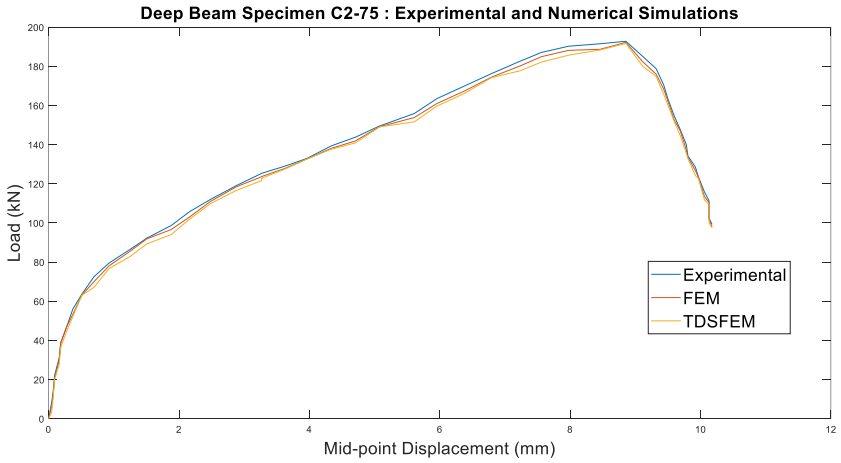

Figure 15: Load v/s mid-point deflection for C2-75

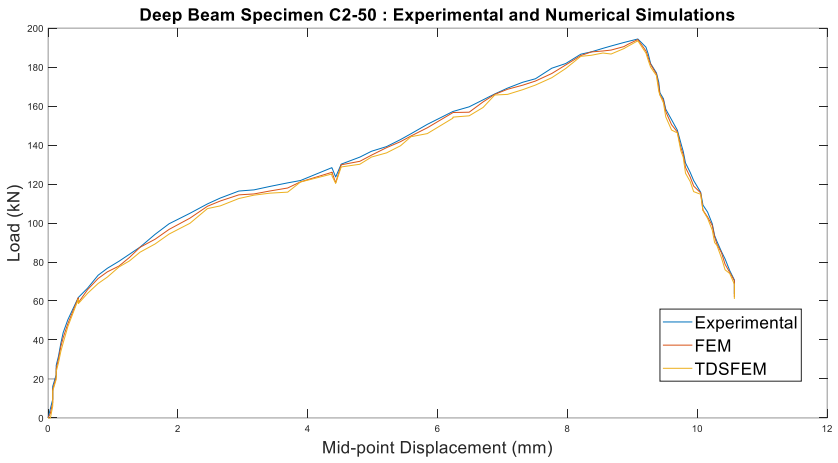

Figure 16: Load v/s mid-point deflection for C2-50

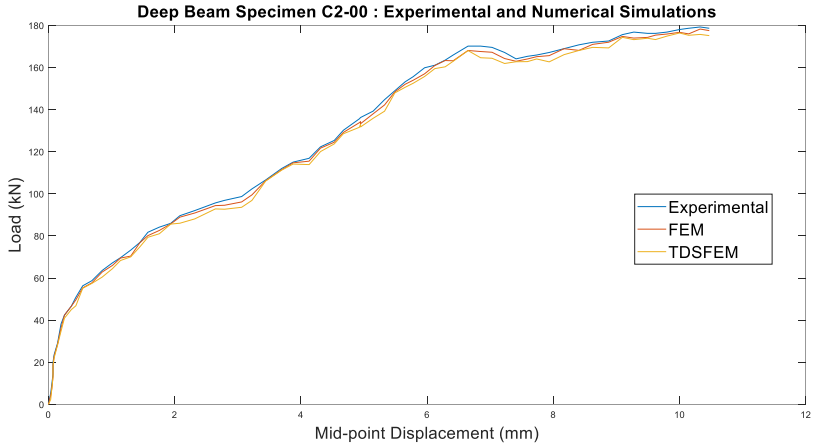

Figure 17: Load v/s mid-point deflection for C2-00

In all the above figures, it is observed that the results of numerical simulations using both FEM and TDSFEM match well with the experimental results. Next, a comparison of computation time is provided in Table 3 for the analysis performed using the FEM and TDSFEM programs. Though the general structure of both the developed algorithms are kept same, the significantly less computation time in case of TDSFEM can be attributed to the nature of the interpolating functions and the integration scheme employed in the procedure. Thus, the TDSFEM can be considered as a viable alternative to the conventional FEM in case of analysis of FRP reinforced concrete deep beams.

Table 5: Comparison of computation time

Specimen	Length (m)	Divisions along length	Depth (m)	Divisions along depth	Total elements	Total DOFs	Time consumed by FEM (s)	Time consumed by TDSFEM (s)
A1-100	1.8	60	0.675	20	1200	2562	4432	2792
A1-75	1.8	60	0.675	20	1200	2562	4391	2766
A1-50	1.8	60	0.675	20	1200	2562	4441	2798
A1-00	1.8	60	0.675	20	1200	2562	4438	2796
B1.5-100	1.8	60	0.5	16	960	2074	3588	2260
C2-100	1.8	60	0.375	12	720	1586	2792	1759
C2-75	1.8	60	0.375	12	720	1586	2813	1772
C2-50	1.8	60	0.375	12	720	1586	2744	1729
C2-00	1.8	60	0.375	12	720	1586	2798	1763

V. Failure modes of concrete deep beams

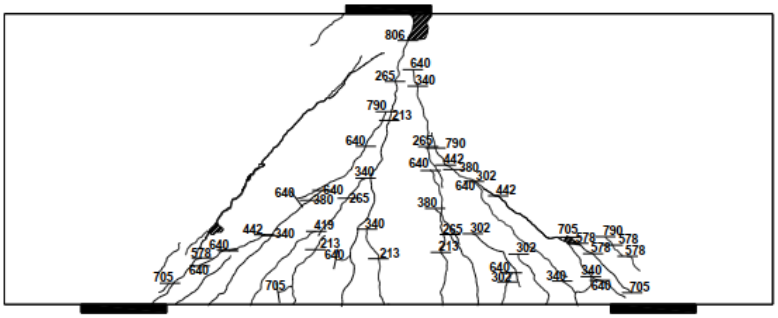

Figure 18: Experimental observed failure pattern of A1-00

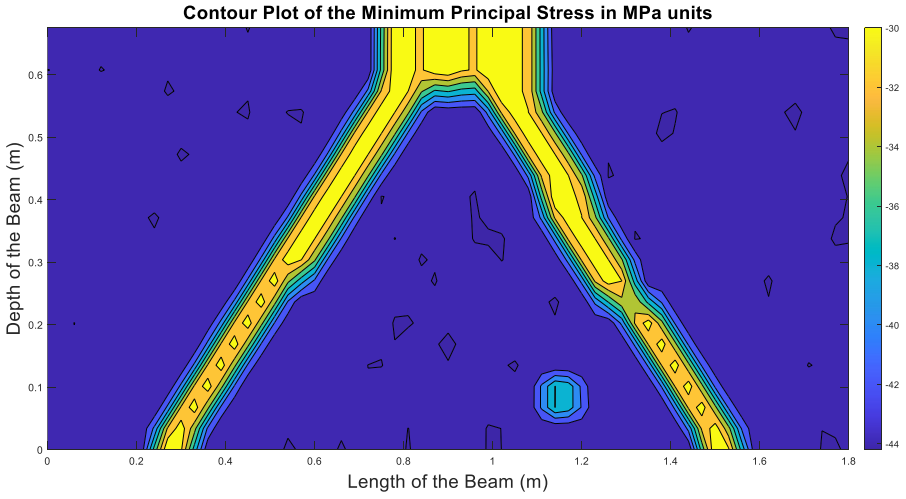

Figure 19: Minimum Principal Stress Contour of A1-00

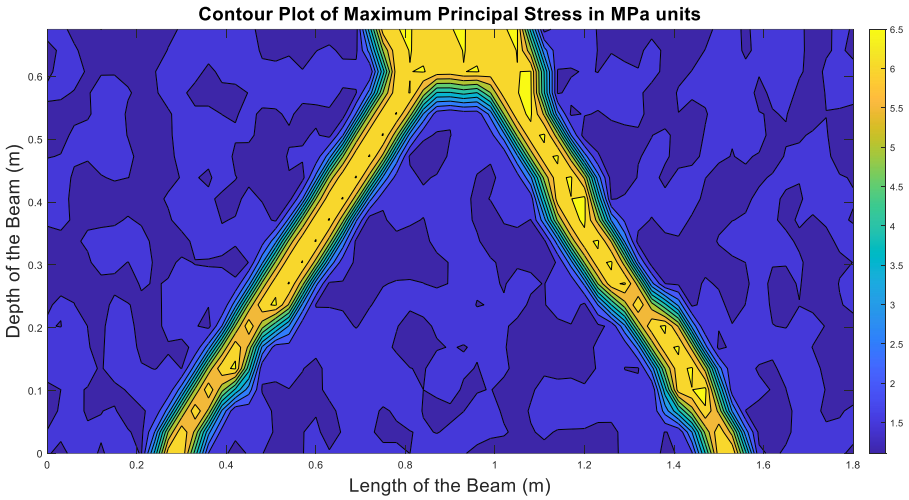

Figure 20: Maximum Principal Stress Contour of A1-00

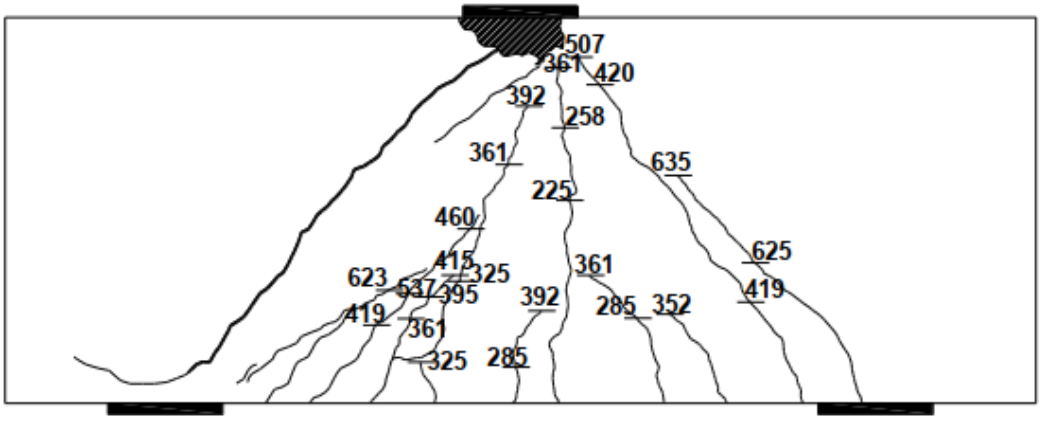

Figure 21: Experimental observed failure pattern of A1-50

Figure 22: Minimum Principal Stress Contour of A1-50

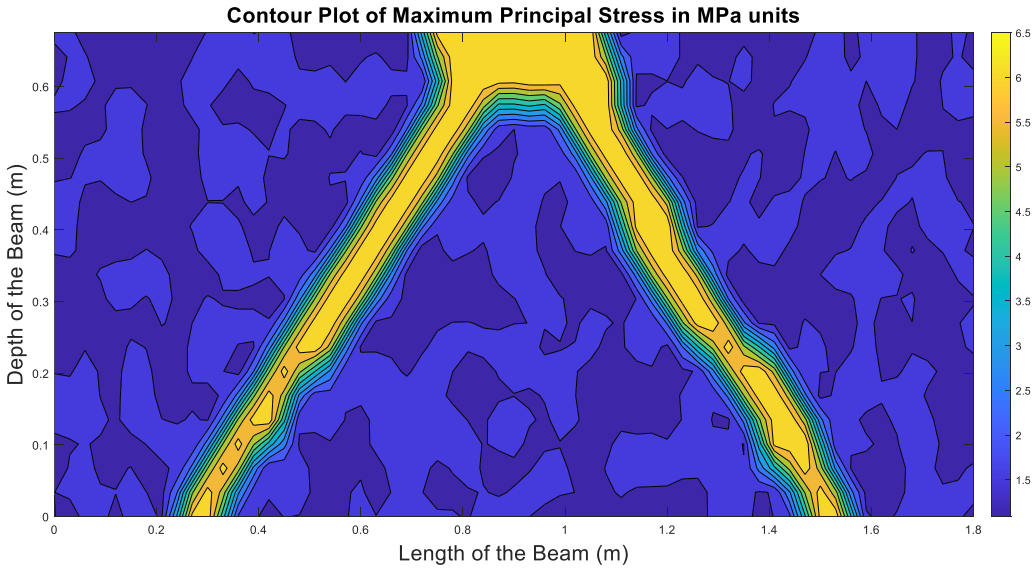

Figure 23: Maximum Principal Stress Contour of A1-50

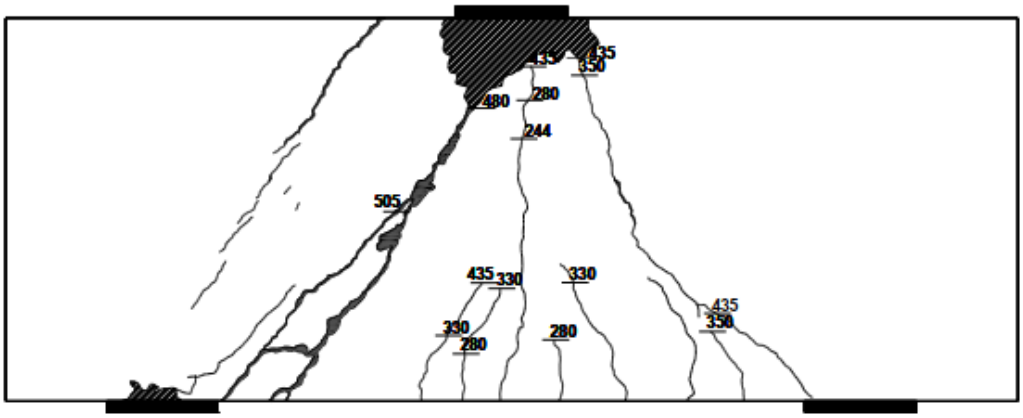

Figure 24: Experimental observed failure pattern of A1-75

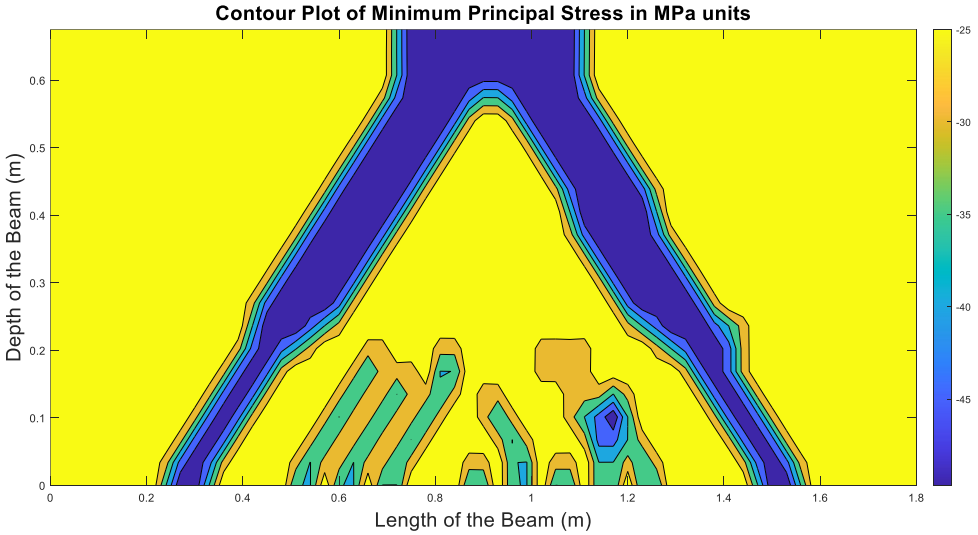

Figure 25: Minimum Principal Stress Contour of A1-75

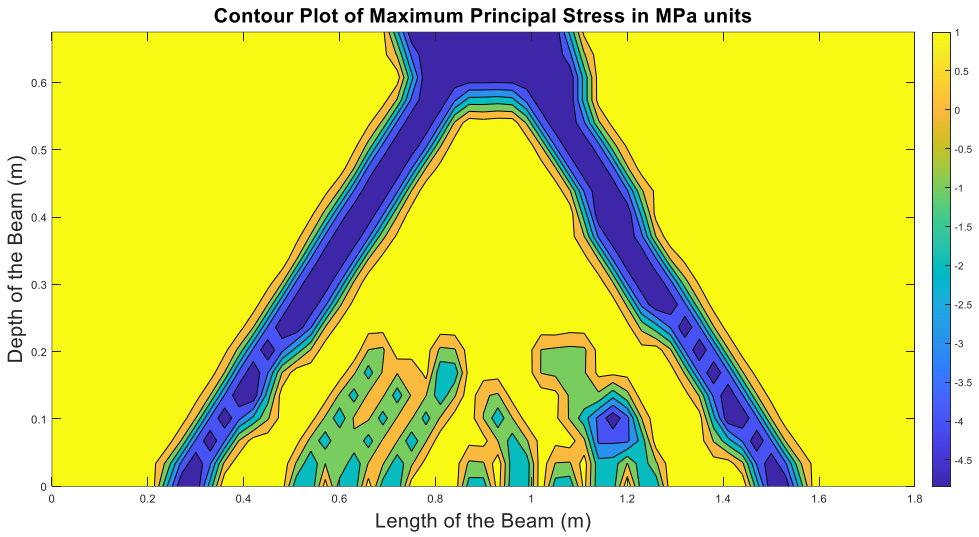

Figure 26: Maximum Principal Stress Contour of A1-75

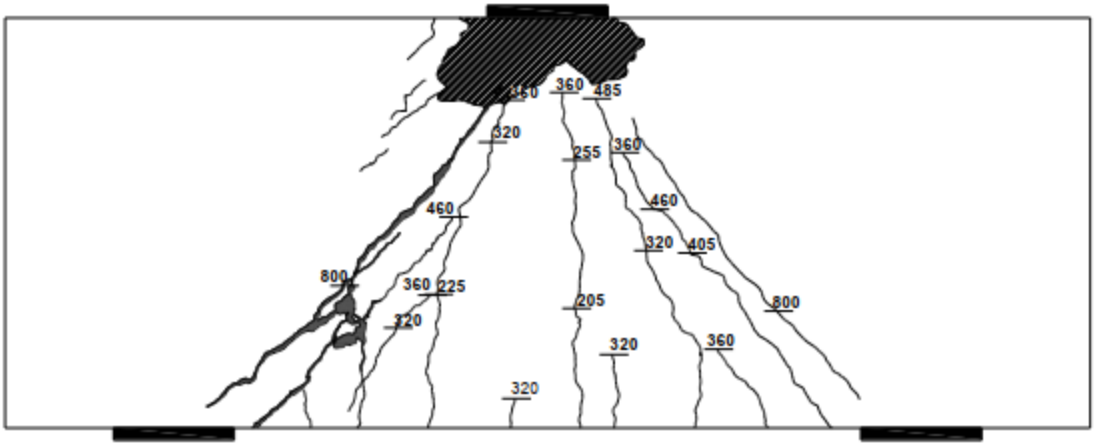

Figure 27: Experimental observed failure pattern of A1-100

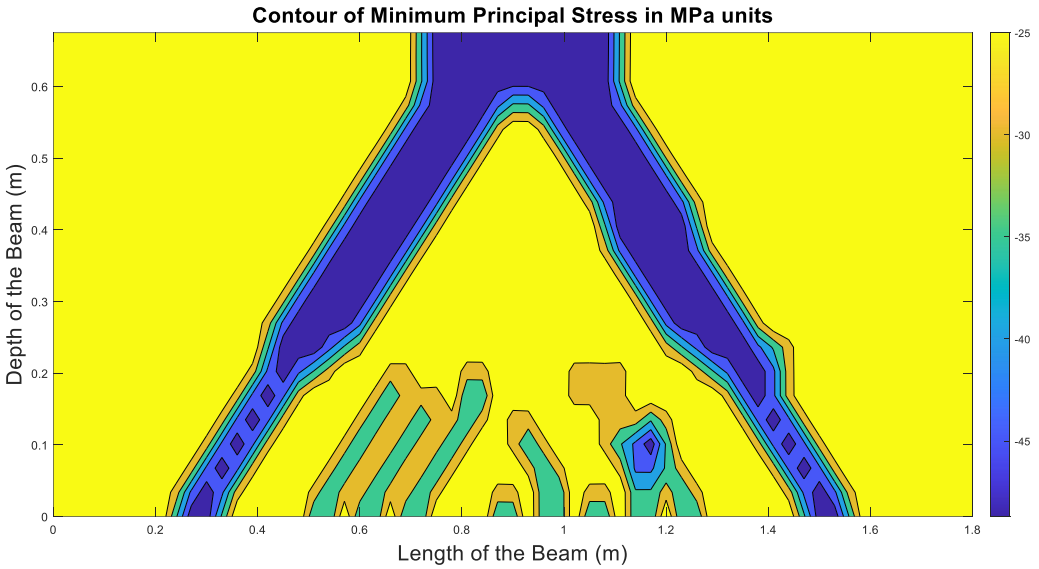

Figure 28: Minimum Principal Stress Contour of A1-100

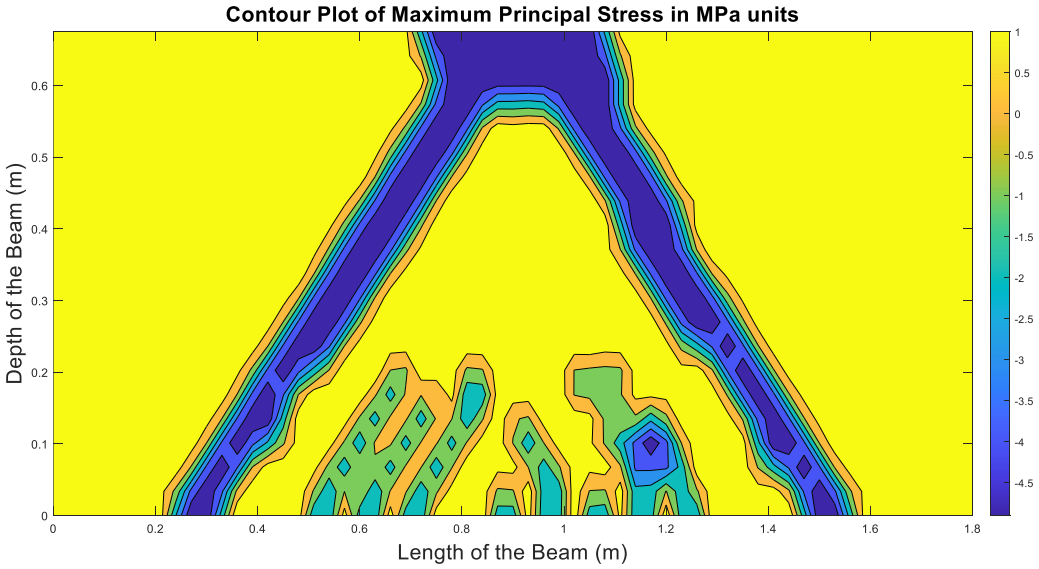

Figure 29: Maximum Principal Stress Contour of A1-100

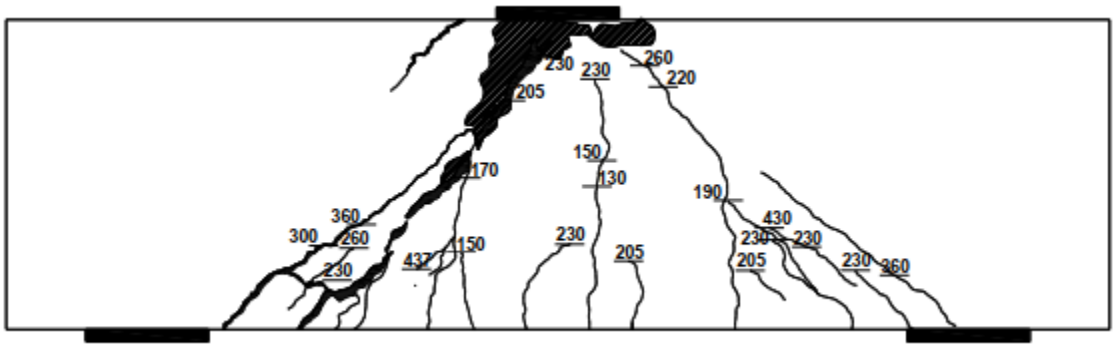

Figure 30: Experimental observed failure pattern of B1.5-100

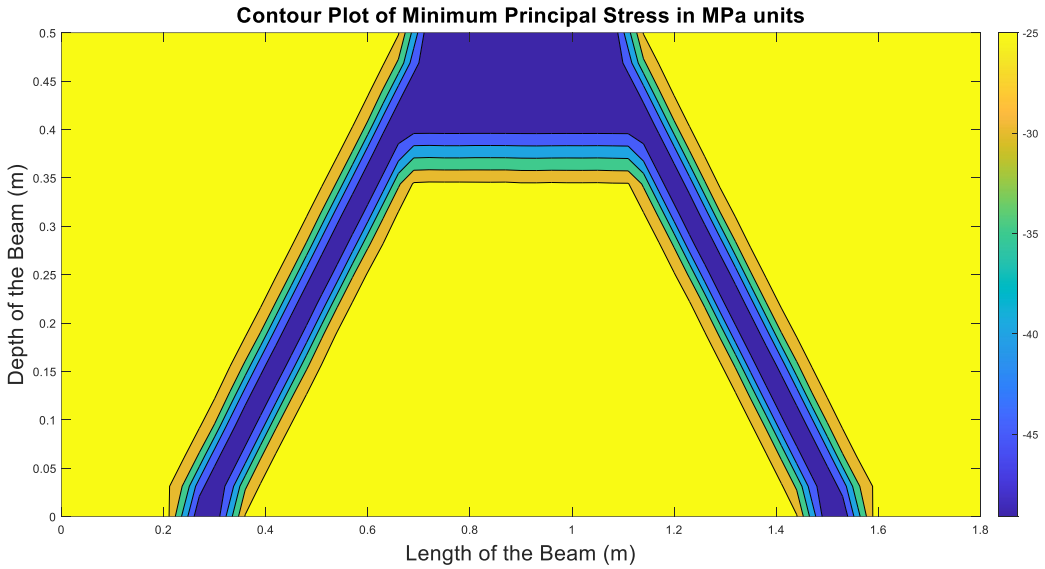

Figure 31: Minimum Principal Stress Contour of B1.5-100

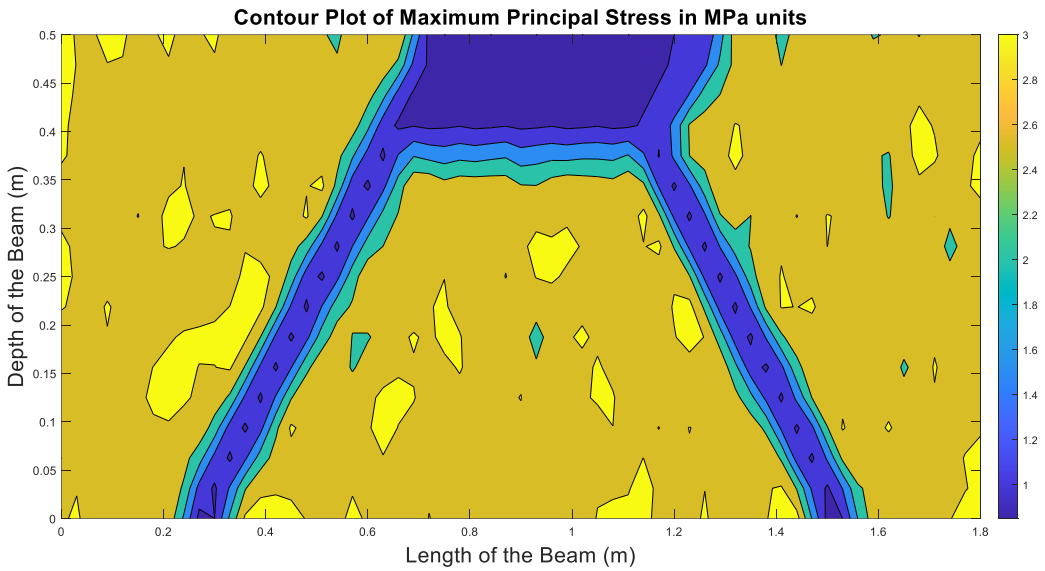

Figure 32: Maximum Principal Stress Contour of B1.5-100

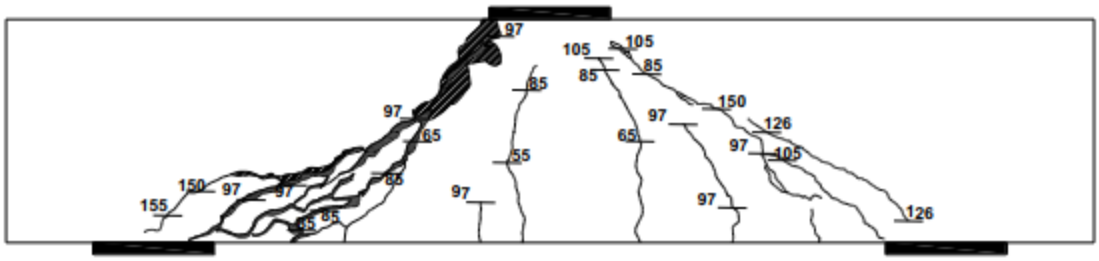

Figure 33: Experimental observed failure pattern of C2-00

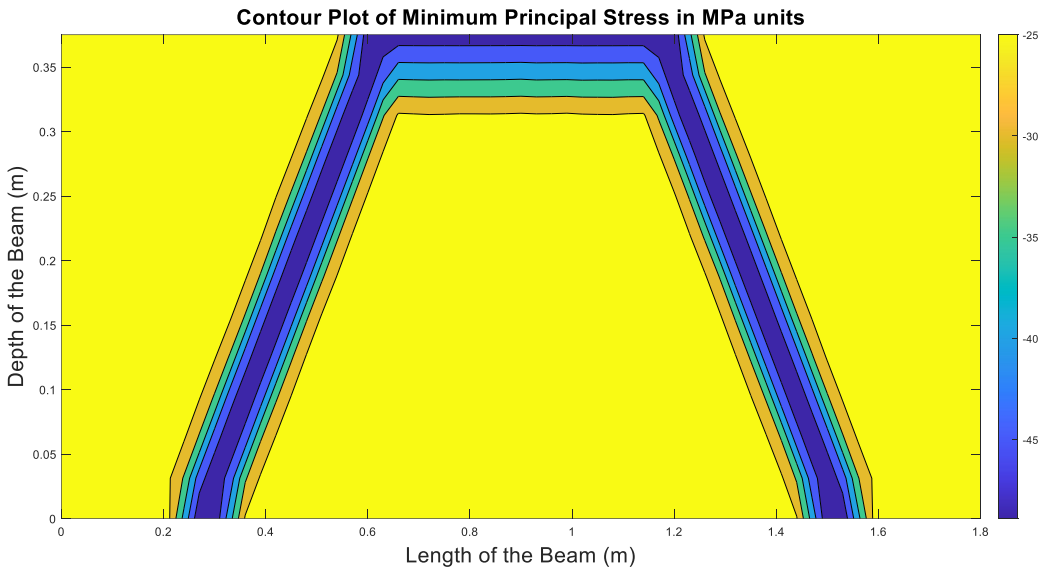

Figure 34: Minimum Principal Stress Contour of C2-00

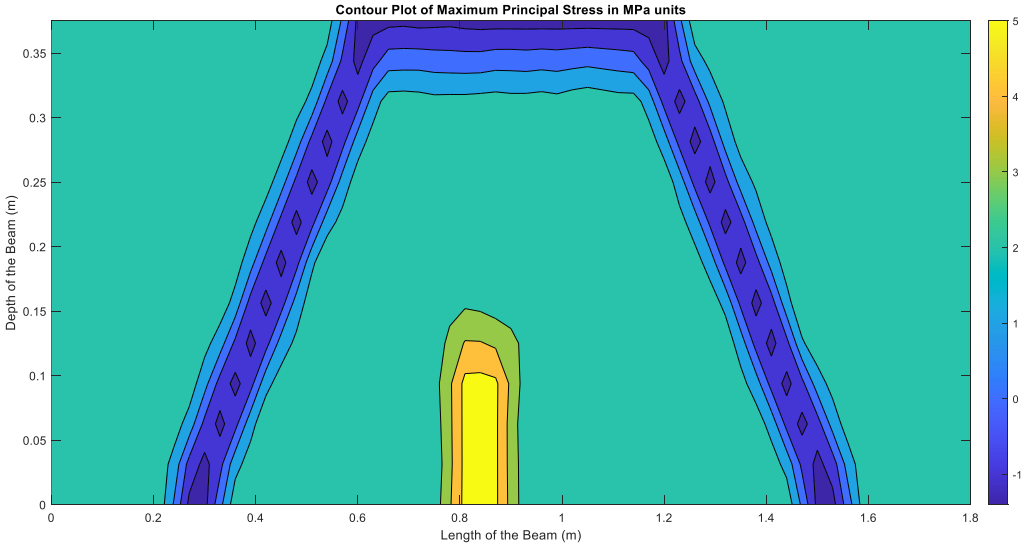

Figure 35: Maximum Principal Stress Contour of C2-00

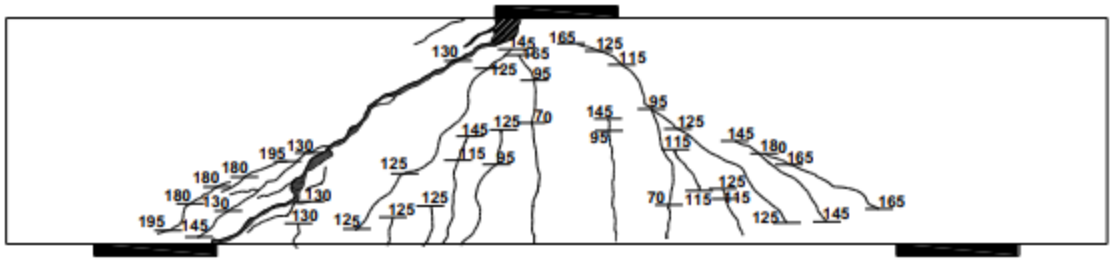

Figure 36: Experimental observed failure pattern of C2-50

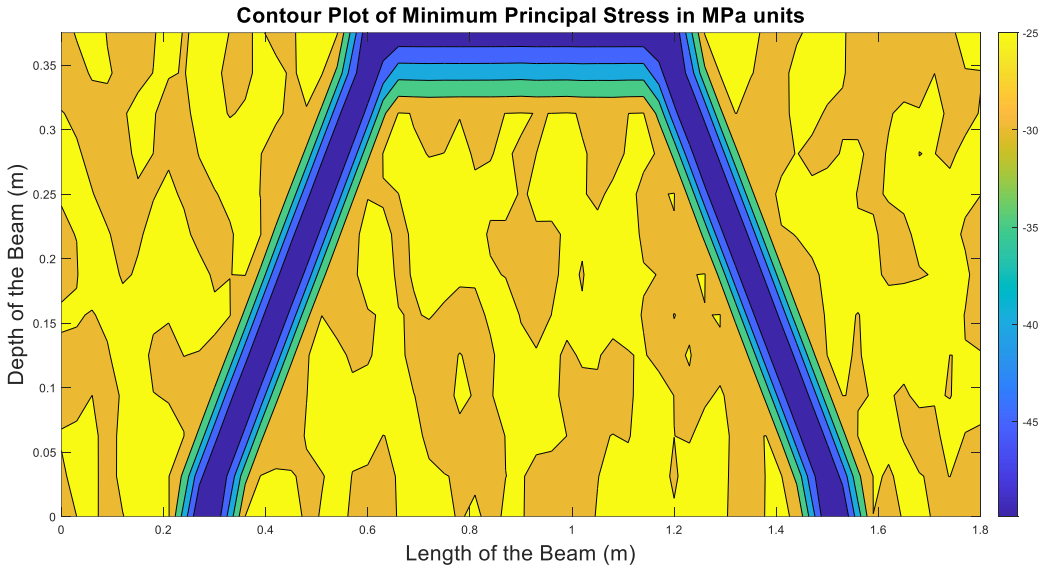

Figure 37: Minimum Principal Stress Contour of C2-50

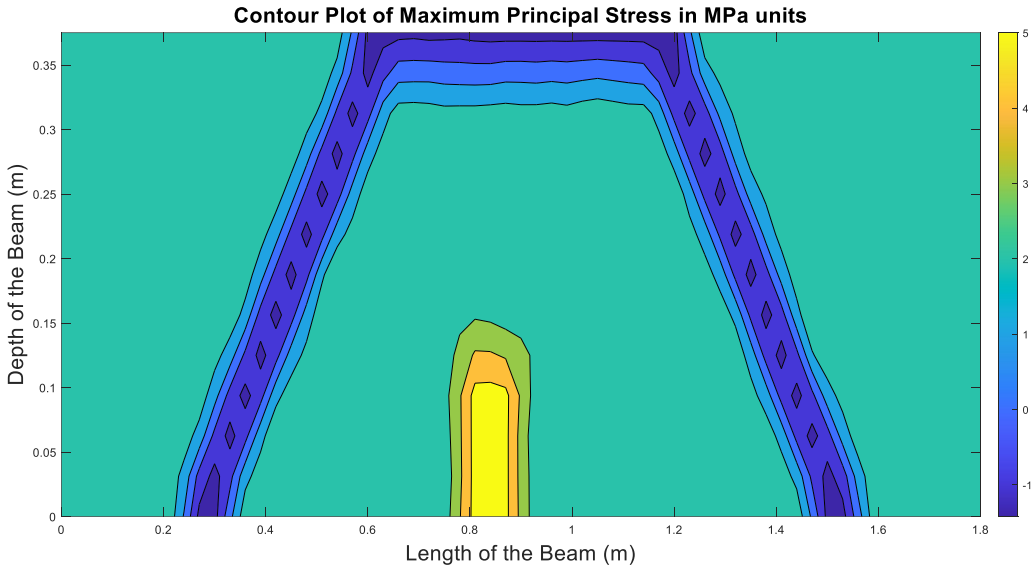

Figure 38: Maximum Principal Stress Contour of C2-50

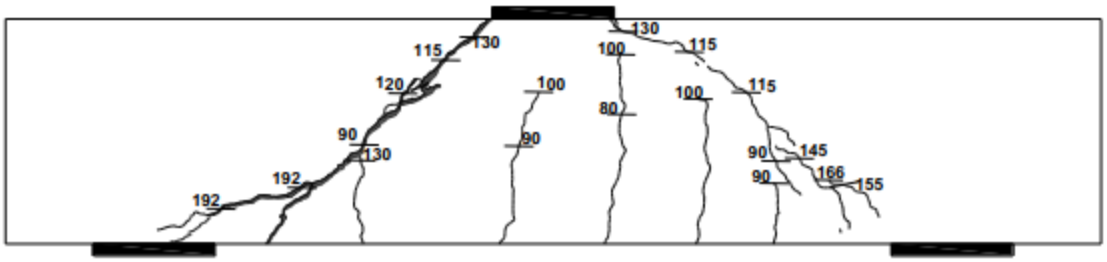

Figure 39: Experimental observed failure pattern of C2-75

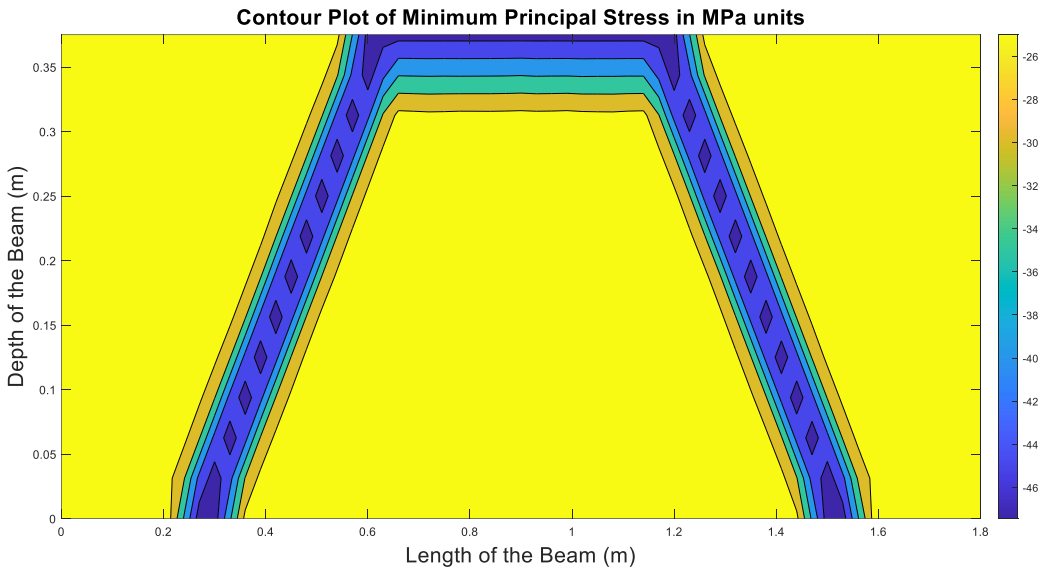

Figure 40: Minimum Principal Stress Contour of C2-75

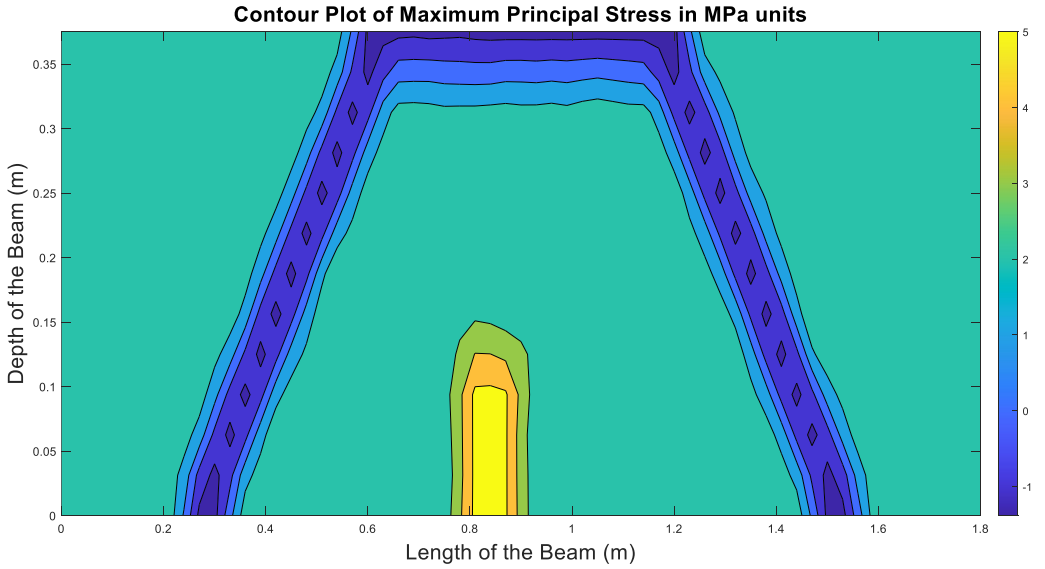

Figure 41: Maximum Principal Stress Contour of C2-75

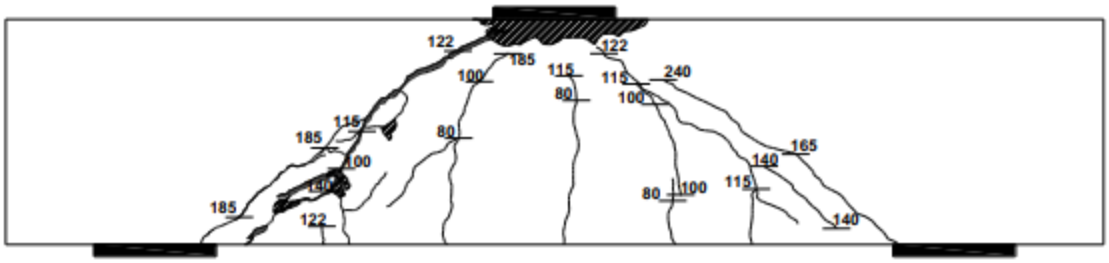

Figure 42: Experimental observed failure pattern of C2-100

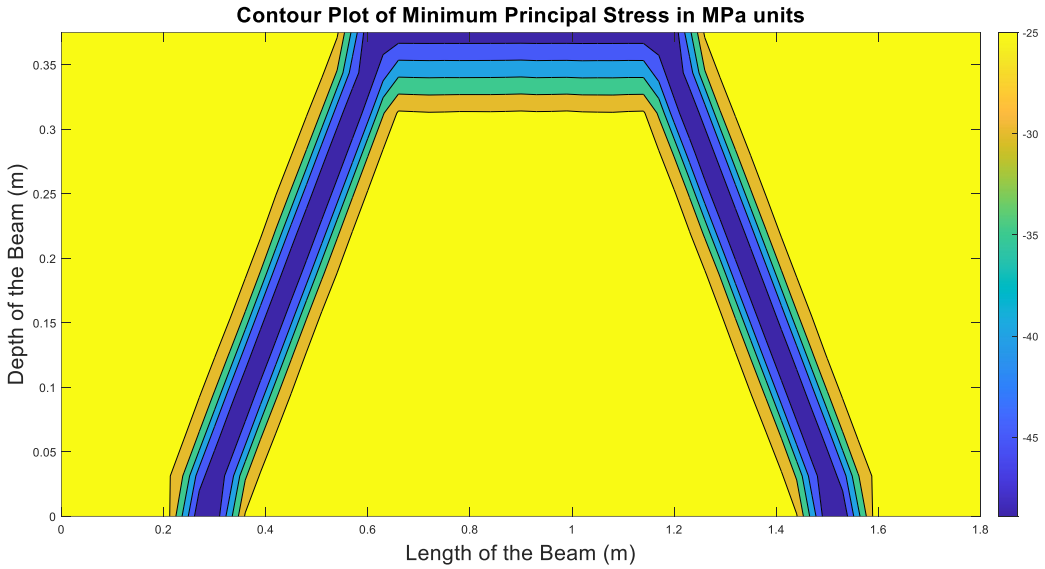

Figure 43: Minimum Principal Stress Contour of C2-100

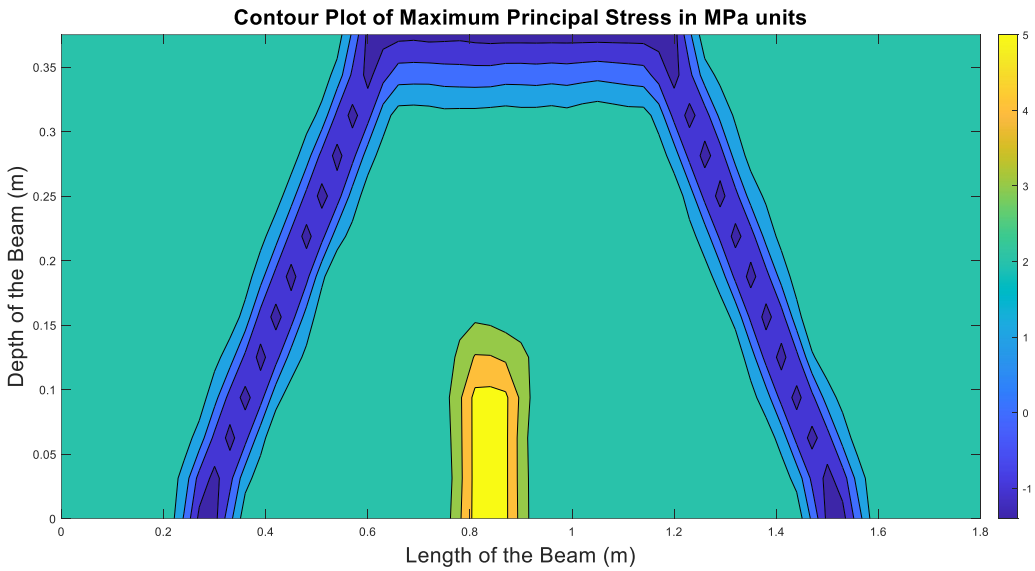

Figure 44: Maximum Principal Stress Contour of C2-100

Table 6: Summary of failure modes of all beams

Specimen	Failure Mode
A1-100	Shear Compression
A1-75	Shear Compression
A1-50	Diagonal Splitting
A1-00	Diagonal Splitting
B1.5-100	Shear Compression
C2-100	Shear Compression
C2-75	Strut Crushing
C2-50	Strut Crushing
C2-00	Strut Crushing

IV. Summary

This chapter presents a detailed verification study of the developed TDSFEM program for static and dynamic analysis. The chapter starts with solving the modal analysis of a simply supported beam and compares the results with the analytical solution and numerical values from available literature. It is observed that the results from the proposed method are comparable to the analytical and the other numerical solution. Further, modal analysis of the well-researched Pine Flat Dam is performed and again the values are comparable to the values available in published literature. This

establishes the linear dynamic analysis program developed in TDSFEM for use in further analysis in the thesis.

For validating the non-linear analysis program, pseudo-static pushover analysis of a set of concrete deep beams with varying geometric dimensions is performed. The results of load-deflection behavior of the beams are matched with the results of the experimental results for the same set of beams. The experiments were previously conducted by Latosh (2014) at the Structural Engineering Laboratory of Concordia University. The numerical analysis of the set of beams using FEM was also conducted by Latosh et al (2019). In this chapter, the numerical analysis results obtained by TDSFEM are validated against the experimental results given in Latosh et al (2019). The failure mechanism of the beams as seen in the numerical simulation results conducted by using TDSFEM in this section match with the experimental and numerical analysis results shown by Latosh (2014) and Latosh et al (2019). In this section, it is also demonstrated that the time of computation required for the TDFSEM programs is less than the similar FEM programs, thus emphasizing the numerical efficiency of TDSFEM with reasonable accuracy.

CHAPTER 5: MODAL AND LINEAR DYNAMIC SEISMIC ANALYSIS OF CONCRETE GRAVITY DAMS USING TDSFEM

I. Introduction

Concrete gravity dams being large structures, application of a computationally efficient analysis procedure has the potential to save considerable amount of computational time and cost. Koyna dam has been considered here as a case study as it is a well-studied dam, particularly for dynamic analysis studies (Chopra and Chakrabarti (1973), Bagchi et al. (2019), Sooch and Bagchi (2012, 2014); Sarkar et al. (2022)) and is also presented in the ABAQUS manual as an example of seismic analysis of concrete gravity dam. Thus, Koyna dam is considered here as a benchmark problem. It has been considered in this paper for modal analysis and time history analysis of concrete gravity dams. The geometry of the dam is shown in Figure 45a. Different meshing scenarios were tried, a typical meshing with 45 elements is shown in Figure 45b. Similar meshing has been done with 190 and 760 elements till convergence is reached.

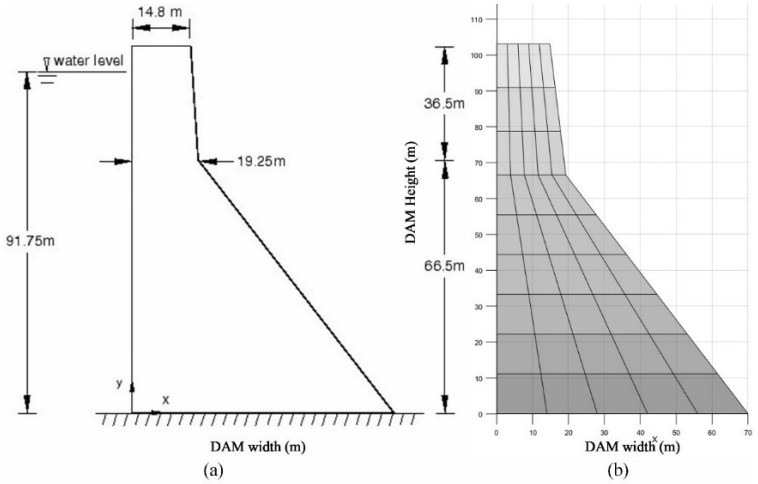

Figure 45: (a) Geometry details of Koyna Dam (ABAQUS Manual), (b) A typical meshing of the dam geometry with 45 elements

It should be noted that while simpler meshes have been used here to model the dam to demonstrate the advantage of the TDSFEM and proposed formulation of the dam-foundation system for modal and dynamic time history analyses, in practice, the meshes could be much finer, leading to large number of degrees of freedom. In such cases, the computational gain with TDSFEM will be quite advantageous, especially when a repetitive analysis is needed with an ensemble of ground motions.

The Young's Modulus for the dam body is considered 31,027 MPa, Poisson's ratio as 0.15 and density as 2,643 kg/m3. Four-noded iso-parametric quadrilateral elements have been considered for modeling the dam. The values of the first four modal frequencies calculated by the developed conventional FEM and TDSFEM are comparable to the values presented in the ABAQUS manual and by Chopra and Chakrabarti (1973). However, the most notable observation is that the time taken by the program for the modal analysis using the TDSFEM is about 40 percent of the time taken by the conventional FEM program. The mode shapes obtained are plotted with undeformed shape in Figure 46.

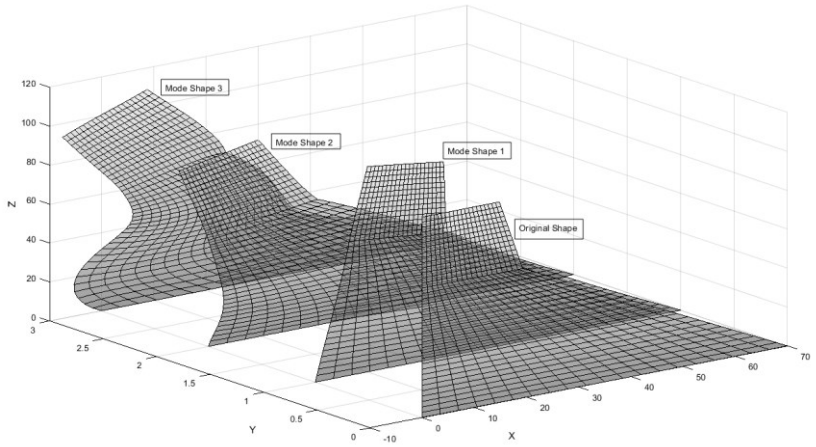

Figure 46: Undeformed shape along with 1st three mode shapes of the dam (760 elements)

While the application of TDSFEM for 2D planar structures for dynamic time history analysis is not reported earlier, it is expected that TDSFEM will be computationally efficient in such cases as well. Therefore, after the modal analysis of the dam, the response history or dynamic time history analysis has been performed using the recorded horizontal and vertical ground motions at the location. The details of the ground motion records were obtained from ABAQUS manual (shown in Figure 47a). Figure 47b shows the response spectra plot for the ground accelerations. The magnitude of the earthquake was 6.7 (1967) on the Richter scale.

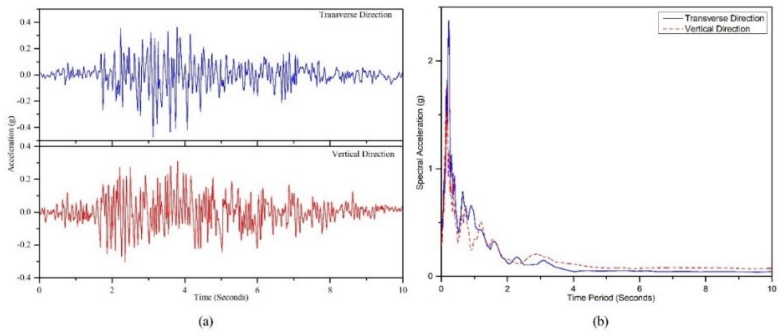

Figure 47: Koyna Earthquake: transverse and vertical ground accelerations a) Acceleration time history b) Response spectrum (ABAQUS manual)

Additionally, two more seismic ground motion records consistent with the seismicity at Koyna have been considered for the time history analysis of the structure in order to account for the variation in frequency content and duration of ground motion records on the behavior of the structure. In the case of both these additional ground motion records, both FEM and TDSFEM have been used to compare the response calculation of these methods. These seismic ground motion records have the ratio of peak ground acceleration to peak ground velocity close to 2, which is similar to the same ratio for the recorded seismic ground motion at Koyna. The details of these seismic records have been provided in Table 3. It is to be noted here for both these ground motion records; transverse and vertical accelerations have been considered simultaneously in the time history analysis of the structure just like the case for Koyna ground motion.

Table 7: Details of additional seismic ground motion records

Earthquake Abbreviation	Earthquake Name	Date	Station	Magnitude	PGA (g)	PGV (m/s)	a/v ratio
EQ-NR	Northridge-01	01/17/1994	Anacapa Island	6.7	0.067	0.032	2.09
EQ-SF	San Fernando	02/09/1971	Castaic - Old Ridge Route	6.6	0.32	0.17	1.88

Newmark's method is used in solving the displacement time history of the dam. Damping is considered to be Rayleigh's stiffness proportional damping and for that the β value is considered as 0.00323 corresponding to critical damping ratio of 0.03 and first modal frequency value as 18.61

rad/s. The horizontal displacement history of the dam crest relative to the ground is shown in Figure 48.

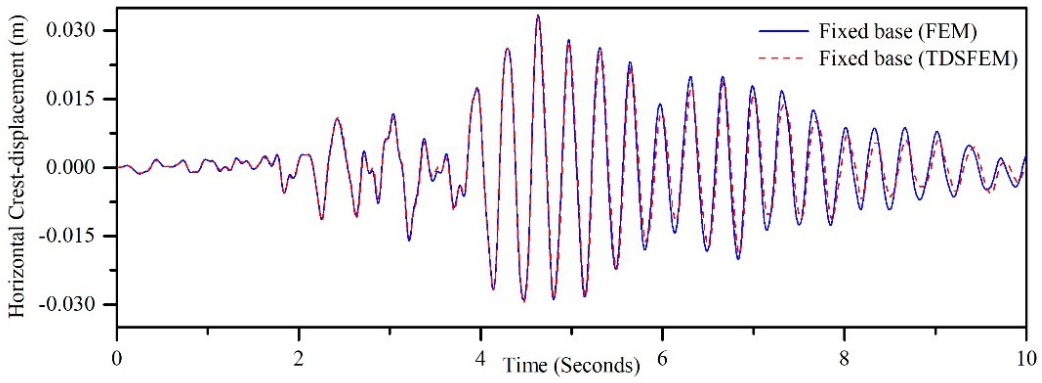

Figure 48: Horizontal Displacement time history of dam crest due to Koyna earthquake: FEM and SFEM comparison (dam only without reservoir, maximum displacement=34mm)

In the time history analysis procedure, time taken by the time domain based spectral finite element program is 690 seconds (approx. 12 mins) while the time taken in the finite element program is 1575 seconds (approx. 27 mins). Thus, like modal analysis, the spectral FEM program consumes much less time (about 40 percent) than that consumed by conventional FEM program in case of time history analysis as well. Sensitivity analysis is carried out in the following section to compare the efficiency of the two methods.

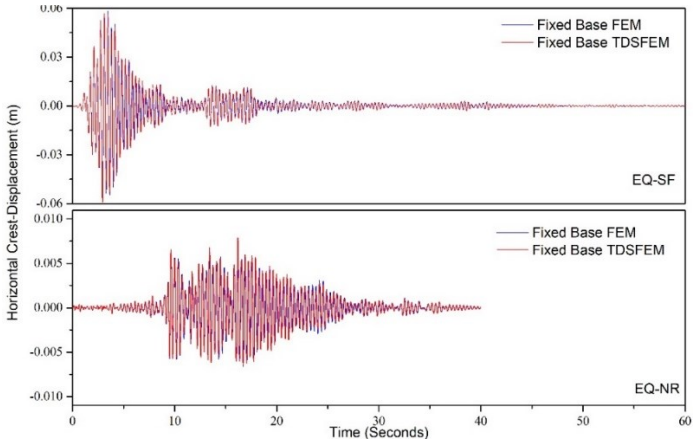

Figure 49: Horizontal Displacement time history of dam crest (fixed base): FEM and SFEM comparison for the ground motions given in Table 3

Figure 49 presents the displacement response history of the dam crest for the additional ground motion records detailed in Table 3. From the ground motion time history analysis, it could be observed that FEM and TDSFEM produce similar results. While one record is of 60 seconds

duration, the other one is of 40 seconds duration as can be seen in Figure 49. Thus, for the three records of different duration and frequency content, FEM and TDSFEM produce similar results and the accuracy of TDSFEM in case of these ground motion parameter variations is also satisfactory. For all further analysis results presented here, only the Koyna earthquake is considered to limit the length of the article. While the results presented in Figures 48 and 49 are generated for the fixed-base condition without the effect of reservoir and the foundation, further analysis is performed considering dam-reservoir, and dam-foundation-reservoir systems.

Effect of reservoir: The dynamic pressure exerted by the reservoir on the upstream face of the dam is modeled by considering added mass technique as proposed by Westergaard (1933). Westergaard proposed that the hydrodynamic pressure exerted by the water on the dam during an earthquake has an effect like the case if a certain mass of water moves back and forth with the dam while the remainder of the reservoir does not interact with the dam. The calculation of added mass at height y, per unit area is given by the equation below.

$$addedmass(y) = (7/8) * \rho_w * \sqrt{h_w * (h_w - y)}; y < h_w, where, \rho_w = 1000 kg/m^3 \quad (36)$$

Modal analysis and time history analysis have been performed considering the effect of reservoir using the added mass technique. The values of the first three modal frequencies considering the reservoir are obtained as 16.95 rad/s, 48.71 rad/s and 58.51 rad/s. The time of computation for TDSFEM is around 40 percent of that in FEM. In the time history analysis, the observed maximum displacement is 39 mm (as shown in Figure 50), which is around 15 percent more than that obtained in time history analysis without considering the effect of reservoir.

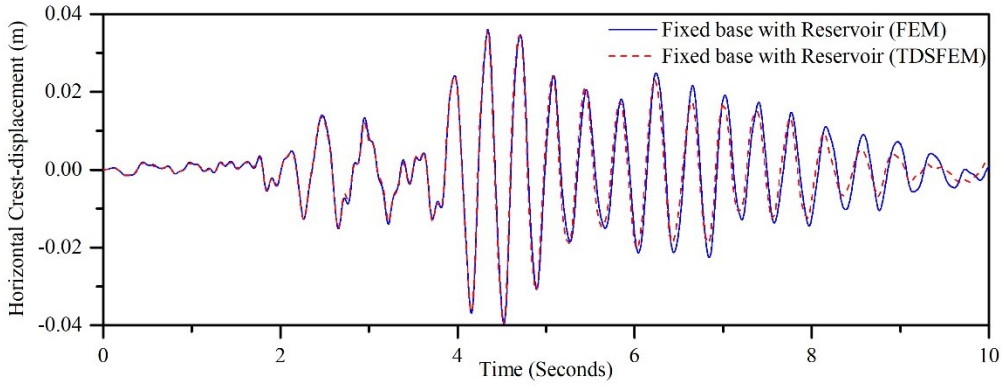

Figure 50: Displacement time history of dam crest due to Koyna earthquake (with reservoir, maximum displacement=39mm)

II. Sensitivity Analysis and Convergence Study

In this section, a sensitivity analysis has been performed by varying the number of elements in the models constructed using conventional FEM and TDSFEM to achieve the convergence of the response parameters such as, the modal frequencies and the maximum horizontal crest displacement of the structure, to the corresponding benchmark values. The computational time taken for each model has also been recorded and compared. Tables 3 to 7 show the convergence of the first three natural frequencies of the considered concrete gravity dam with the changing number of elements and the corresponding time of computation, for both FEM and TDSFEM models. As a TDSFEM model produces a diagonal mass matrix, for the comparison of FEM and TDSFEM, both consistent and lumped mass matrices have been considered for FEM. It needs to be pointed out here that the structure of the developed codes for conventional FEM and TDSFEM are essentially the same. However, the order of computation in conventional FEM is larger with respect to TDSFEM for the same size of a problem considered. This is due to the locations of the Gauss integration points in each element. The integration points in conventional FEM (2-point Gauss quadrature points) are at locations corresponding to the irrational numbers $-1/\sqrt{3}$ and $1/\sqrt{3}$ which lead to an additional step (square root) in computation of the stiffness matrix. This increases the order of computation in conventional FEM, which is not necessary for the TDSFEM elements as the integration point coincides with the nodes. To evaluate the impact of the square root function in the time for computation, simplified values of $1/\sqrt{3}$ has been used in the integration scheme for conventional FEM, in which case, the value of $1/\sqrt{3}$ is replaced by its approximate decimal values, making the order of computation similar to TDSFEM. Comparisons of modal frequency calculations by the number of elements and computation time has been performed amongst four different models, including, conventional FEM with consistent mass matrix, conventional FEM with diagonal mass matrix, conventional FEM with diagonal mass matrix and Gauss integration points simplified as decimal numbers and TDSFEM. The results are demonstrated in Tables 4 to 8 and Figures 51 and 52.

Table 8: SFEM and FEM Comparison for 45 elements

SFEM and FEM Comparison for 45 elements					
	ABAQUS (Benchmark)	FEM-Consistent Mass Matrix	FEM-Diagonal Mass Matrix	FEM-Diagonal Mass Matrix-Simplified Gauss Points	SFEM
No. of elements		45	45	45	45
Time of computation (s)		79	71	46	30
1st Frequency (rad/s)	18.86	20.17	20.87	21.41	21.25
2nd Frequency (rad/s)	49.97	52.56	53.27	53.96	53.55
3rd Frequency (rad/s)	68.16	70.06	70.2	70.81	70.23

Table 9: SFEM and FEM Comparison for 190 elements

SFEM and FEM Comparison for 190 elements					
	ABAQUS (Benchmark)	FEM-Consistent Mass Matrix	FEM-Diagonal Mass Matrix	FEM-Diagonal Mass Matrix-Simplified Gauss Points	SFEM
No. of elements		190	190	190	190
Time of computation (s)		336	296	190	117
1st Frequency (rad/s)	18.86	19.63	19.92	20.26	20.13
2nd Frequency (rad/s)	49.97	51.85	52.01	52.48	52.11
3rd Frequency (rad/s)	68.16	69.81	69.89	70.39	69.95

It is observed from Tables 4-8 that for a fixed value of element number, TDSFEM program needs much less computation time than that for conventional FEM (consistent mass matrix) program. However, when FEM with diagonal mass matrix is used, the time taken by conventional FEM gets reduced. The use of FEM with diagonal mass matrix and with Gauss points considered as approximate decimal numbers reduces the computation time in FEM even further. However, diagonalization of the mass matrix in the FEM models lead to a loss of accuracy to some extent with respect to FEM models with consistent mass matrix as shown in the values of frequencies in

Tables 4 to 8. Figure 51 shows the plot of convergence of 1st frequency over number of elements for TDSFEM and various FEM models considered here. It is noticed from the plot that conventional FEM with consistent mass matrix is closest to the ABAQUS benchmark values for a given number of elements. The two FEM cases with diagonal mass matrix (with same values, thus overlapped lines in Figure 51) produce the frequency values between those from FEM with consistent mass matrix and SFEM.

Table 10: SFEM and FEM Comparison for 405 elements

SFEM and FEM Comparison for 405 elements					
	ABAQUS (Benchmark)	FEM-Consistent Mass Matrix	FEM-Diagonal Mass Matrix	FEM-Diagonal Mass Matrix-Simplified Gauss Points	SFEM
No. of elements		405	405	405	405
Time of computation (s)		730	641	406	255
1st Frequency (rad/s)	18.86	19.11	19.29	19.43	19.36
2nd Frequency (rad/s)	49.97	50.72	51.21	51.76	51.55
3rd Frequency (rad/s)	68.16	68.94	69.06	69.41	69.13

Table 11: SFEM and FEM Comparison for 760 elements

SFEM and FEM Comparison for 760 elements					
	ABAQUS (Benchmark)	FEM-Consistent Mass Matrix	FEM-Diagonal Mass Matrix	FEM-Diagonal Mass Matrix-Simplified Gauss Points	SFEM
No. of elements		760	760	760	760
Time of computation (s)		1492	1287	908	616
1st Frequency (rad/s)	18.86	18.94	19.01	19.12	19.04
2nd Frequency (rad/s)	49.97	50.12	50.86	51.38	51.21
3rd Frequency (rad/s)	68.16	68.61	68.77	69.12	68.87

Table 12: SFEM and FEM Comparison for 1125 elements

SFEM and FEM Comparison for 1125 elements					
	ABAQUS (Benchmark)	FEM-Consistent Mass Matrix	FEM-Diagonal Mass Matrix	FEM-Diagonal Mass Matrix-Simplified Gauss Points	SFEM
No. of elements		1125	1125	1125	1125
Time of computation (s)		2498	2036	1352	940
1st Frequency (rad/s)	18.86	18.89	18.92	18.98	18.93
2nd Frequency (rad/s)	49.97	50.05	50.74	51.25	51.14
3rd Frequency (rad/s)	68.16	68.52	68.76	68.98	68.81

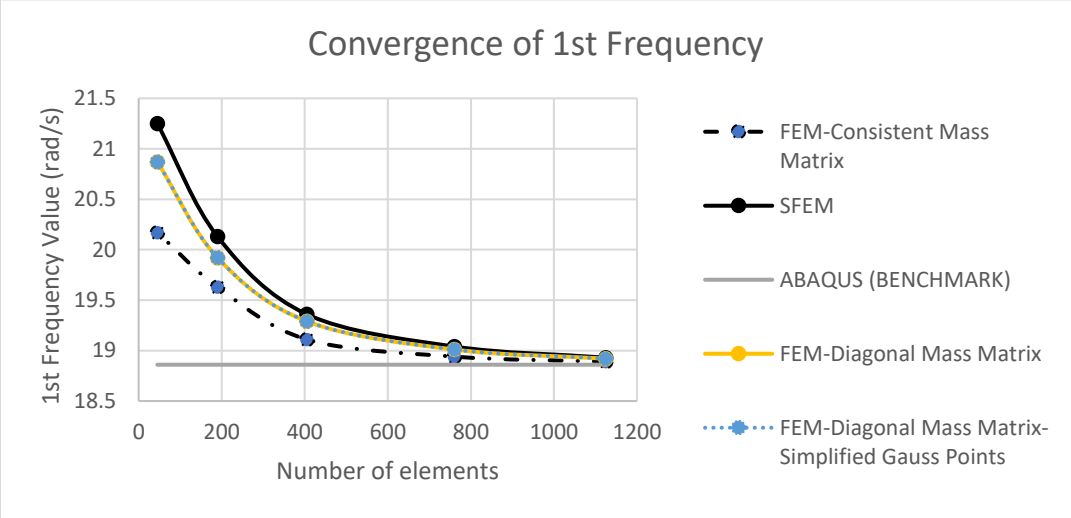

Figure 51: Convergence of 1st frequency

A plot of the time taken by the SFEM and FEM (consistent mass matrix, diagonal mass matrix, diagonal mass matrix with gauss points converted to decimal numbers) programs to converge is shown in Figure 52 for the 1st natural frequency. It is observed that the FEM with consistent mass matrix requires the maximum computation time, followed by FEM with diagonal mass matrix and Gauss points at irrational coordinate, while FEM with diagonal mass matrix and simplified Gauss points requires considerably less computation time. SFEM consumes the least amount of computation time.

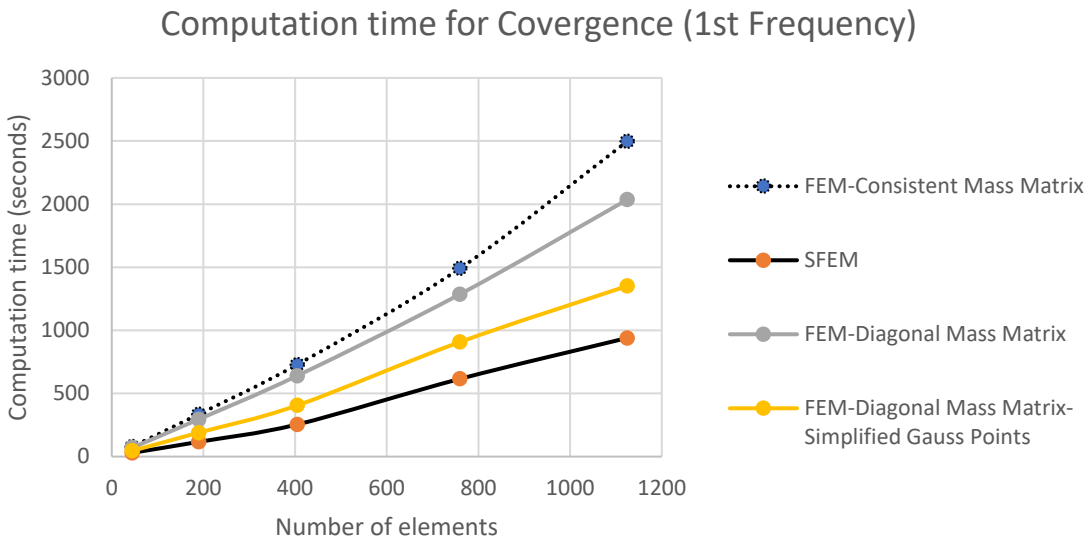

Figure 52: Computation time for modal analysis

It is observed from Figure 52 that the computational time for TDSFEM model is considerably lower than the three FEM models. This is attributed to the facts that the order of complexity of computation O(n) in TDSFEM is lower than conventional FEM with consistent mass matrix due to the additional square root function computation in the latter and also diagonalization of the mass matrix in SFEM. When the diagonal mass matrix is considered in FEM, the computation time gets reduced with respect to FEM with consistent mass matrix, however, the computational complexity and thus order of computation is still higher due to the calculation of the square root function. Finally, the use of diagonal mass matrix along with Gauss points reduced to approximate decimal values for the Gauss points reduces the computation time in conventional FEM to a great extent, but it is still higher than SFEM. This can be attributed to the fact that the shape function matrix and the strain matrix (i.e., B matrix) in case of SFEM contains a lot of zeroes due to the fact that the shape functions and the integration points are orthogonal to each other in the GLL integration technique used in SFEM.

Table 13: SFEM and FEM Comparison for Horizontal Crest Displacement

No. of elements	FEM-Consistent Mass Matrix		FEM-Diagonal Mass Matrix		FEM-Diagonal Mass Matrix-Simplified Gauss Points		SFEM	
	Crest Displacement (mm)	Time of Computation (seconds)	Crest Displacement (mm)	Time of Computation (seconds)	Crest Displacement (mm)	Time of Computation (seconds)	Crest Displacement (mm)	Time of Computation (seconds)
45	32.7	81	31.4	74	31.4	50	30.6	31
190	33.3	340	33	301	33	193	31.9	123
405	33.8	753	33.7	660	33.7	421	33.4	264
760	34.3	1575	34.2	1360	34.2	983	34.1	690
1125	34.4	2607	34.3	2143	34.3	1448	34.2	1037

Similar results are produced for time history analysis. The parameter chosen for the sensitivity analysis using time history analysis is the maximum horizontal crest displacement. Table 9 presents the results of convergence of horizontal crest displacement and the corresponding time of computation and number of elements for the four cases- FEM with consistent mass matrix, FEM with diagonal mass matrix, FEM with diagonal mass matrix and Gauss points considered as decimals and time domain SFEM. The results are also shown graphically in Figures 53 (the two FEM cases with diagonal mass matrix produce same results, thus overlapped lines) and Figure 54. As the diagonalization of the stiffness matrix and many zero values in the stiffness matrix occur naturally due to the choice of the shape function and the integration scheme in TDSFEM, it is proved to be computationally efficient as compared to the conventional FEM.

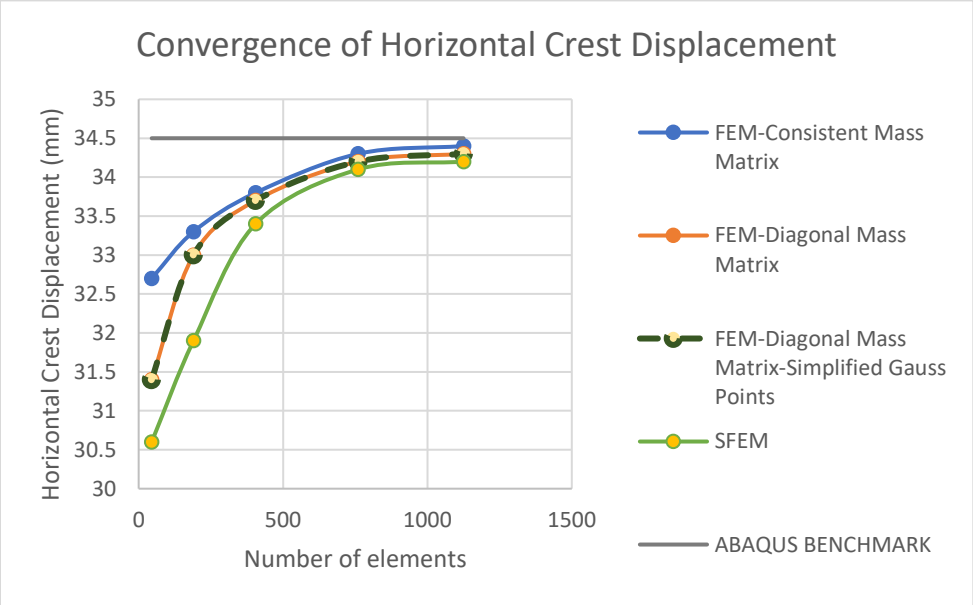

Figure 53: Convergence of Horizontal Crest Displacement

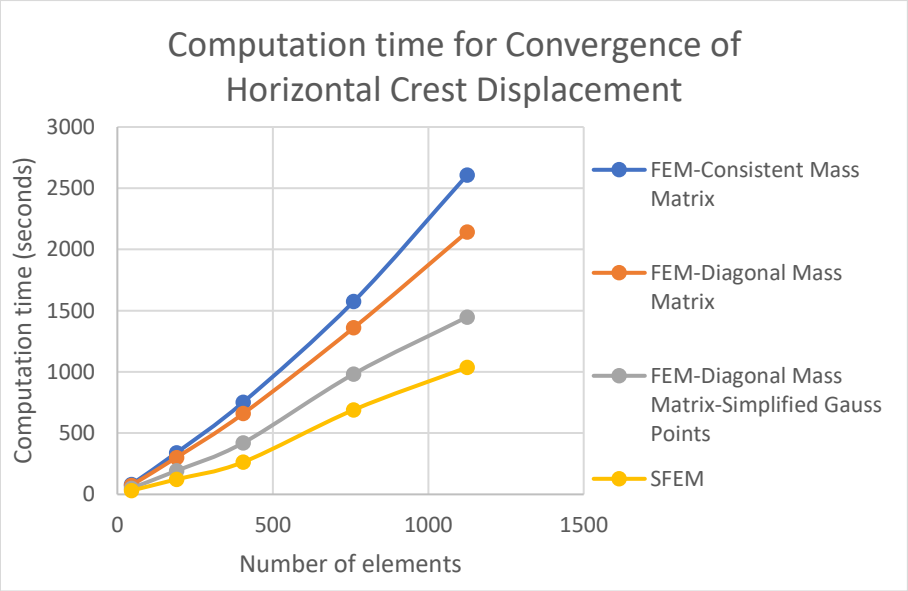

Figure 54: Computation time for time history analysis

From Table 9 and Figures 53 and 54, it is observed that the convergence analysis results on the horizontal crest displacement by time history analysis confirm to the results of convergence study on modal frequencies by modal analysis. FEM with consistent mass matrix consumes maximum time with highest accuracy, while FEM with diagonal mass matrix consumes little less time with some loss of accuracy. When FEM with diagonal mass matrix is considered with simplified Gauss points considered as decimal values, the reduction of computational order leads to significant decrease in computation time with values same as FEM with diagonal mass matrix normal case. SFEM model takes the least computation time amongst all four cases considered and starts with maximum error (when element number is least), converging to the expected value as element number increases.

III. Performance of TDSFEM with higher order elements

To investigate the comparative performance of FEM and TDSFEM in the case of higher order elements, 9 noded rectangular elements with quadratic shape functions in both directions have been used to model the dam geometry. Modal analysis and time history analysis have been performed for both FEM and TDSFEM using the 9-noded elements. The results from the previous section have shown that FEM with consistent mass matrix produces the most accurate results and consumes less time when the simplified Gauss quadrature points are considered as decimal values.

Thus, for all further simulations of FEM, consistent mass matrix with the simplified Gauss points considered as decimal values are used to get acceptable accuracy and optimized time of computation. In order to compare the performance of the models 9-noded elements (quadratic shape functions) with the model with 4-noded elements (linear shape functions), the total number of degrees of freedom in both models are kept the same. The convergence of the 1st natural frequency from modal analysis and computation time for TDSFEM and FEM are shown in Figures 55 and 56 respectively. Similar plots for the maximum horizontal crest displacement from time history analysis are shown in Figures 57 and 58.

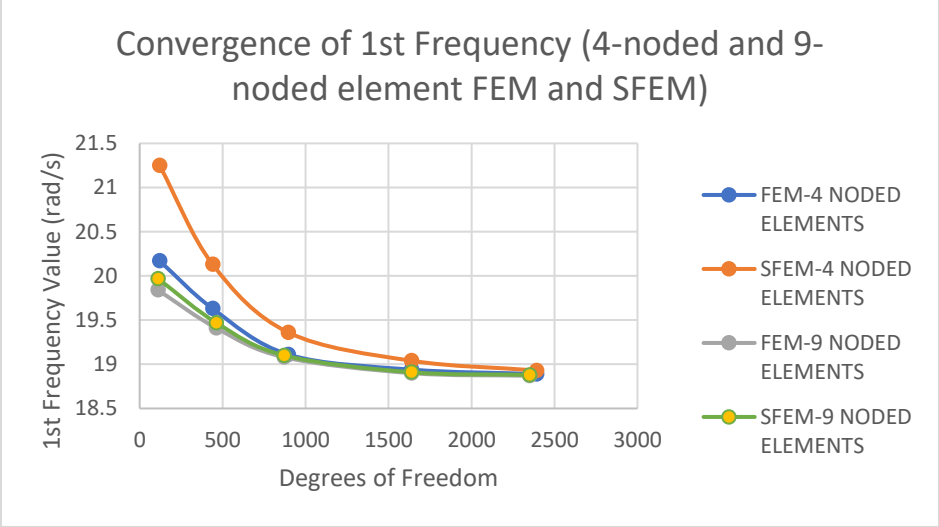

Figure 55: Convergence of 1st frequency for 4-node and 9-node elements using FEM and TDSFEM

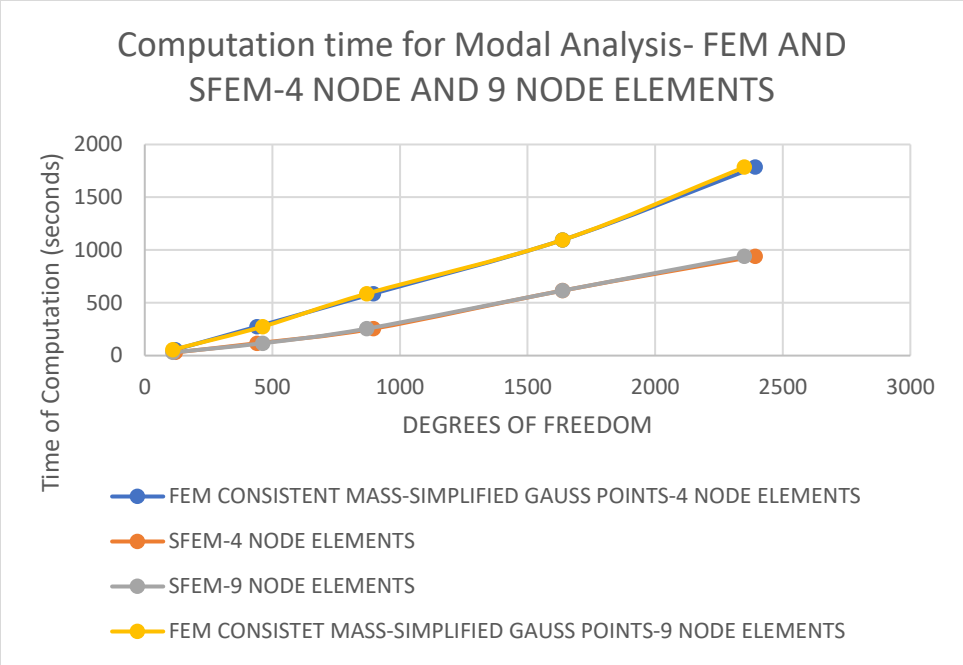

Figure 56: Computation time of modal analysis for 4-node and 9-node elements using FEM and TDSFEM

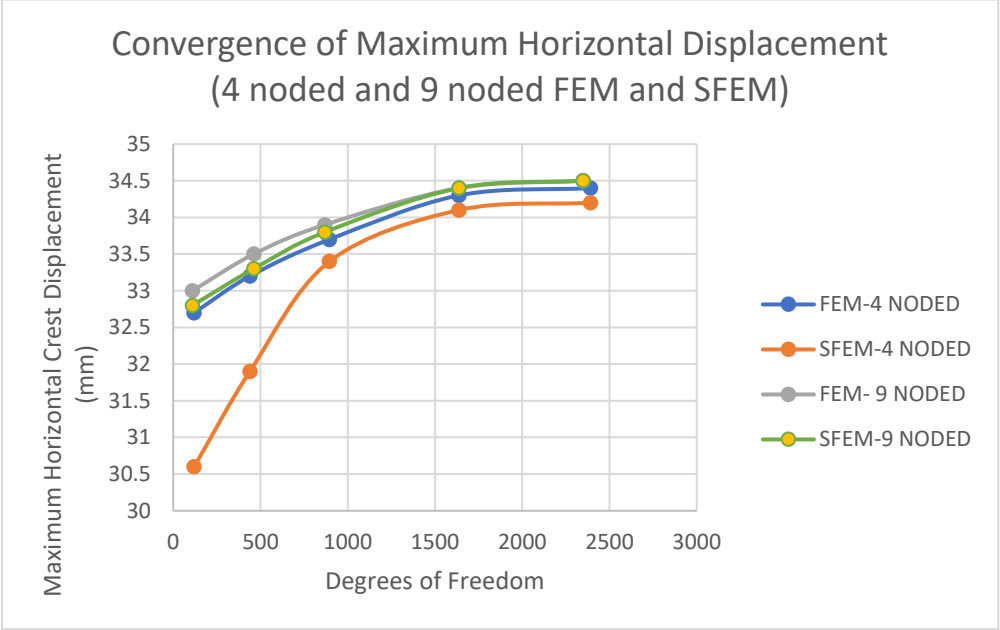

Figure 57: Convergence of Maximum horizontal crest displacement for 4-node and 9-node elements using FEM and TDSFEM

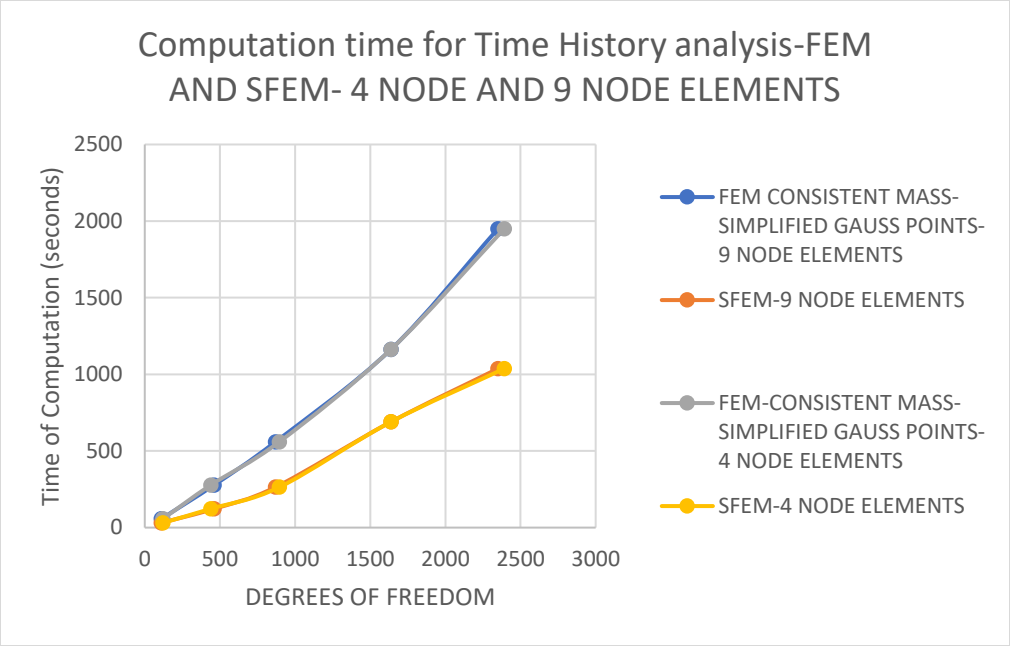

Figure 58: Computation time for time history analysis for 4-node and 9-node elements using FEM and TDSFEM

The results demonstrate the better performance of 9-noded TDSFEM elements with respect to the 4-noded TDSFEM elements. In the case of 9-noded TDSFEM elements, the errors in the results of frequency and horizontal crest displacement are reduced and almost match with the results of 9-noded FEM elements with consistent mass, with significant reduction of computation time. In the present study, the total degrees of freedom for the models with 4-noded and 9-noded elements were considered similar (so 9-noded element models have lesser number of element than the corresponding models with 4-noded elements) to compare them directly and achieve consistent results (same or similar number of degrees of freedom provide same flexibility to the models and thus produce comparable results). Thus, TDSFEM with higher order elements, which provide accurate results with significant saving in computation time, can be considered as a viable alternative to conventional FEM for dynamic analysis of large structures.

IV. Modeling of dam foundation with infinite elements

In order to consider the effect of foundation on the behavior of the dam, infinite elements have been developed to model the foundation system. Rectangular six-noded elements with two degrees of freedom at each node are considered, with three nodes in the infinite direction. Isoparametric formulation is used with the master element being a 2x2 square element. The master element and typical actual element is shown in Figure 59. The infinite element formulation in FEM is typically

demonstrated in literature (Bhatti, 2005). The shape functions for the displacements are as given in Equation 37 to 42.

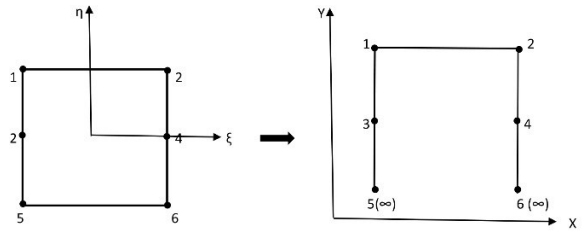

Figure 59: Six-noded Infinite element formulation

$$N1 = 0.25 * \eta * (\eta + 1) * (1 - \xi) \quad (37)$$

$$N2 = 0.25 * \eta * (\eta + 1) * (1 + \xi) \quad (38)$$

$$N3 = -0.5 * (\eta - 1) * (\eta + 1) * (1 - \xi) \quad (39)$$

$$N4 = -0.5 * (\eta - 1) * (\eta + 1) * (1 + \xi) \quad (40)$$

$$N5 = 0.25 * \eta * (\eta - 1) * (1 - \xi) \quad (41)$$

$$N6 = 0.25 * \eta * (\eta - 1) * (1 + \xi) \quad (42)$$

The mapping for the co-ordinates from the master element to the actual element is as mentioned in Equation 43 and 44.

$$x(\xi,\eta) = \frac{\eta * (1-\xi)}{(1+\eta)} x_1 + \frac{\eta * (1+\xi)}{(1+\eta)} x_2 + \frac{(1-\eta) * (1-\xi)}{2(1+\eta)} x_3 + \frac{(1-\eta) * (1+\xi)}{2(1+\eta)} x_4 \quad (43)$$

$$y(\xi,\eta) = \frac{\eta * (1-\xi)}{(1+\eta)} y_1 + \frac{\eta * (1+\xi)}{(1+\eta)} y_2 + \frac{(1-\eta) * (1-\xi)}{2(1+\eta)} y_3 + \frac{(1-\eta) * (1+\xi)}{2(1+\eta)} y_4 \quad (44)$$

It could be observed that the mapping functions considered in Equations 43 and 44 make the co-ordinates of the mapped points 5 and 6 go to infinity. Using the above-mentioned shape functions and mapping functions, the element matrices for the foundation elements are calculated for both FEM and TDSFEM. In FEM, the integration is carried out using Gauss quadrature while for

TDSFEM, the integration is carried out using Gauss-Lobatto-Legendre quadrature as mentioned in the earlier sections. Though the use of infinite elements to model foundation is prevalent in conventional FEM literature, the use of infinite elements in TDSFEM was not reported in the literature to the best of the authors' knowledge. Therefore, adapting the infinite element formulation to 2D TDSFEM represents an addition to the body of knowledge. Once the element matrices for the foundation are calculated, they are assembled with the dam structure element matrices and the whole structure dam-foundation global matrices are formed. The total width of the foundation considered is 805 m, the elastic modulus considered is 31027 MPa, density as 2643 kg/m3 and Poisson's ratio as 0.33. For the foundation model, the Rayleigh damping coefficients α and β are considered as 1.64 and 0.0012.

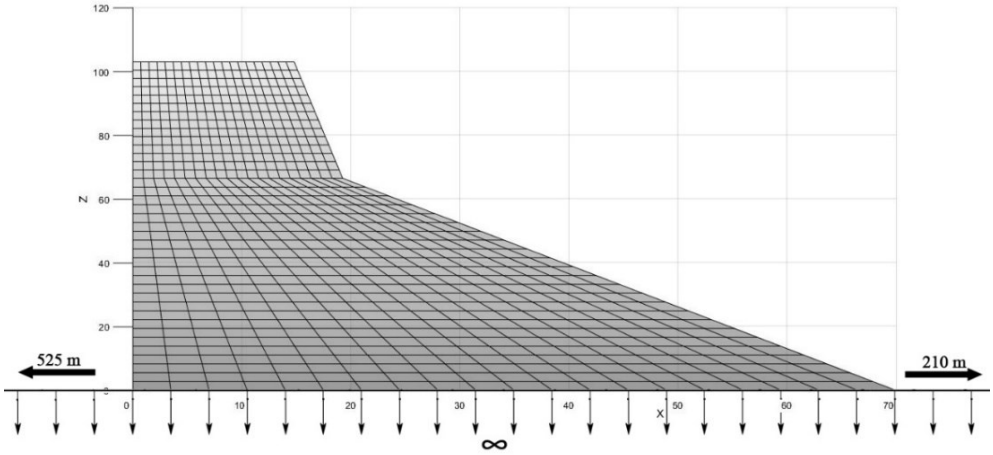

Figure 60: Dam-foundation assembly with infinite elements

Figure 60 shows the plots of the dam with the foundation elements extending to infinity. The width of the foundation is considered to be about 12 times the height of the dam. Time history analysis has been performed and the crest displacement has been shown in Figure 60.

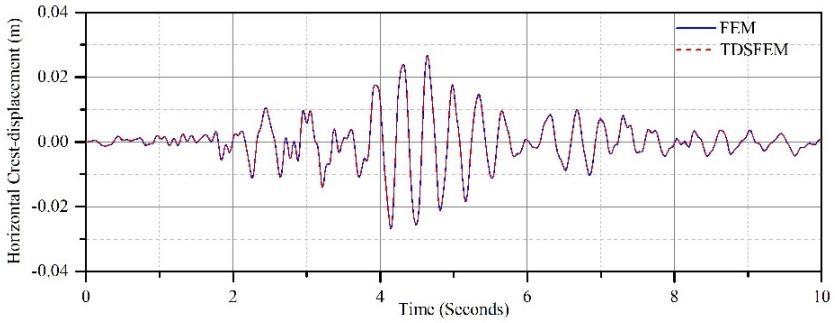

Figure 61: Horizontal crest-displacement history considering dam-foundation system for FEM and TDSFEM (subjected to Koyna earthquake)

Figure 61 shows a reasonably good match in the results for FEM and TDSFEM. It is observed that the maximum displacement of the crest is around 28 mm, which is less than that for the dam with fixed base condition. Another set of analysis is carried out considering the dam-foundation-reservoir system thus taking account the effect of both foundation and reservoir on the behavior of the dam. The foundation has been modeled with infinite elements as mentioned in the preceding segment and the reservoir has been modeled by Westergaard added mass technique. Figure 62 shows the crest displacement history of the dam-foundation-reservoir system with both FEM and TDSFEM.

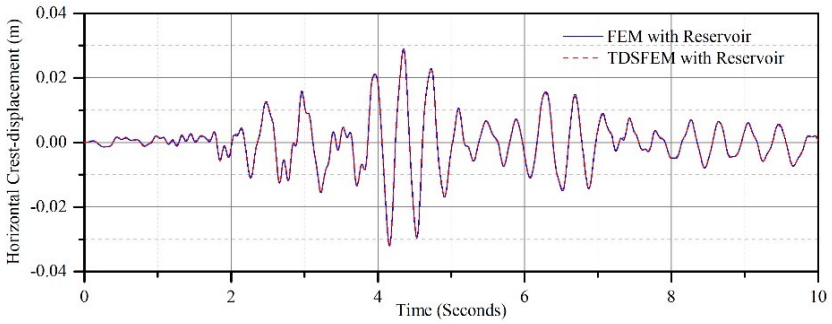

Figure 62: Horizontal crest-displacement history considering dam-foundation-reservoir system for FEM and TDSFEM (subjected to Koyna earthquake)

The analysis time required for the computations with foundation in Section 9 is again significantly less for TDSFEM than that for FEM, which is consistent with the results obtained in the previous sections.

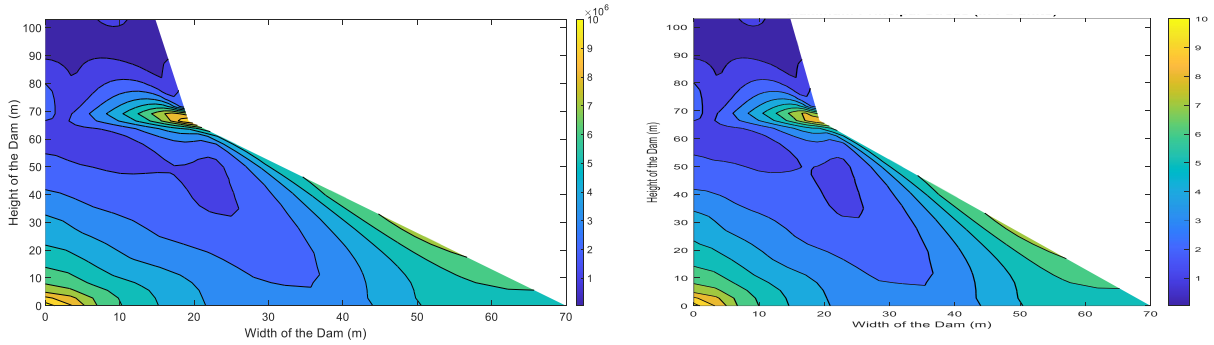

(a) (b)

Figure 63: Envelope of maximum principal stress for dam-foundation-reservoir system (subjected to Koyna earthquake) in Pa units a) FEM, b) TDSFEM

Figure 63 presents the plot of the envelope of maximum principal stress (tensile) over the dam body for dam-foundation-reservoir case. It is observed that maximum stress values are obtained at

the dam heel and neck, which are regions of possible dam failure due to tensile stress exceeding the maximum tensile capacity of the dam.

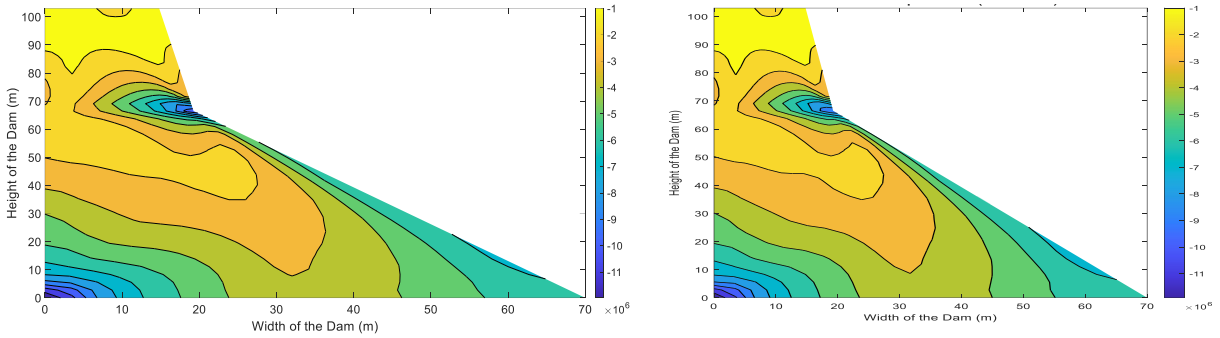

(a) (b)

Figure 64: Envelope of minimum principal stress for dam-foundation-reservoir system (subjected to Koyna earthquake) in Pa units: a) FEM, b) TDSFEM

Figure 64 presents the plot of the envelope of minimum principal stress (compressive) over the dam body for dam-foundation-reservoir case. The compressive stress values do not exceed the yield strength of concrete in compression. It is observed from Figures 63 and 64 that FEM and TDSFEM stress plots match exactly for the dam-foundation-reservoir case. This can be attributed to the exact match in the horizontal crest displacement history for both TDSFEM and FEM as observed in Figure 62. It could be concluded from Figures 63 and 64 that damage in the dam body occurs due to tensile cracking and not yielding in compression. The linear dynamic stress analysis aids in understanding that under the action of the applied seismic ground motion, the behavior of the dam in tension goes beyond its tensile capacity (i.e., at the dam heel and neck regions) and thus non-linear analysis would provide a better insight into the response of the structure. But it also needs to be noted that the material non-linearity in the dam body occurs only at localized regions of the dam heel and neck, while the other parts of the dam body do not exhibit the material non-linearity due to lower stresses (Chopra & Chakrabarti (1973), Bhattacharjee & Léger (1993), Tidke et al (2022)). The same phenomenon is observed in the present study (refer, Figure 63 and 64). Thus, linear analysis is very important and deemed sufficient in normal circumstances. Nonlinear analysis with material nonlinearity will be warranted if the linear analysis indicates the tensile and compressive stresses in the dam body exceed the limits significantly. The present work focuses on linear dynamic analysis showcase the computational efficiency of TDSFEM in terms of computational time and accuracy of TDSFEM. Non-linear analysis models with TDSFEM to be developed in the future are expected to provide higher efficiency than conventional FEM due to

the fact that the stiffness matrices would need to be updated at different steps and the dynamic equation need to be solved for the incremental response at each of those steps. Figures 65 and 66 present the plot of maximum and minimum principal stress envelopes for the dam without reservoir for the fixed base case while Figures 67 and 68 present the same for the dam with reservoir.

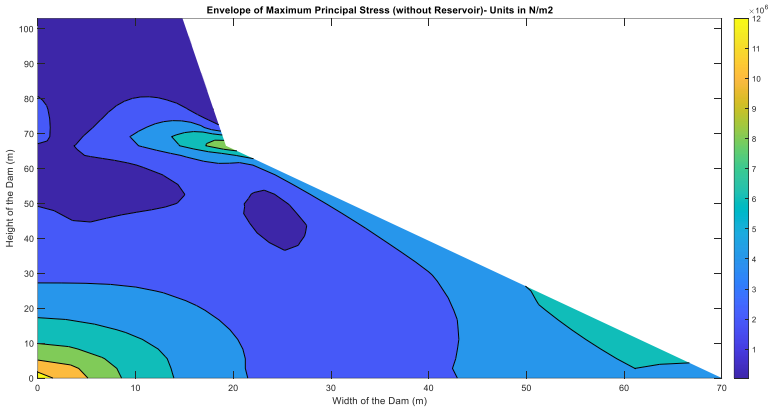

Figure 65: Envelope of Maximum Principal Stress (Dam without reservoir) (fixed base case)

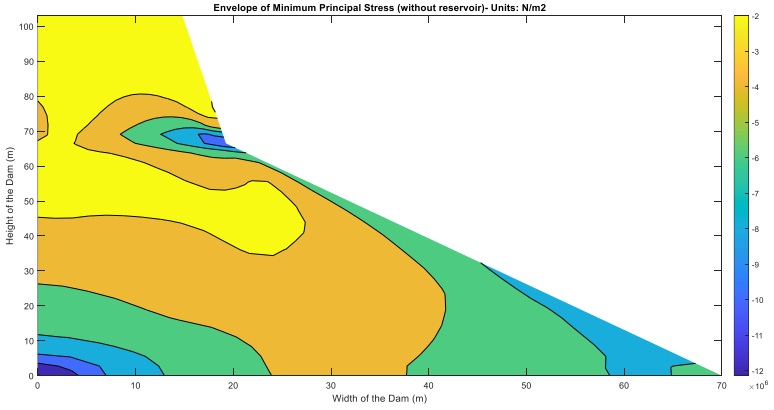

Figure 66: Envelope of Minimum Principal Stress (Dam without reservoir)(fixed base case)

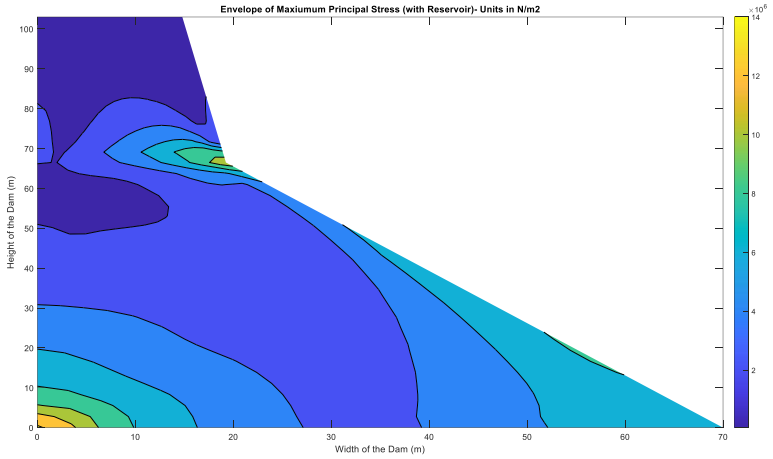

Figure 67: Envelope of Maximum Principal Stress (Dam with reservoir) (fixed base case).

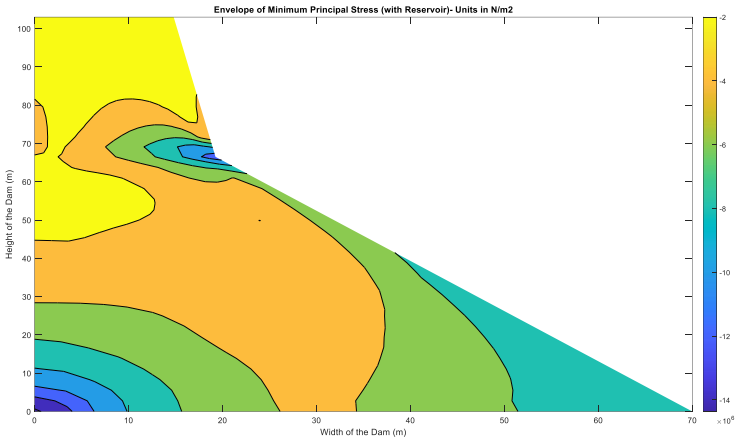

Figure 68: Envelope of Minimum Principal Stress (Dam with reservoir) (fixed base case)

V. Damage identification and localization in concrete gravity dams based on modal parameters

A. Modeling of damage in concrete gravity dams

Damage is introduced to the structure in terms of reduction in Young's Modulus. For four elements on the vertical upstream face of the dam, Young's Modulus considered in the second analysis is 1 percent of that in the pristine structure. So, for the damaged elements, Young's Modulus value considered is 310.27 MPa. The geometry of the model with the location of the damaged elements is shown in Figure 69.

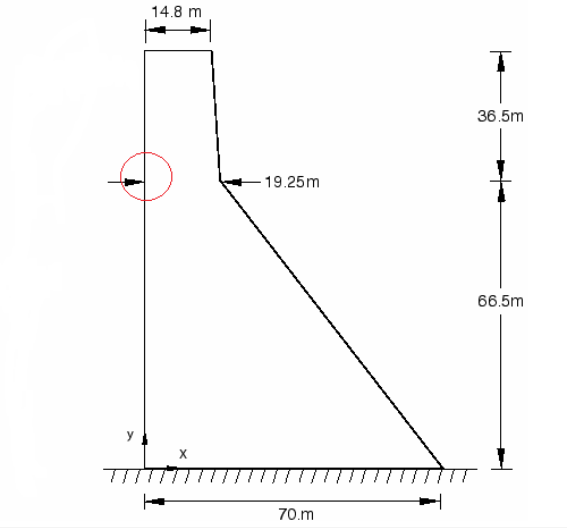

Figure 69: The geometry of the dam, showing damage location

The natural frequencies of the structure along with the corresponding displacement mode shapes, curvature mode shapes, and strain energy mode shapes are compared between the pristine and damaged state of the structure.

Damage indices are defined for the displacement mode shape and strain energy mode shape. For the displacement mode shape, damage index values are calculated as the change in modal displacements of the nodes from the pristine to the damaged structure (for modes 1 to 3) normalized by the modal displacements of the nodes in the pristine structure. Similarly, for the strain energy mode shapes damage index values are calculated as the change in modal strain energy from the pristine to damaged structure (for modes 1 to 3) normalized by the strain energy values of the corresponding nodes in the pristine condition. For the curvature mode shapes, a similar calculation is done only for the vertical upstream face of the dam. For all the nodes on the vertical upstream face, the curvature mode shape damage index is calculated by the change in curvature values normalized by the curvature of the pristine model (for modes 1 to 3).

The analysis procedure followed as explained above is performed for both TDSFEM and FEM by developed codes in MATLAB and the computation time is observed for the two.

B. Estimation of damage using modal parameters

At first, the change in modal frequencies, obtained for the pristine and damaged structure, is presented in Table 10. For the analysis performed, sensitivity analysis is performed, and 760 elements are found to be adequate to accurately calculate the modal frequency values.

Table 14: Change in 1st three modal frequencies

MODE	PRISTINE STATE	DAMAGED STATE
1st	19.04	19.02
2nd	51.21	51.18
3rd	68.87	68.81

The Changes in natural frequency values do identify the presence of damage in the structure. However, the change is so small, that it may be obfuscated by the presence of noise in measured data in the field. Here, as the overall change in the structure due to damage in 4 elements is very less, the change in frequency values is very less. Also, frequencies being a global parameter are not able to provide adequate information on the location and quantification of damage. The other parameter which is compared between the pristine and damaged structure is the displacement mode shapes. Figures 70 to 72 represent the modal damage indices based on the first three mode shape vectors.

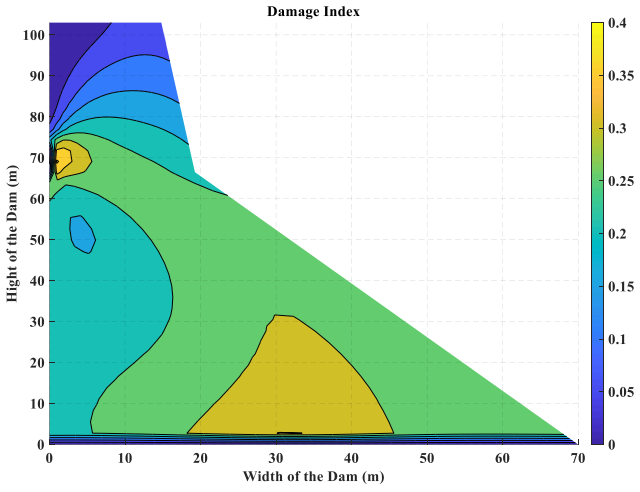

Figure 70: Damage index (Displacement Mode 1)

From the results, it is observed that the displacement mode shape change (normalized and denoted as damage index) over the structure though characterizes the presence of damage, it is not

consistent in accurately localizing the damage location in all the modes. Thus, displacement mode shapes are also not reliable properties to be considered for damage localization of structures.

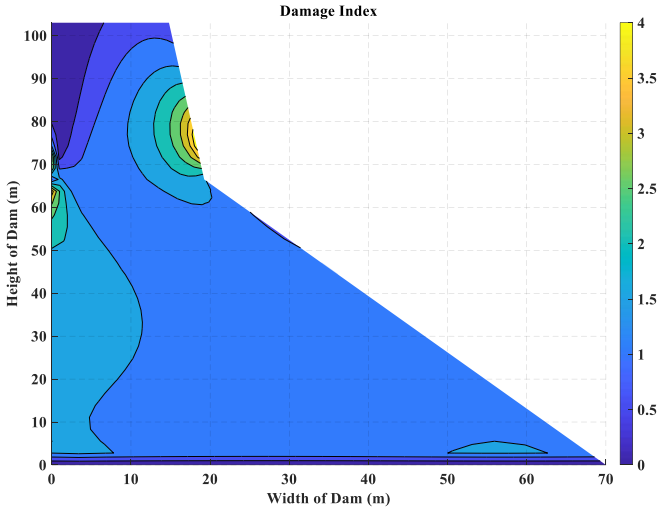

Figure 71: Damage index (Displacement Mode 2)

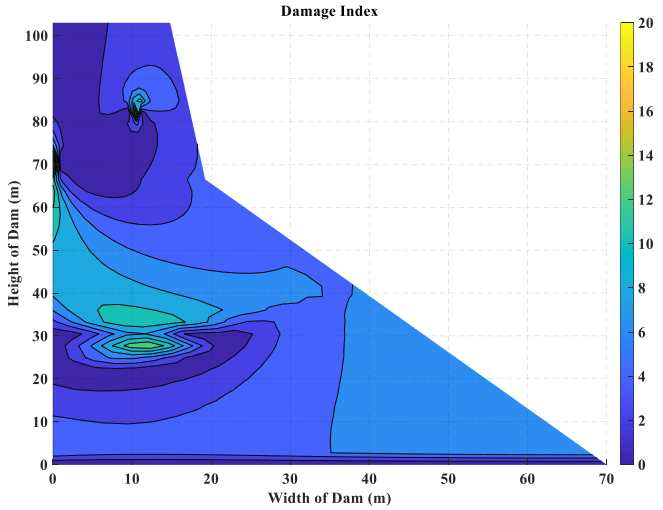

Figure 72: Damage index (Displacement Mode 3)

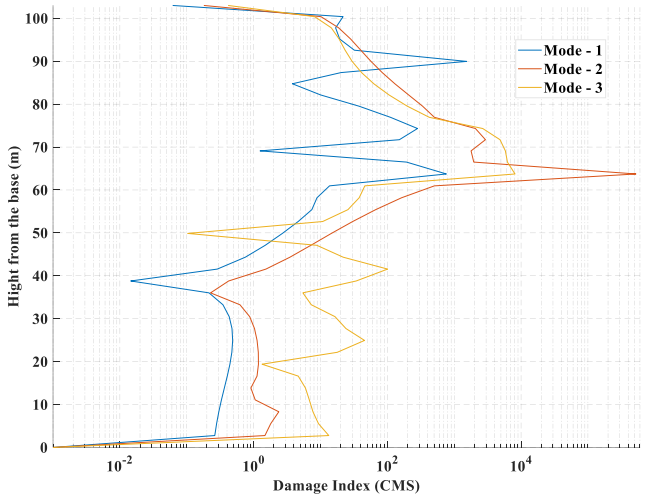

Figure 73: Damage index (Curvature mode shape)

The curvature mode shape has been identified in literature (Pandey et al, 1991) to be a better predictor in terms of damage location than the other modal parameters. The modal curvature damage index for the vertical upstream face of the dam is shown in Figure 73.

In these plots, it is observed that in Mode 2 and Mode 3, the location of damage is accurately predicted in terms of the Curvature Damage Index, however in Mode 1, the Curvature damage index is not accurately able to predict the location of the damage as it predicts higher value of damage index further from the damage location.

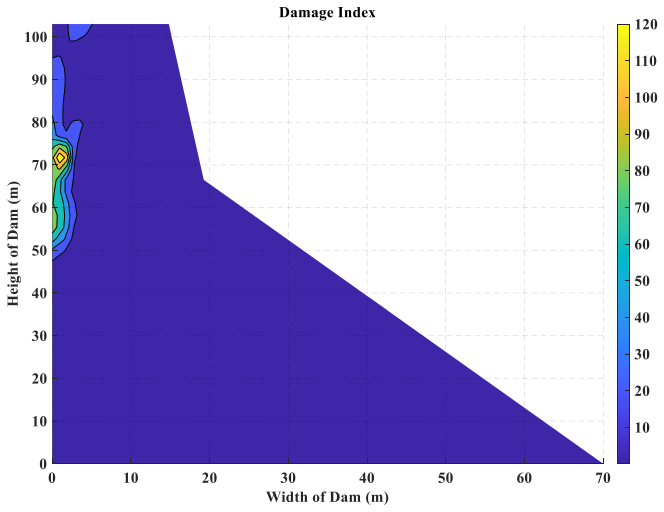

Figure 74: Damage index (Strain Energy Mode 1)

The final parameter studied is the strain energy mode shape. The Figures 74 to 76 show the damage index corresponding to the three modes.

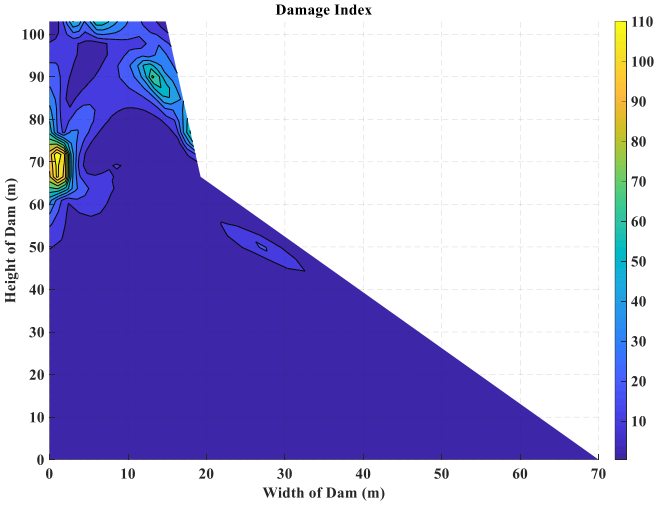

Figure 75: Damage index (Strain Energy Mode 2)

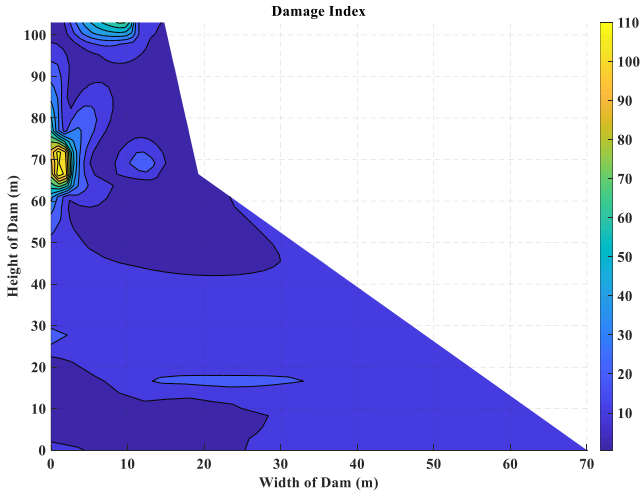

Figure 76: Damage index (Strain Energy Mode 3)

From the Figures 74 to 76, it is observed that the modal strain energy-based damage index accurately indicates the location of damage by providing maximum values of damage index at the exact location of damage. Thus, strain energy can be considered the most suitable parameter for localization of damage amongst the four modal parameters studied.

For all the above-mentioned analysis, similar results have been obtained with both TDSFEM and conventional FEM, thus emphasizing the fact that other than the computational aspect, both the

methods provide similar results. An important observation made here is that the analysis time required by conventional FEM is recorded as 2517 s, while the analysis time required by TDSFEM is 1545 s. Thus, TDSFEM provides a huge reduction in the computational time over the conventional FEM which is very important for analysis of large structures.

In this chapter, two aspects have been studied: the efficiency of modal parameters in detection of damage location and the computational efficiency of TDSFEM over conventional FEM. From the results of analysis, it is observed that amongst the modal parameters, modal strain energy is the most accurate predictor of damage location. Frequency, though able to identify the presence of damage in a structure, is not able to predict the location of damage. Also, for minute change in structural properties, the change in frequency is very less, thus making it an unreliable parameter for damage detection. Displacement mode shape also does not provide accurate results in terms of damage localization.

Curvature mode shape is found to be a better parameter than frequency and displacement mode shape in terms of judging the location of damage. However, it provides inconsistent results in some cases. As observed, in case of Mode 1, curvature mode shape is not able to predict the location of damage. On the other hand, Modal Strain Energy provides the best estimate for damage location with good consistency for all the modes. Finally, the application of TDSFEM in analysis of dams causes huge reduction in the computational time which is of a great importance. This method can be used in cases where a large number of analyses needs to be performed, achieving significant reduction of computational time.

VI. Discussions, Conclusions and Summary

The results of dynamic analysis of concrete gravity dam show that the TDSFEM is computationally more efficient than the conventional FEM for dynamic analysis of large structures, as the time consumed for analysis is reduced considerably. The reason for less time consumption can be attributed to the reduced complexity (also referred to as the order of complexity) of the spectral finite element formulation than the conventional FEM program. Order of complexity is a parameter which describes the runtime of an algorithm based on amount of input data (Cormen et al, 2001) and is generally denoted by the big-O notation O(n), O(n2), etc. In the case of the MATLAB programs developed here, the structure of the algorithms developed is the same for both conventional FEM and TDSFEM. The difference lies in the way system matrices

are formed in TDSFEM, and in the fact that the stiffness formulation uses GLL quadrature rule for numerical integration of the element matrices rather than the Gaussian quadrature as used in conventional FEM. This leads to the diagonalization of the mass matrix. Also, the conventional FEM uses Gauss points for integration which are $-1/\sqrt{3}$ and $1/\sqrt{3}$ for 2-point integration. The additional function for evaluating the non-rational number increases the computation complexity in the case of conventional FEM. Now, the order of complexity which depends on the number of times a particular operation is performed in an algorithm, that remains the same in the developed TDSFEM and FEM algorithms (due to same number of degrees of freedom which is the size of the matrix to be solved), but the time consumed in each step reduces drastically in SFEM due to sparsity in the mass and stiffness matrices (due to zeroes in shape function and B matrix in SFEM as a result of integration points being orthogonal to shape functions). In the conventional FEM, the diagonal mass matrix is also considered, and the comparisons shown with TDSFEM. It needs to be pointed out that the additional advantage in computational time in the case of TDSFEM can be attributed to the integration points (GLL points) in TDSFEM (-1 and 1 in case of 2-point integration) which coincide with the element nodes, contrary to the conventional FEM using Gauss integration points ($-1/\sqrt{3}$ and $1/\sqrt{3}$) in case of 2-point integration. For GLL quadrature, up to 3 integration points, the integration points are rational numbers and thus will provide computational time reduction compared to conventional FEM having irrational numbers as integration points. However, it has been observed that in case of conventional FEM, while using Gauss points as integration points, if the irrational numbers are replaced by decimal values, the computation of an additional square root function is reduced, and thus the computation time is reduced. TDSFEM with higher order elements gets rid of the inaccuracy encountered in TDSFEM with lower order elements and provides significant saving in computation time over the conventional FEM.

This chapter presents FEM-based alternative computational methods for dynamic analysis of two-dimensional structures. The methods reviewed here include the two most common SFEM methods found in literature- frequency or Fast Fourier Transform (FFT) based spectral finite element (FDSFEM) and time domain based spectral finite element method (TDSFEM). From the discussion, the TDSFEM is considered more suitable than the FDSFEM for application to dynamic analysis of structures with any arbitrary geometry and boundary conditions. A set of MATLAB based programs were developed to demonstrate the computational efficiency of the TDSFEM for dynamic analysis of large structures (validation studies have been performed using a simply

supported beam and the Pine Flat concrete gravity dam (U.S.A)). For the present study, a benchmark structure has been considered i.e., the Koyna Dam (India) and its geometric and material properties used to validate the results with available literature (Chopra & Chakrabarti (1973), Bhattacharjee & Leger (1993), Tidke et al (2022)). However, the developed codes could be adopted for any two-dimensional structure.

The significant reduction of computation time in the TDSFEM (due to diagonalization obtained by using the GLL integration points) compared to the conventional FEM demonstrates that this method could be successfully implemented for dynamic analysis of large structures with a similar level of accuracy as demonstrated in the results of modal analysis and dynamic time history analysis. The performance of TDSFEM considering higher order elements is particularly beneficial as the accuracy is same as conventional FEM with significant reduction of computational time (refer, Figure 56 and 58). Thus, the results of the study demonstrate the suitability of considering higher order TDSFEM elements as a viable alternative to the conventional FEM for the dynamic analysis of large structures.

The foundation has been modeled using infinite elements using both FEM and TDSFEM techniques. The use of infinite elements using TDSFEM for foundation modeling is an advancement in this domain. The modeling of dam-foundation-reservoir system as a whole has also been taken up leading to the saving in computational time (as the size of matrix solved is even greater than the dam with fixed base case).

The main findings of the study can be summarized as: 1) The conventional FEM requires considerable computation time for dynamic analysis of large structures. TDSFEM is comparatively more efficient and consumes much less amount of time for the analysis, and provides reasonable accuracy, especially when higher order elements are used; 2) Both the modal analysis and time history analysis results show a similar level of computational efficiency of TDSFEM over the conventional FEM, 3) The computational efficiency of TDSFEM is also demonstrated when the whole dam-foundation-reservoir model is considered for dynamic analysis.

The scope of future work includes system identification, damage detection, uncertainty quantification of large structures using the TDSFEM. It will also be interesting to study the efficiency of TDSFEM in the non-linear dynamic response history analysis of large practical structures like concrete gravity dams. For the non-linear analysis, the concrete damage plasticity

model can be used to simulate the material behavior. As the present article does not address the abovementioned issues, they are cited as some of the limitations of scope of the present work. It needs to be pointed out here that the adopted methodology in this work can also be extended to 3D structures with complex geometry. In the case of three-dimensional modeling of dams, the computational efficiency achieved by TDSFEM methodology could lead to enormous saving of computation time. While the above aspects are out of scope of the present article, they will be considered in the future.

CHAPTER 6: NONLINEAR ANALYSIS OF CONCRETE GRAVITY DAMS

I. Dynamic analysis of concrete gravity dams using TDFEM considering material nonlinearity

Concrete is a brittle material and like other brittle and quasi-brittle materials, it follows the non-associative plasticity in which the yield function and the plastic flow function are not the same. In the present work, the Concrete Damage Plasticity (CDP) model for concrete as suggested by Lee and Fenves (1998), which is a modified version of the one suggested by Lubiner et al (1989), has been considered. In this approach, the tensile and compressive damage are considered using separate variables which is a realistic way of modeling the behavior of concrete undergoing both tensile and compressive stresses. The yield functions and the plastic flow potential function considered are mentioned in the following equations.

In recent years, other researchers have developed modified concrete damage plasticity models for specific applications like Grassl (2009), Unger et al. (2011). For the return mapping algorithm, an elastic predictor-plastic corrector methodology is adopted along with the Newton-Raphson method for solving the set of non-linear equations as suggested by Simo and Taylor (1986).

II. Effect of reservoir

The dynamic pressure exerted by the reservoir on the upstream face of the dam is modeled by considering added mass technique as proposed by Westergaard (1933). Westergaard proposed that the hydrodynamic pressure exerted by the water on the dam during an earthquake has an effect like the case if a certain mass of water moves back and forth with the dam while the remainder of the reservoir does not interact with the dam. The calculation of added mass at height y, per unit area is given by the equation below.

$$addedmass(y) = (7/8) * \rho_w * \sqrt{h_w * (h_w - y)}; y < h_w, where, \rho_w = 1000 kg/m^3$$

III. Effect of foundation

In order to consider the effect of foundation on the behavior of the dam, infinite elements have been developed to model the foundation system. Rectangular six-noded elements with two degrees of freedom at each node are considered, with three nodes in the infinite direction. Isoparametric formulation is used with the master element being a 2x2 square element. The master element and typical actual element is shown in Figure 77. The infinite element formulation in FEM is typically demonstrated in literature (Bhatti, 2005). The shape functions for the displacements are as given in Equation 37 to 44 in Chapter 5.

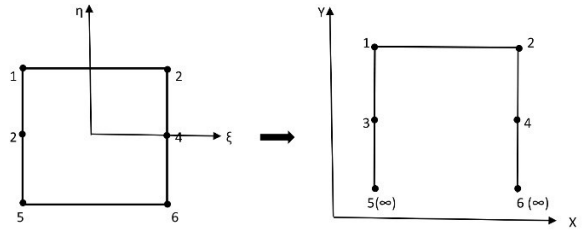

Figure 77: Six-noded Infinite element formulation

It could be observed that the mapping functions considered in Equations 28 and 29 make the co-ordinates of the mapped points 5 and 6 go to infinity. Using the above-mentioned shape functions and mapping functions, the element matrices for the foundation elements are calculated for both FEM and TDSFEM. In FEM, the integration is carried out using Gauss quadrature while for TDSFEM, the integration is carried out using Gauss-Lobatto-Legendre quadrature as mentioned in the earlier sections. Though the use of infinite elements to model foundation is prevalent in conventional FEM literature, the use of infinite elements in TDSFEM was showcased by the authors (Sarkar et at (2024)). However, in this chapter, the reported work has been extended by considering a full-scale model of the foundation where the depth of the foundation and the width of the foundation has been considered as per guidelines for non-linear analysis of dams (USBR guidelines) (as shown in Figure 78). Once the element matrices for the foundation are calculated, they are assembled with the dam structure element matrices and the whole structure dam-foundation global matrices are formed. The elastic modulus considered is 31027 MPa, density as 2643 kg/m3 and Poisson's ratio as 0.33. For the foundation model, the Rayleigh damping coefficients α and β are considered as 1.64 and 0.0012.

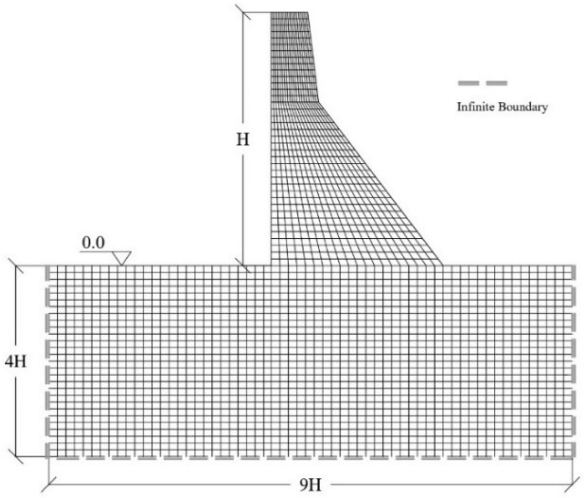

Figure 78: Dam-foundation assembly with infinite elements

IV. Deconvolution of ground motion

In the case of considering the foundation, the ground motion is applied at the bottom of the foundation. In order to do the same, the recorded ground motion is deconvoluted using DEEPSOIL, a program developed at the Department of Civil Engineering, University of Illinois at Urbana-Champaign, United States of America (USA). In this program, the deconvolution is performed using the frequency domain approach. This approach is the same as the frequency-domain linear equivalent linear analysis approaches except that the input motion can be applied at the ground surface or anywhere else in the soil column. The corresponding rock motion is then computed. The deconvolution procedure requires the definition of soil properties of each layer like soil thickness, unit weight, shear modulus and damping ratio. The values of these properties are considered as defined in the foundation properties. The concept of deconvolution comes from the theories of wave propagation and is briefly discussed here. The objective of the procedure is to obtain a ground motion to be applied at the bed rock level which will produce the same effects as the ground motion at the surface produces. An iterative procedure is adopted for this purpose where the frequency content of a trial ground motion at the bed rock level is matched with the frequency content of the ground motion recorded at the surface level by following the wave propagation principles where the intermediate soil strata is considered as a two-dimensional shear column layer based on its shear wave velocity. The deconvolved ground motions are applied at the bottom of the foundation.

V. Results of non-linear time history analysis

The results of the nonlinear time history analysis are represented in this section in terms of the horizontal displacement of the crest. The ground motion considered for the analysis is the recorded ground motion at the site of the Koyna Dam as shown in Figure 47 in Chapter 5. The Figures 79 to 82 show the plots of the horizontal displacement history of the crest for the 1) dam only case (fixed base)-D, 2) dam (fixed base) with reservoir case-DR, 3) dam only with foundation case-DF and 4) dam with foundation with reservoir case -DFR for both TDSFEM and the conventional FEM. It is seen from the plots that the results of TDSFEM and FEM match considerably well. The comparison of computation time for the two analysis procedures in all the four cases is shown in Table 15. The results of dynamic analysis of concrete gravity dam show that the TDSFEM is computationally more efficient than the conventional FEM for dynamic analysis of large structures, as the time consumed for analysis is reduced considerably. The reason for less time consumption can be attributed to the reduced complexity (also referred to as the order of complexity) of the spectral finite element formulation than the conventional FEM program. Order of complexity is a parameter which describes the runtime of an algorithm based on amount of input data (Cormen et al, 2001) and is generally denoted by the big-O notation O(n), O(n2), etc. In the case of the MATLAB programs developed here, the structure of the algorithms developed is the same for both conventional FEM and TDSFEM.

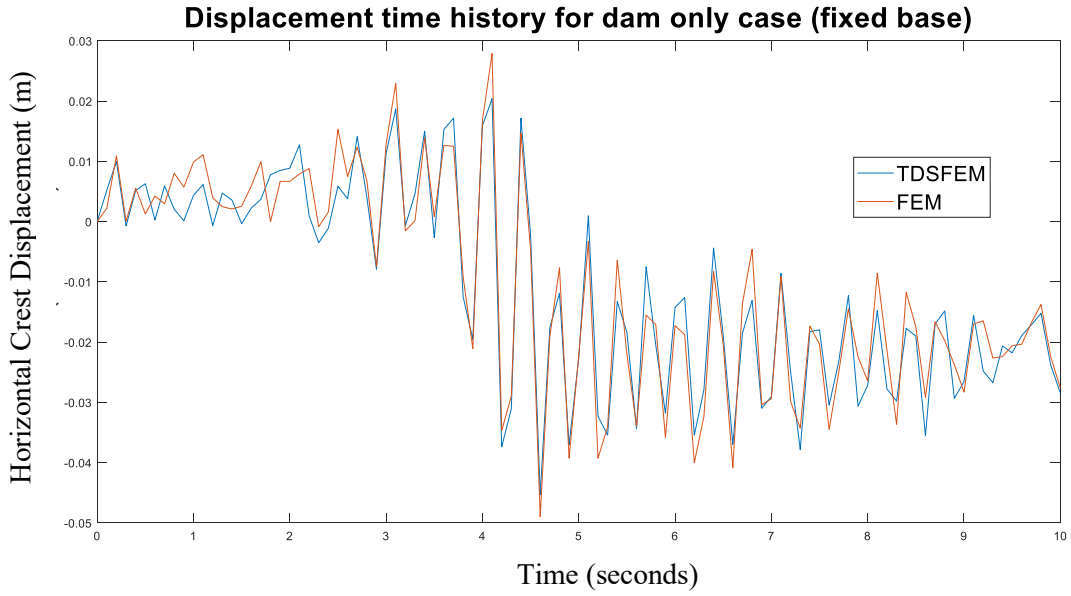

Figure 79: Time history of horizontal crest displacement for dam only fixed base condition (both FEM and TDSFEM)

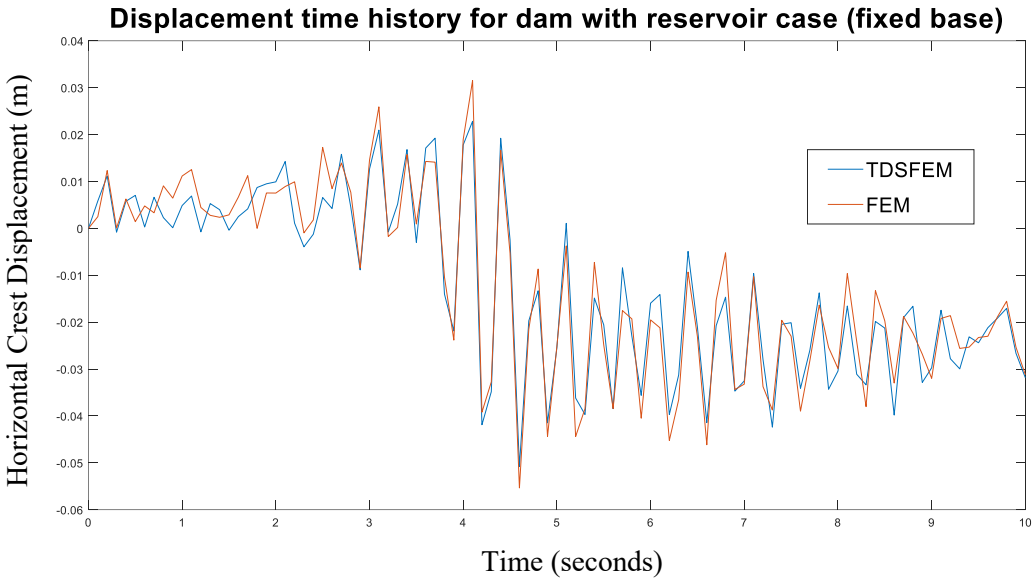

Figure 80: Time history of horizontal crest displacement for dam with reservoir fixed base condition (both FEM and TDSFEM)

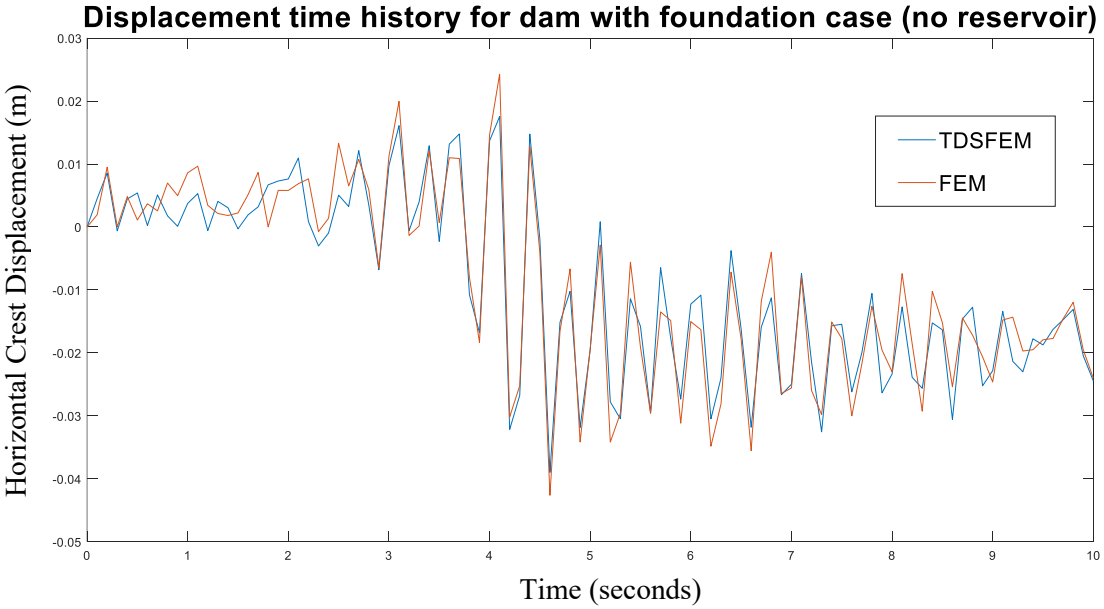

Figure 81: Time history of horizontal crest displacement for dam with foundation (both FEM and TDSFEM)

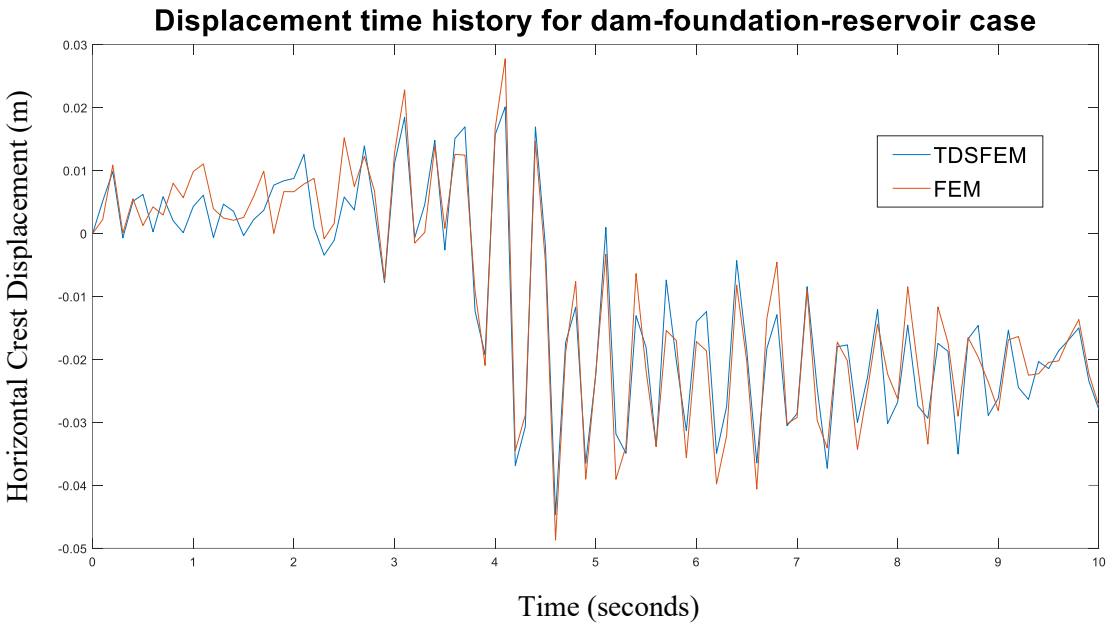

Figure 82: Time history of horizontal crest displacement for dam-foundation-reservoir case (both FEM and TDSFEM)

Table 15: Comparison of computation time

Case	Computation time FEM (seconds)	Computation time TDSFEM (seconds)
D	9357	4024
DR	9481	4211
DF	20017	8954
DFR	20238	9180

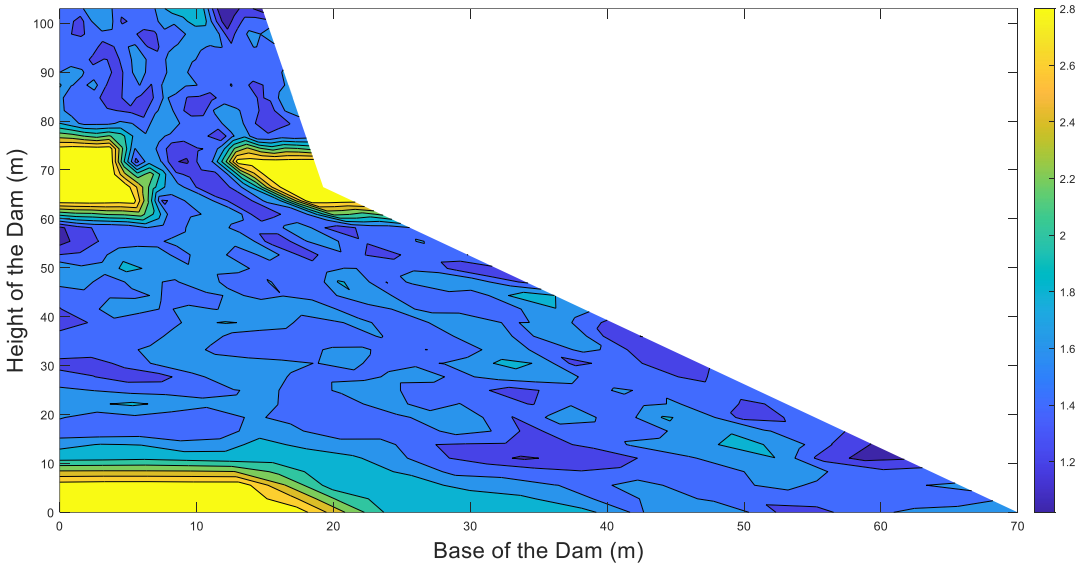

Figure 83: Maximum principal stress of dam body for Dam-foundation-reservoir case (FEM) in MPa units

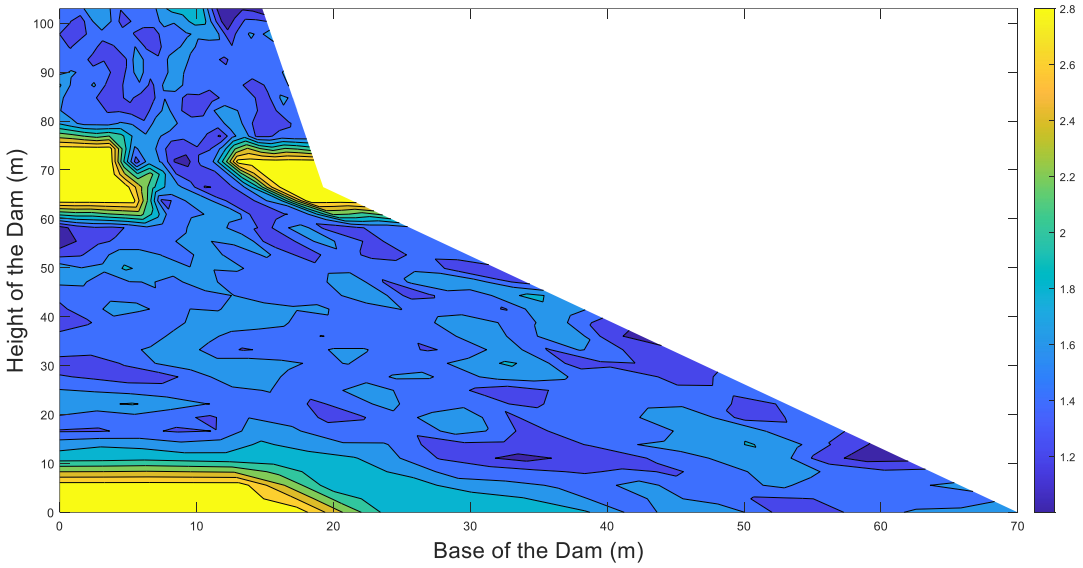

Figure 84: Maximum principal stress of dam body for Dam-foundation-reservoir case (TDSFEM) in MPa units

In Figures 83 and 84, the plot of the maximum principal stress contour over the dam body is shown in case of FEM and TDSFEM. These plots provide an idea of the possible failure pattern of the dam under the applied ground motion at the neck and heel region due to the tensile stresses exceeding the permissible limits. The reported failure pattern of the dam in literature (Chopra &

Chakrabarti (1973), Bhattacharjee & Leger (1993), Tidke et al (2022)) matches with the present findings.

VI. Discussions, Conclusions and Summary

This chapter presents FEM-based alternative computational methods for dynamic analysis of two-dimensional structures. The method considered here is the time domain based spectral finite element method (TDSFEM). From the discussion, the TDSFEM is considered more suitable than the time domain based spectral finite element method (FDSFEM) for application to dynamic analysis of structures with any arbitrary geometry and boundary conditions. A set of MATLAB based programs were developed to demonstrate the computational efficiency of the TDSFEM for dynamic analysis of large structures For the present study, a benchmark structure has been considered i.e., the Koyna Dam (India) and its geometric and material properties used to validate the results with available literature (Chopra & Chakrabarti (1973), Bhattacharjee & Leger (1993), Tidke et al (2022)). However, the developed codes could be adopted for any two-dimensional structure.

The significant reduction of computation time in the TDSFEM (due to diagonalization obtained by using the GLL integration points) compared to the conventional FEM demonstrates that this method could be successfully implemented for dynamic analysis of large structures with a similar level of accuracy as demonstrated in the nonlinear dynamic time history analysis.

The foundation has been modeled using infinite elements using both FEM and TDSFEM techniques. The use of infinite elements using TDSFEM for foundation modeling is an advancement in this domain. The modeling of dam-foundation-reservoir system as a whole has also been taken up leading to the saving in computational time (as the size of matrix solved is even greater than the dam with fixed base case).

The main findings of the study can be summarized as: 1) The conventional FEM requires considerable computation time for dynamic analysis of large structures. TDSFEM is comparatively more efficient and consumes much less amount of time for the analysis, and provides reasonable accuracy, especially when higher order elements are used; 2) The computational efficiency of TDSFEM is also demonstrated when the whole dam-foundation-reservoir model is considered for dynamic analysis.

The scope of future work includes utilizing the benefits of the computational efficiency achieved by TDSFEM in various analysis and applications of concrete gravity dams. In the case of analysis types like fragility analysis, inverse problems, etc. where the solution involves repeated iterations to be performed on the set of matrix equations, TDSFEM could prove to be highly advantageous. Also, integration of the TDSFEM procedure into the commercially available software packages could be highly beneficial for both academia and industry as it would reduce the computational time for repeated analysis scenarios. In the present work, for modeling the effects of the reservoir, a simplified approach has been considered. This could be extended to more advanced methods of modeling the reservoir using coupled Euler-Lagrangian approach or the acoustic formulation. While these are out of scope of the present work, it can be considered in the future as an extension of the present work. It will also be interesting to consider other boundary conditions for the foundation like viscous boundary, non-reflecting boundary, etc. and study the effect on the response of the structure. As the present article does not address the abovementioned issues, they are cited as some of the limitations of scope of the present work. It needs to be pointed out here that the adopted methodology in this work can also be extended to 3D structures with complex geometry. In the case of three-dimensional modeling of dams, the computational efficiency achieved by TDSFEM methodology could lead to enormous saving of computation time. While the above aspects are out of scope of the present article, they will be considered in the future.

CHAPTER 7: MODELING OF ALKALI-AGGREGATE REACTIONS IN CONRETE GRAVITY DAMS USING TDSFEM

I. AAR effects causing deterioration in concrete structures

Concrete as a material undergoes deterioration over time which impacts the performance of concrete structures and sometimes leads to devastating effects and requires severe repair and retrofitting measures. One of the major deterioration effects which is observed in concrete structures is the damage caused by chemical changes in the compositions of concrete, namely the alkali-aggregate reaction often referred to as AAR. AAR causes major changes in concrete structures due to differential expansion created in different parts of the structures causing major cracks.

Alkali-aggregate reaction (AAR) is the predominant chemical process observed in concrete, leading to gradual deterioration over time and the formation of a network of both small and large cracks within the concrete structure. AAR results in permanent expansion and contributes to the weakening of concrete dams. This deterioration can compromise the stability of a dam, particularly when existing cracks, induced by AAR, extend further during powerful earthquakes. The interaction of these cracks could potentially lead to the failure of the dam. Therefore, it is crucial to assess the damage caused by AAR as part of the seismic safety evaluation of concrete dams prior to significant seismic events.

Several macroscopic models have been developed to analyze the structural expansion resulting from alkali-aggregate reaction (AAR), with Charlwood's model (1992) being one of the most commonly utilized approaches. Charlwood's model assumes a constant rate of swelling during the AAR reaction, which does not align well with the kinetics observed in experimental tests. While the model can estimate the final amount of expansion displacement in AAR-affected concrete dams, it lacks accuracy in reproducing the structural deformation process, especially when nonlinearities are considered. Consequently, more sophisticated models have been developed to incorporate both AAR kinetics and mechanical behavior, such as those by Huang and Pietruszczak (1996), Ulm et al. (2000), and Steffens et al. (2003). Among these, Ulm's model, which integrates

reaction kinetics from Larive (1998), has gained wide acceptance. These models are effectively used to quantitatively assess AAR expansion in both time and space within concrete structures. Numerous studies have been conducted to predict expansion deformation during the AAR process in concrete dams and validate these predictions through field measurements of crest displacements. For an extensive overview of research on the modeling of alkali-aggregate reaction (AAR), readers can consult the work of Pan et al. (2012).

In all simulations for large structures like concrete gravity dams, computational time is a challenging aspect. Thus, a computationally efficient analysis procedure is extremely beneficial for analysis of large structures. The efficiency of time domain based spectral finite element method in analysis of large dams have been demonstrated in literature (Sarkar et al, 2024), (Sarkar & Bagchi, 2023), (Sarkar et al, 2022). In this paper, the authors have extended the procedure established in mentioned literature for AAR effects on dams.

In summary, the literature demonstrates a growing interest in developing sophisticated models and simulation techniques to assess and understand the detrimental effects of AAR on concrete dams. These contributions underscore the complexity of AAR as a phenomenon and highlight the critical need for further research to refine these models for more accurate damage assessment and mitigation strategies, particularly focusing on the creation of simplified thermo-mechanical models tailored for concrete gravity dams. This review indicates the field's progression towards more accurate and practical solutions to combat the challenges posed by AAR in maintaining the integrity and safety of concrete dam structures globally.

II. AAR kinetics

Rotter et al. (1998) and Saouma et al. (2006) contribute to understanding the mechanical impacts of AAR and modeling approaches. Rotter focuses on determining the specific fracture energy of AAR-affected concrete, while Saouma introduces a novel model for AAR expansion. Comi et al. (2009) proposes a model to simulate the swelling and deterioration of concrete, a concept further investigated by Sellier et al. (2009) through an innovative method assessing AAR kinetics and residual swelling capability. Pan et al. (2013), Pan et al. (2014) introduced models for analyzing cracking and predicting the long-term behavior of AAR-affected concrete dams, highlighting the importance of considering anisotropic expansion and seismic response in such structures. Moreover, suggestions have been made to incorporate mechanical and microscopic tools such as

the Stiffness Damage Test (SDT) and the Damage Rating Index (DRI) for evaluating the condition of AAR-affected concrete (Shayan & Grimstad, 2006) and (Sanchez et al., 2017).

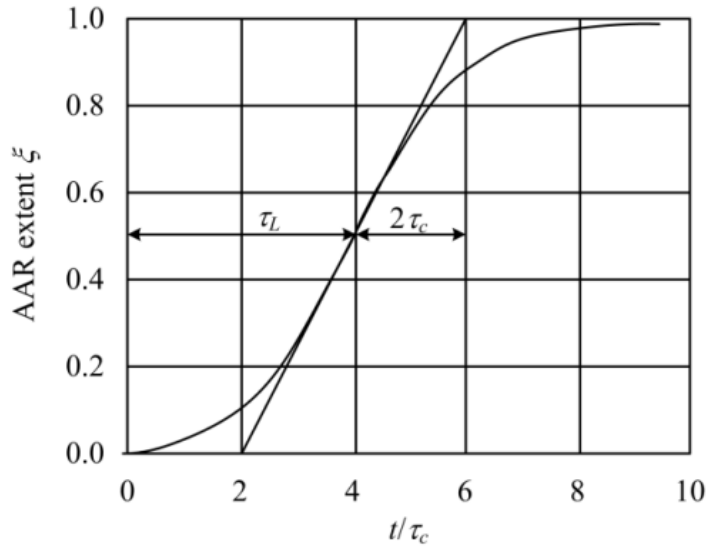

Figure 85: AAR progression over time

III. Simulation of AAR effects in concrete gravity dams using TDSFEM

In this section, a novel thermo-mechanical approach is adopted for analysis of AAR effects on concrete gravity dams using the time domain based spectral finite element method (TDSFEM). The Koyna dam, located in Maharashtra, India, plays crucial roles in water storage, hydroelectric power generation, and flood control within its region. The cross-section of the Koyna dam used in the numerical simulation is depicted in Figure 85. With a crest length of 853.5 meters and a height of 85.34 meters above the riverbed, descending to a depth of 103.02 meters below the deepest foundation, the Koyna dam stands as a substantial structure. It consists of 27 monoliths, each spanning 15.24 meters in width. The elastic modulus of the dam structure is estimated at 31027 MPa, with a density of 2643 kg/m^3, and a Poisson's ratio of 0.15.

First, an initial thermal analysis of the Koyna Dam is performed to find the temperature variation of the dam body. The details of the above procedure are presented in the methodology chapter of the thesis (refer Figure 3). Based on the internal nodal temperature variation of the dam body, a pseudo thermal analysis is performed to calculate the AAR strain and stress variation in the dam body.

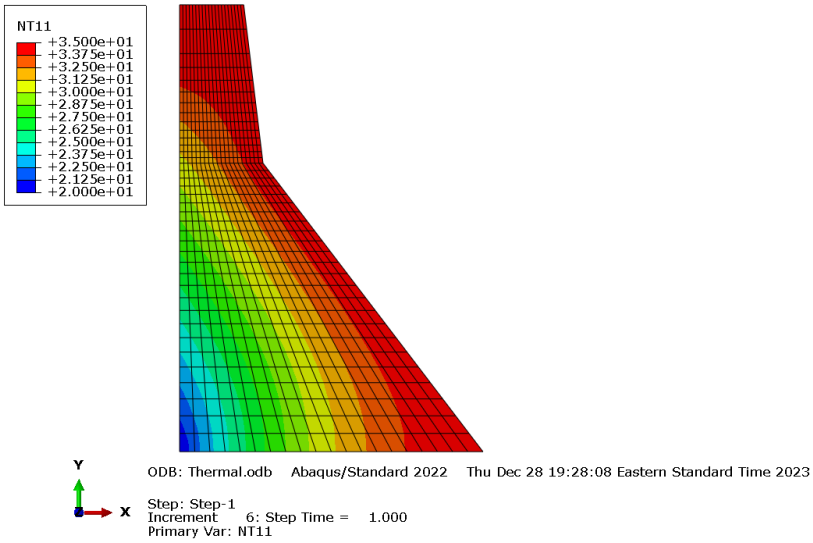

Figure 86: Temperature variation of the dam obtained from thermal analysis

A few stages of analysis are performed. First, a static analysis is performed considering only hydrostatic load and temperature effects on the dam, without any AAR effects. Second, static analysis is performed with hydrostatic loads and temperature effects, along with full AAR effects. In this analysis, the modulus of elasticity is reduced as per the AAR effects. Third, dynamic analysis is performed by applying seismic loads along with the previously considered loads and full AAR effects to analyze the structure. The stress variation in the structure helps to ascertain the probable failure zones of the dam considering the effect of AAR. he analysis integrates the combined effects of ambient temperature, gravity, hydrostatic, and hydrodynamic loading on the system. To assess the seismic response of the Koyna dam, ground motion data obtained from an accelerometer in one of the dam's galleries during the earthquake on December 11, 1967, with a moment magnitude of Mw=6.5, was utilized. The analysis considered ground motion characterized by peak horizontal accelerations of 0.473g (perpendicular to the dam axis) and peak vertical accelerations of 0.311g, as depicted in Figure 47(a). Additionally, the response spectra of these accelerographs are illustrated in Figure 47(b).

Here, a stepwise analysis approach is adopted. Initially, a static analysis is conducted, considering hydrostatic forces and thermal impacts on the dam. Two analysis stages are undertaken: one without considering Alkali-Aggregate Reaction (AAR) effects and another incorporating full AAR strain effects. Subsequently, the second stage of analysis involves linear dynamic analysis, incorporating seismic, hydrodynamic, and thermal effects on the dam. Once again, two analysis

stages are considered: one without AAR effects and one with full AAR effects. To simulate the impact of AAR, a pseudo-temperature load is applied to the structure. The full AAR strain is assumed to be 0.003 (Saouma & Perotti, 2006). The analysis utilizes a time-domain-based spectral finite element method, employing the Gauss-Lobatto-Legendre quadrature for integration, as opposed to the conventional Gauss quadrature utilized in typical finite element methods. The matrix formulations and other methodological details are outlined in Chapter 3.

IV. Results of static and dynamic analysis with full AAR effects on whole dam body

This section presents the results obtained from the analysis conducted. Figure 86 illustrates the internal temperature variation within the dam body. This temperature fluctuation serves as the basis for applying temperature loads to calculate the mechanical stresses exerted on the dam body. In the analysis where full Alkali-Aggregate Reaction (AAR) effects are considered, a pseudo temperature load is computed to replicate the same effects as the full AAR strain. The results of the analysis, comparing scenarios with no AAR and full AAR effects, are depicted in the figures within this section. Figures 87 and 88 display contour plots illustrating the maximum and minimum principal stresses for static analysis under hydrostatic and thermal loads, excluding the effects of AAR. Conversely, Figures 89 and 90 portray contour plots of the maximum and minimum principal stresses for static analysis under hydrostatic and thermal loads, considering full AAR effects. Similarly, for dynamic analysis, a comparable comparison is conducted between scenarios without AAR and with full AAR. Figures 91, 92, and 93 present the crest displacement, contour plot of maximum, and minimum principal stresses, respectively, for dynamic analysis considering hydrodynamic and seismic forces, alongside temperature loads but excluding AAR effects. The corresponding results for the full AAR situation are presented in Figures 94, 95, and 96.

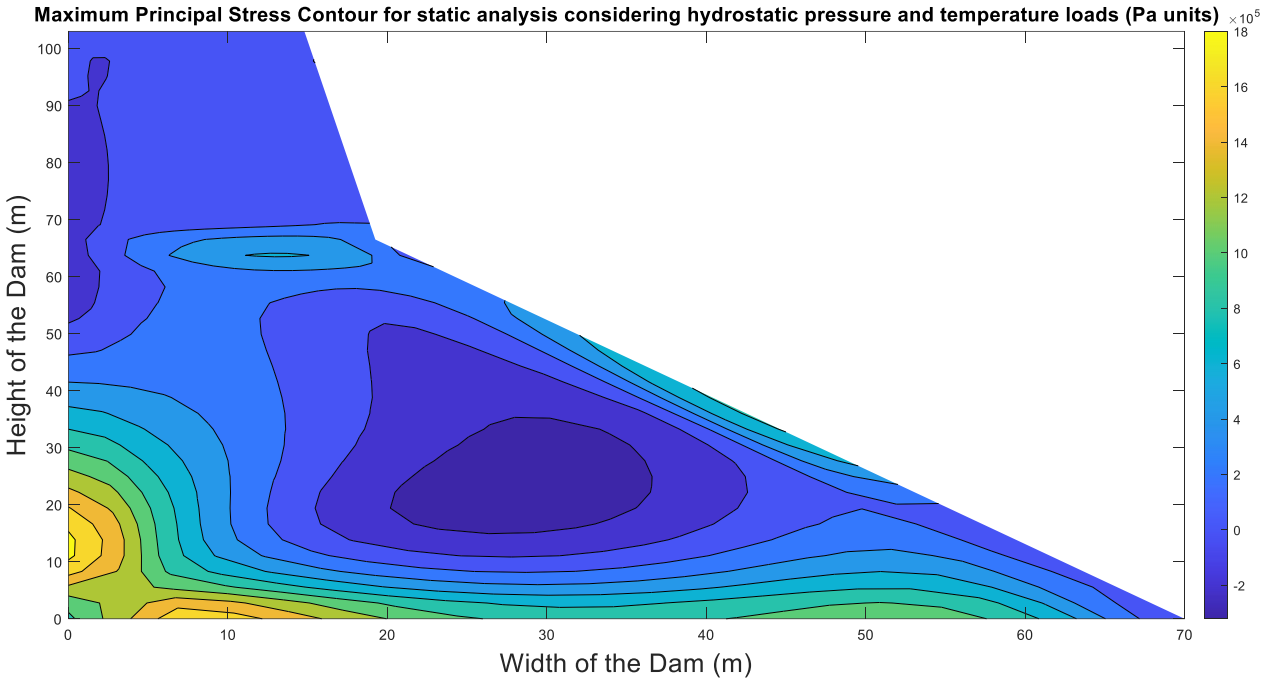

Figure 87: Maximum Principal stress plot for static analysis no AAR effect

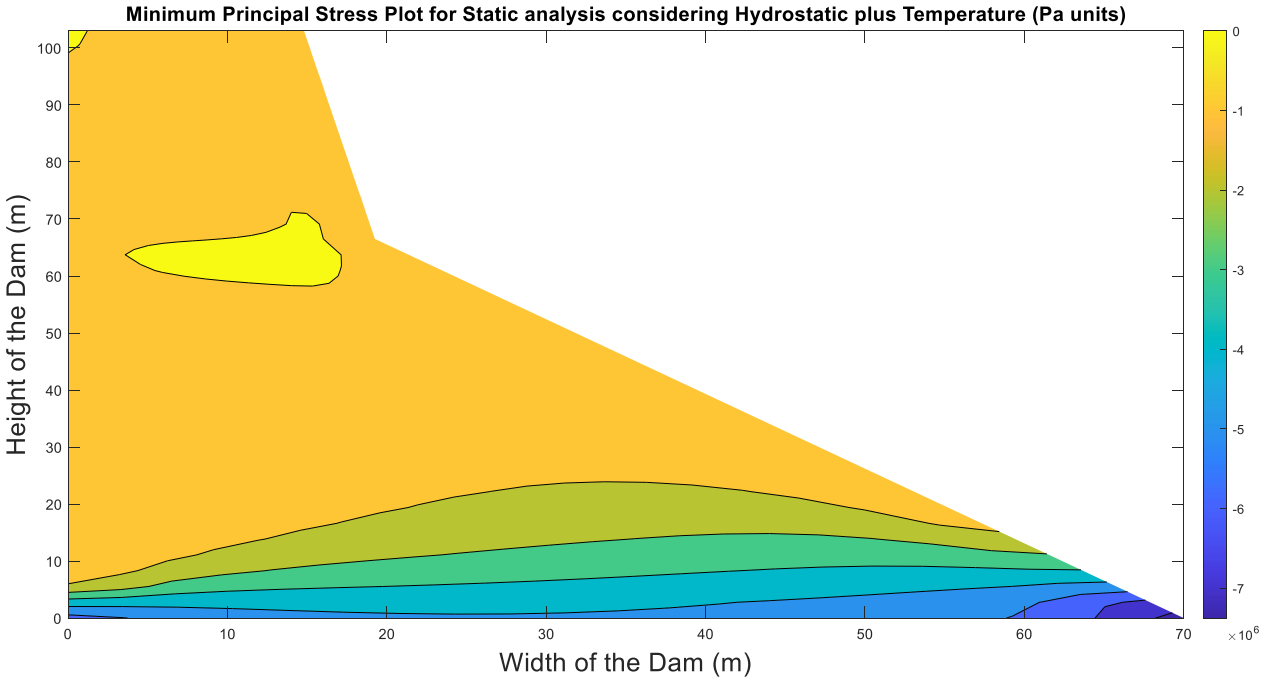

Figure 88: Minimum Principal stress plot for static analysis no AAR effect

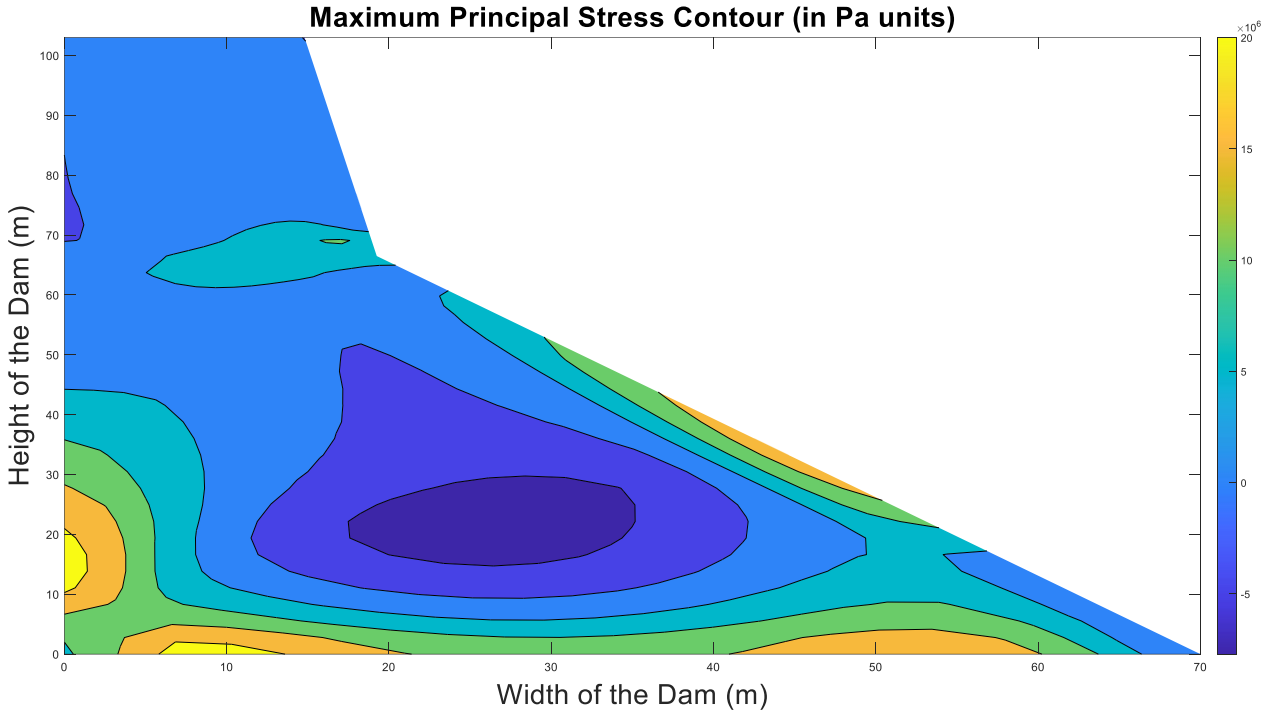

Figure 89: Maximum Principal Stress plot for static analysis with full AAR effect

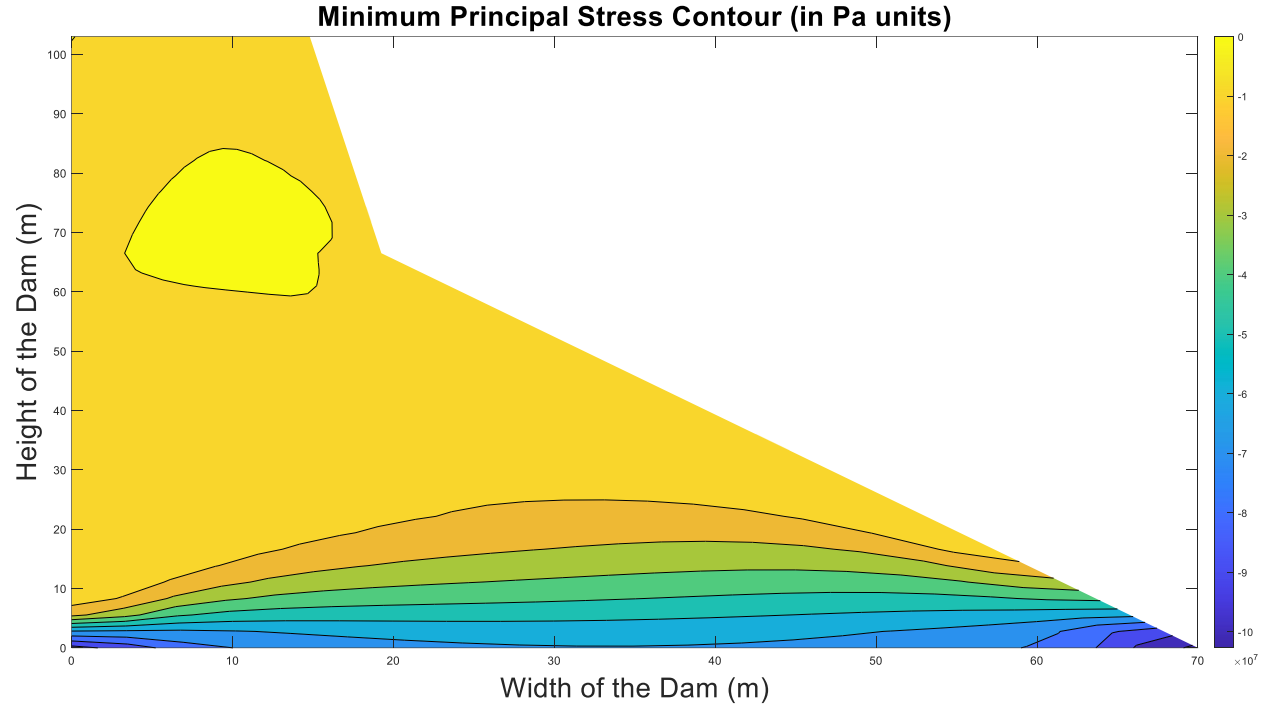

Figure 90: Minimum Principal Stress plot for static analysis with full AAR effect

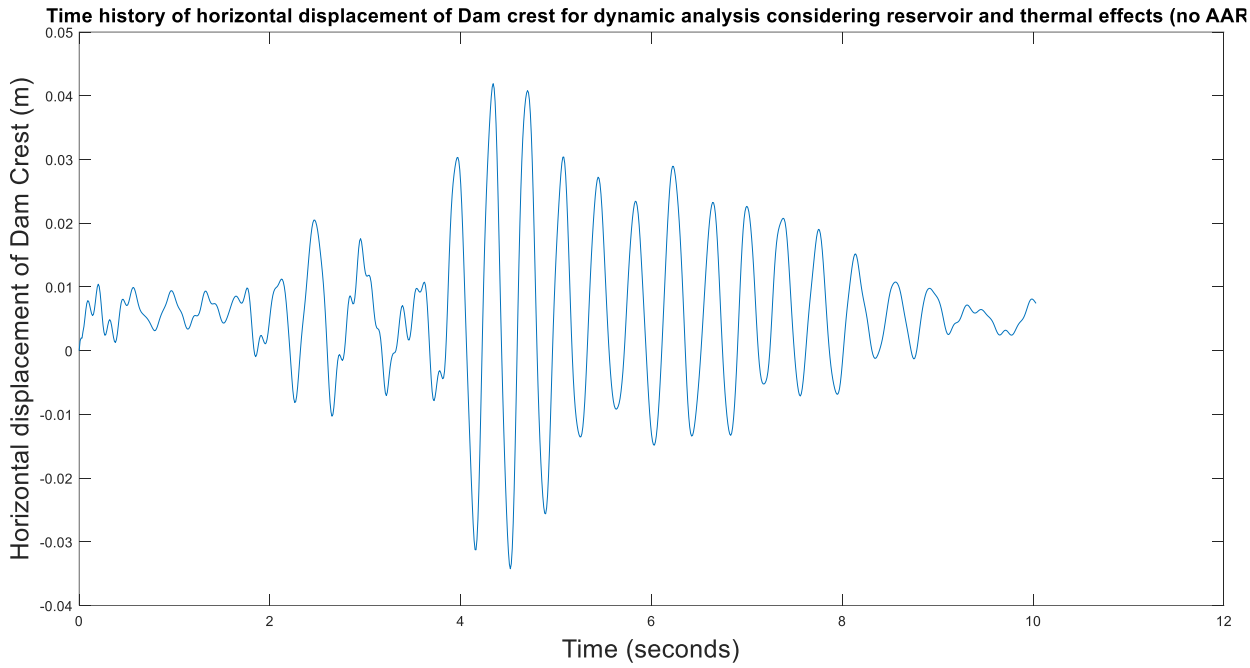

Figure 91: Crest Displacement history for dynamic analysis considering seismic, reservoir and thermal effects without AAR effects

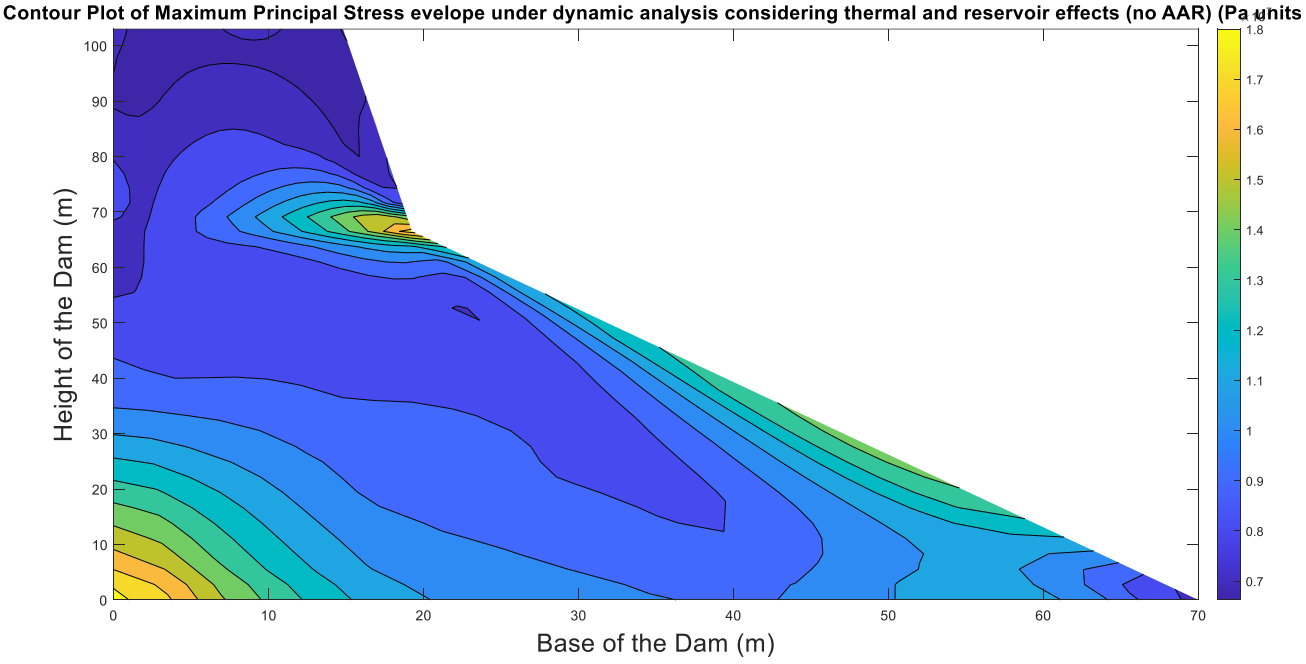

*Figure 92: Contour Plot of Maximum Principal Stress envelope for dynamic analysis considering seismic, thermal and reservoir effects without AAR effects (in MPa *10 units)*

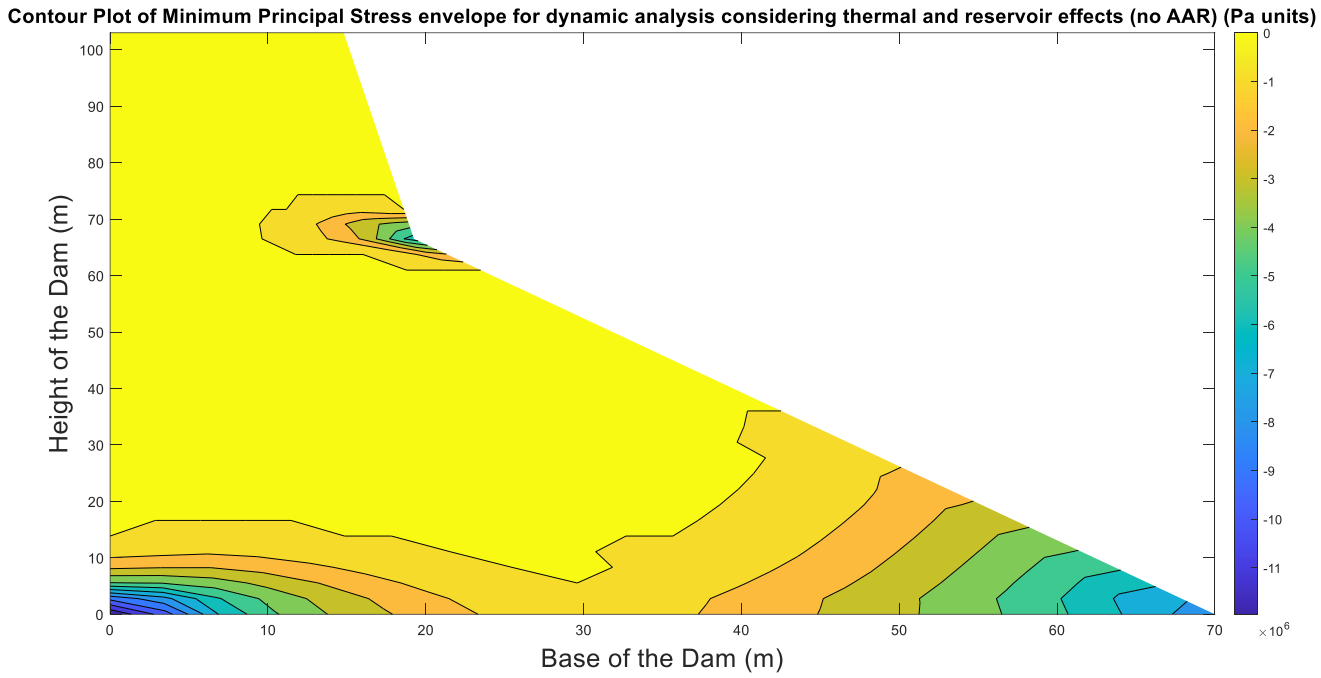

Figure 93: Contour Plot of Minimum Principal Stress envelope for dynamic analysis considering seismic, thermal and reservoir effects without AAR effects (in Pa units)

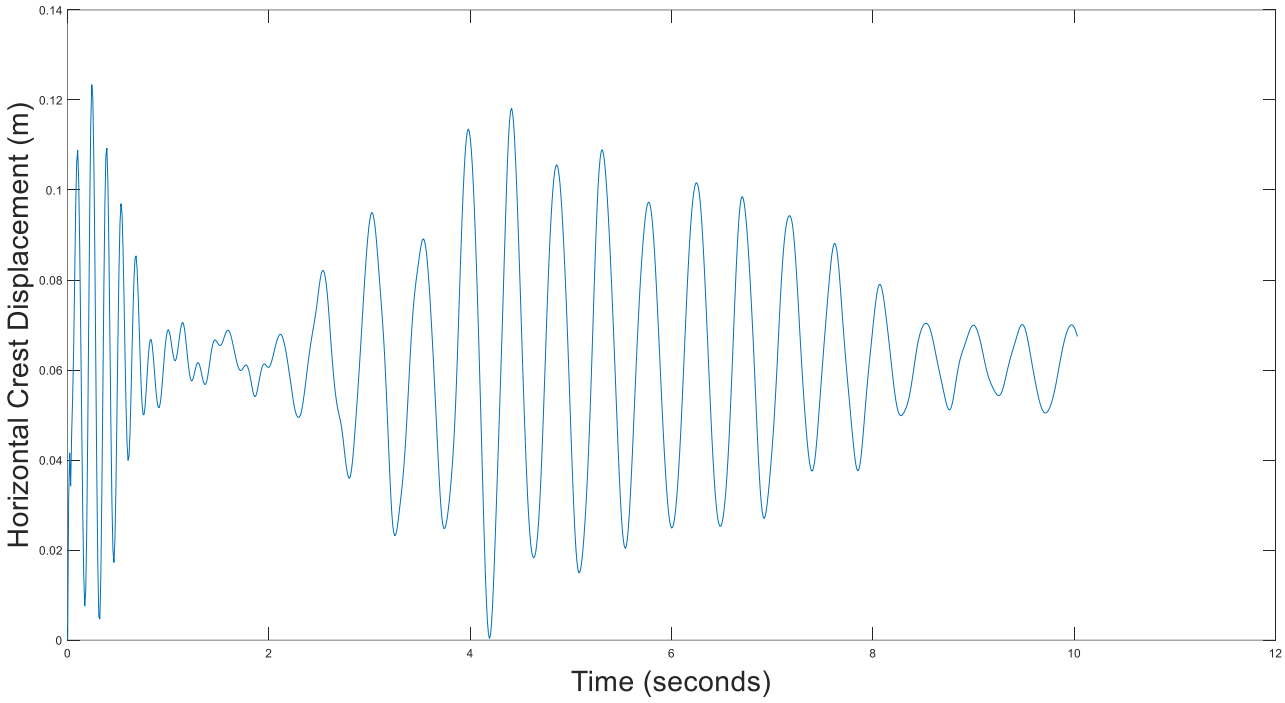

Figure 94: Crest Displacement history for dynamic analysis considering seismic, reservoir and thermal effects with full AAR effects

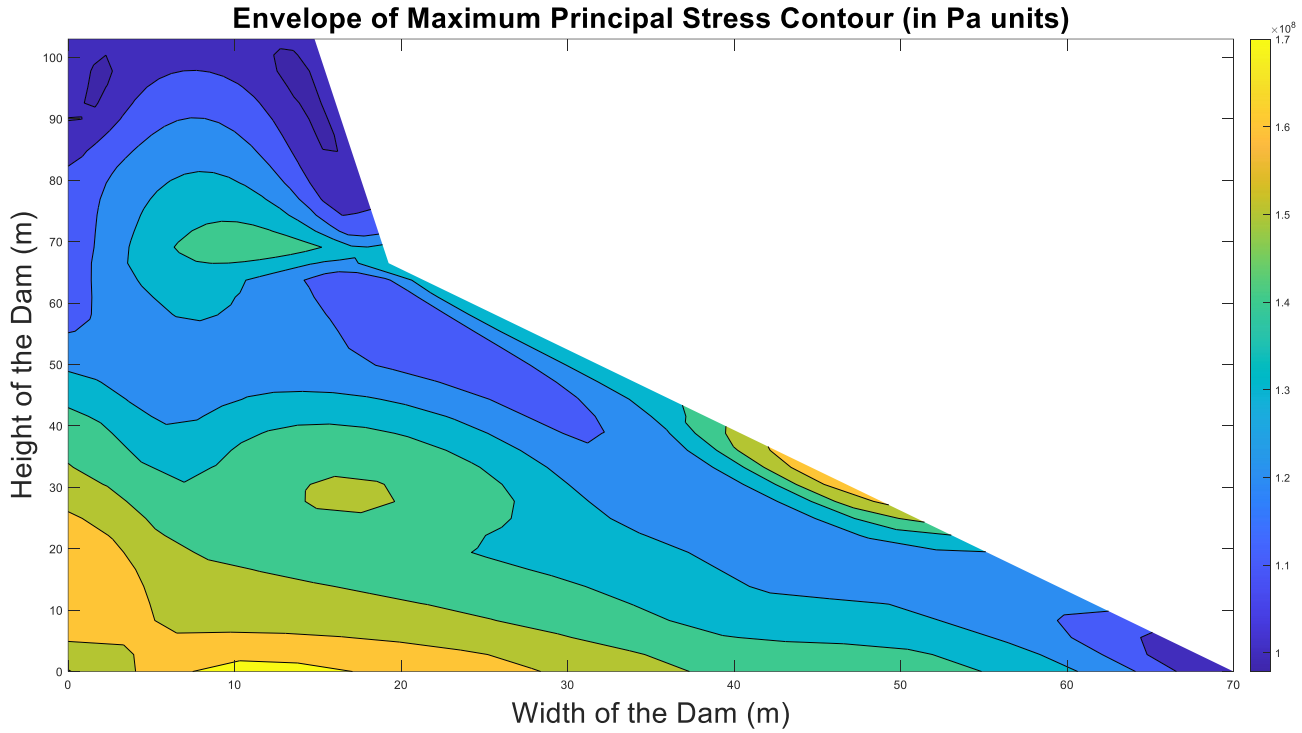

Figure 95: Contour plot of Maximum Principal Stress for dynamic analysis considering seismic, thermal and reservoir effects with full AAR effects (in Pa units)

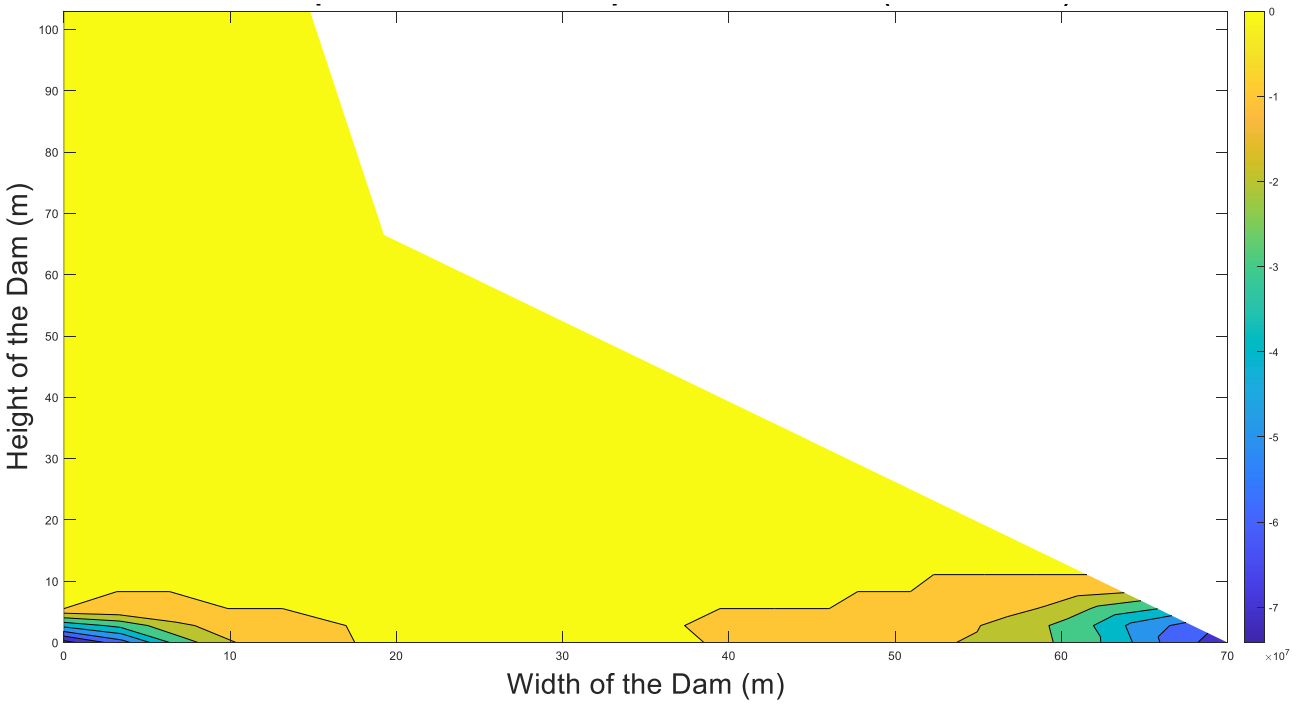

Figure 96: Contour plot of Minimum Principal Stress for dynamic analysis considering seismic, thermal and reservoir effects with full AAR effects (in Pa units)

V. Stepwise progression of AAR effects on the behavior of dam

While the above section showcases a situation where the whole dam body is subjected to the same level of AAR strain effects, the simulations in this section consider differential AAR strains across the dam body based on the differential temperature increase across the body of the dam. Also, in the previous section, only two stages are considered i.e. the nascent state of the dam without any AAR effect and finally, the state where the maximum AAR strain has affected the dam, while in this section, the stepwise progression of AAR strain is taken into consideration.

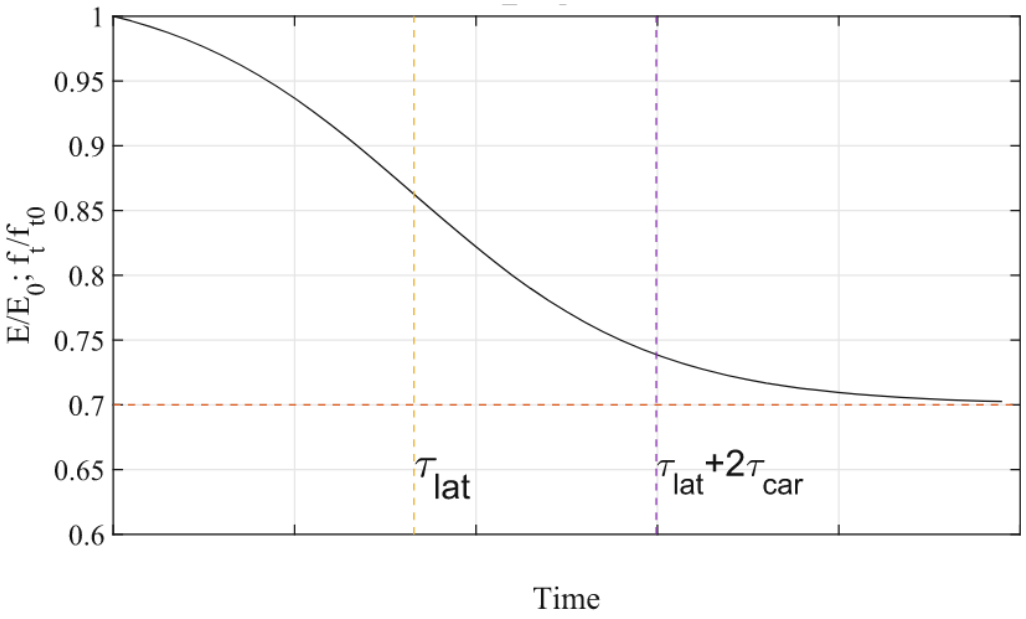

Figure 97: Degradation of material properties due to progression of AAR over time (Saouma et at, 2006)

In this section, four different situations are considered for the stagewise progression of AAR over the dam body. In the first scenario, the dam is affected by 25 percent of the maximum possible AAR strain with the strains varying over the dam body as a function of its temperature. In the second scenario, the maximum strain in the dam body is 50 percent of the maximum possible AAR strain with the strains across the dam body varying as per the temperature distribution of the dam body. In the third and fourth scenarios, the maximum strain in the dam body is considered as 75 percent and 100 percent of the maximum possible AAR strain with the strains in the dam body varying as a function of the temperature of the dam body. The variation of the material properties of the dam are considered as given in Figure 97. The temperature variation across the dam body for the calculation of the AAR strain variation is considered as shown in Figure 86. In all the four cases, dynamic analysis is carried out with seismic ground motions (Figure 47) applied at the base

of the dam. All other forces acting on the dam like thermal, hydrostatic and hydrodynamic as considered in the previous section are also considered for all the analysis performed in this section. The results of the dynamic analysis due to the stagewise progression of AAR over time and the variation of AAR over the dam body as a function of temperature is shown in terms of maximum principal stress contour of the dam body and time history of horizontal crest displacement at each of these four stages. Figure 98 and Figure 99 respectively showcase the plots of horizontal crest displacement history and envelope of maximum principal stress contour of the dam for the first scenario i.e. the maximum strain in the dam body is 25 percent of the maximum possible AAR strain of 0.003 with the strain across the dam body varying as a function of temperature. Similar plots for the other stages i.e. maximum strain values in the dam body reaching 50, 75 and 100 percent of the maximum possible AAR strain are shown in Figures 100-101, Figures 102-103 and Figures 104-105 respectively. While the previous section depicts a theoretical maximum situation where the whole dam body is equally impacted by the maximum possible AAR strain, the results of this section consider more practical scenarios where the impact of AAR strain is considered as a function of the temperature variation of the dam body and helps to evaluate the failure progression of the dam as the impact of AAR increases over time.

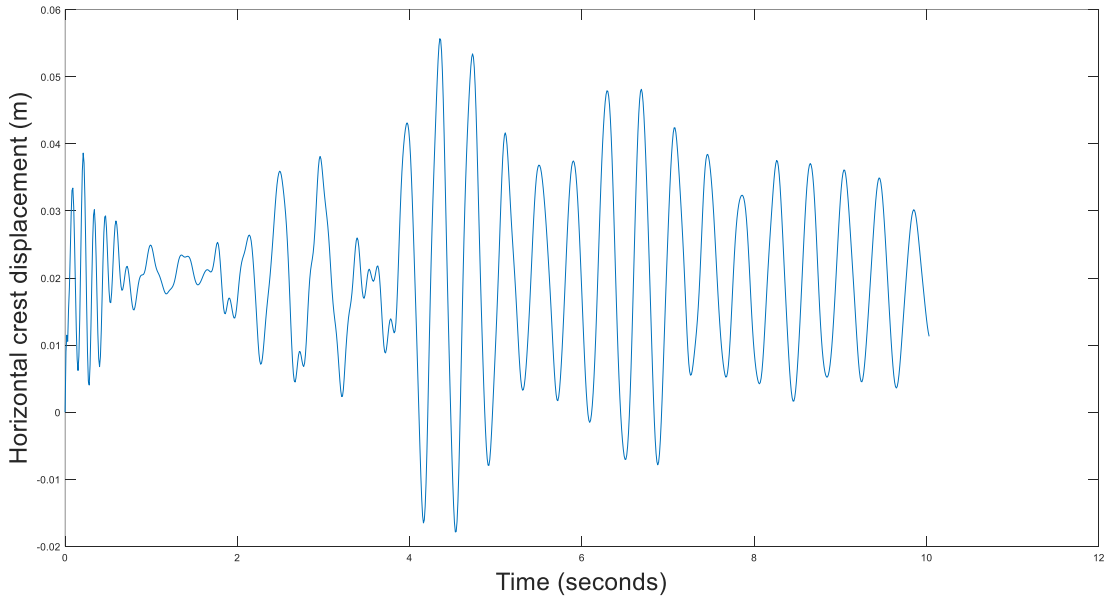

Figure 98: Time history of horizontal crest displacement for dynamic analysis with maximum AAR strain as 25 percent of maximum possible AAR strain

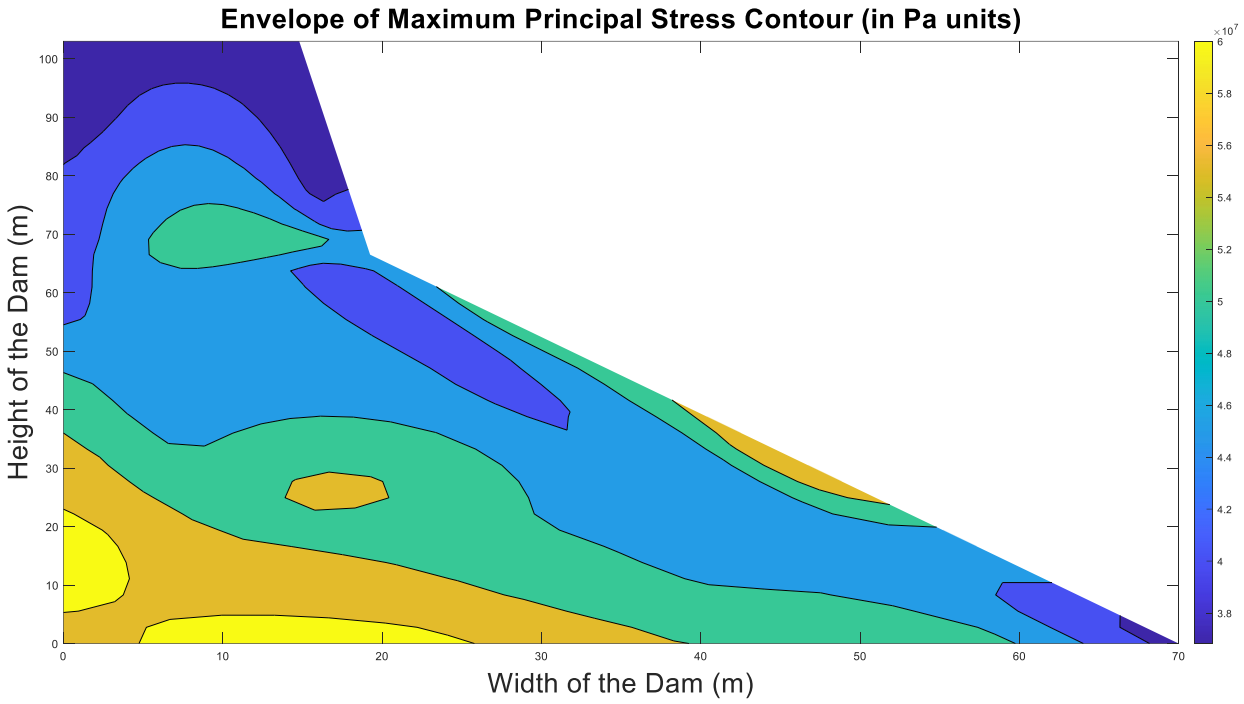

Figure 99: Contour plot of Maximum Principal Stress for dynamic analysis with maximum AAR strain as 25 percent of maximum possible AAR strain (in Pa units)

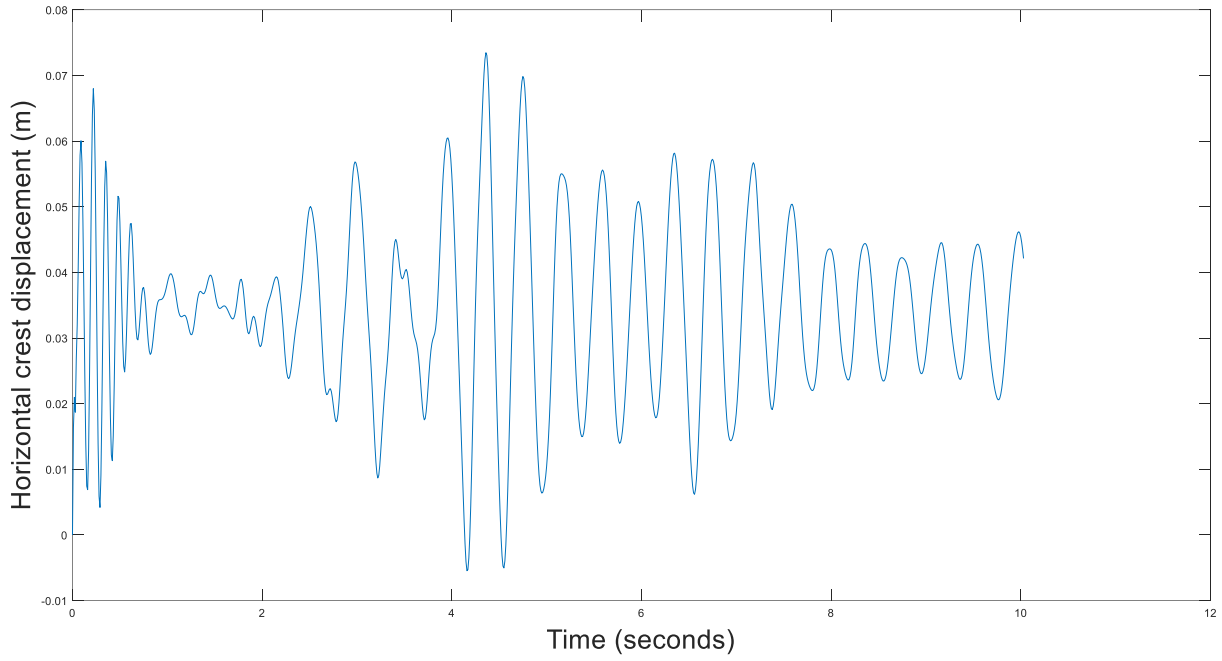

Figure 100: Time history of horizontal crest displacement for dynamic analysis with maximum AAR strain as 50 percent of maximum possible AAR strain

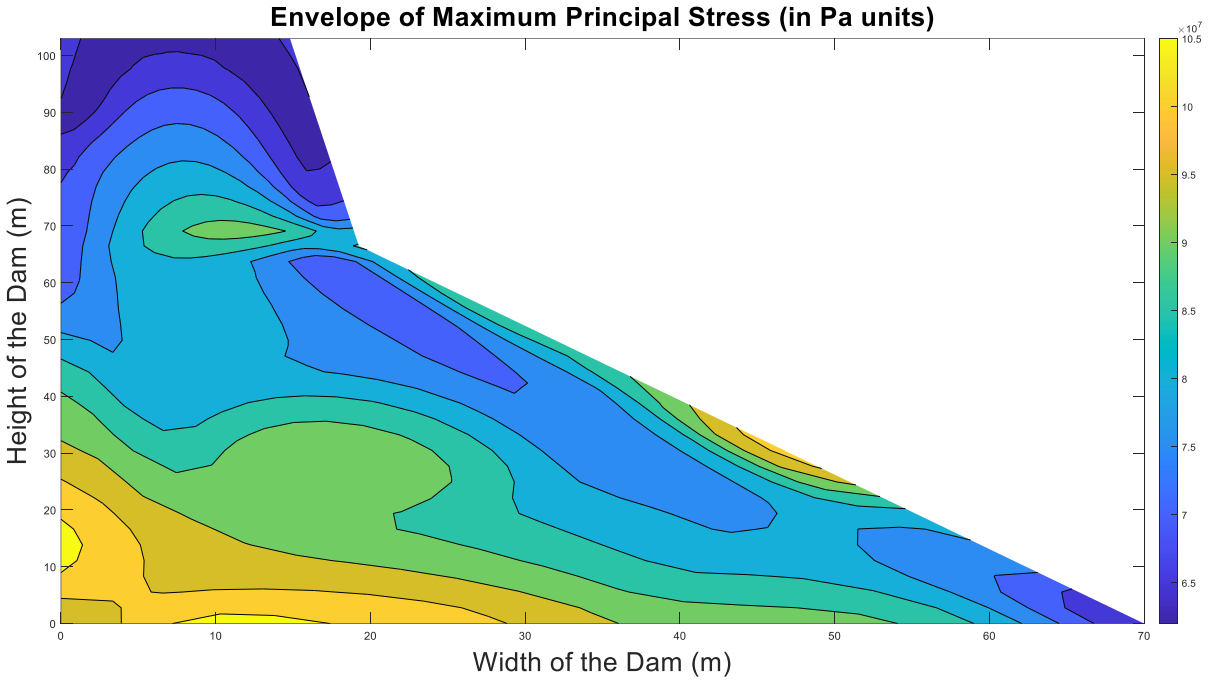

Figure 101: Contour plot of Maximum Principal Stress for dynamic analysis with maximum AAR strain as 50 percent of maximum possible AAR strain (in Pa units)

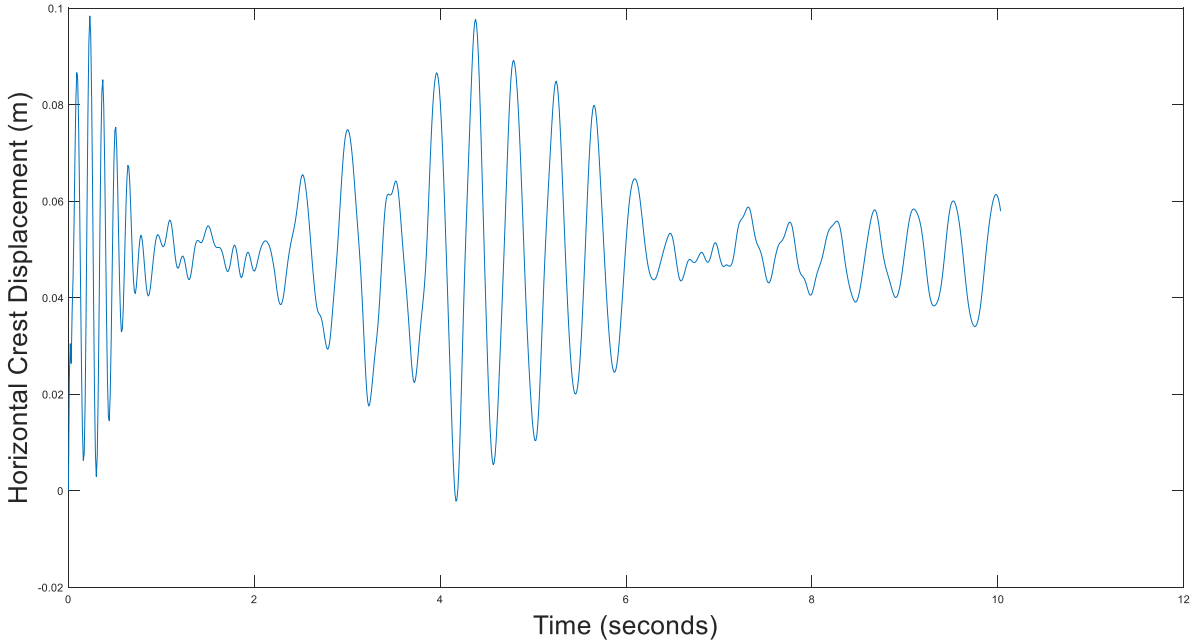

Figure 102: Time history of horizontal crest displacement for dynamic analysis with maximum AAR strain as 75 percent of maximum possible AAR strain

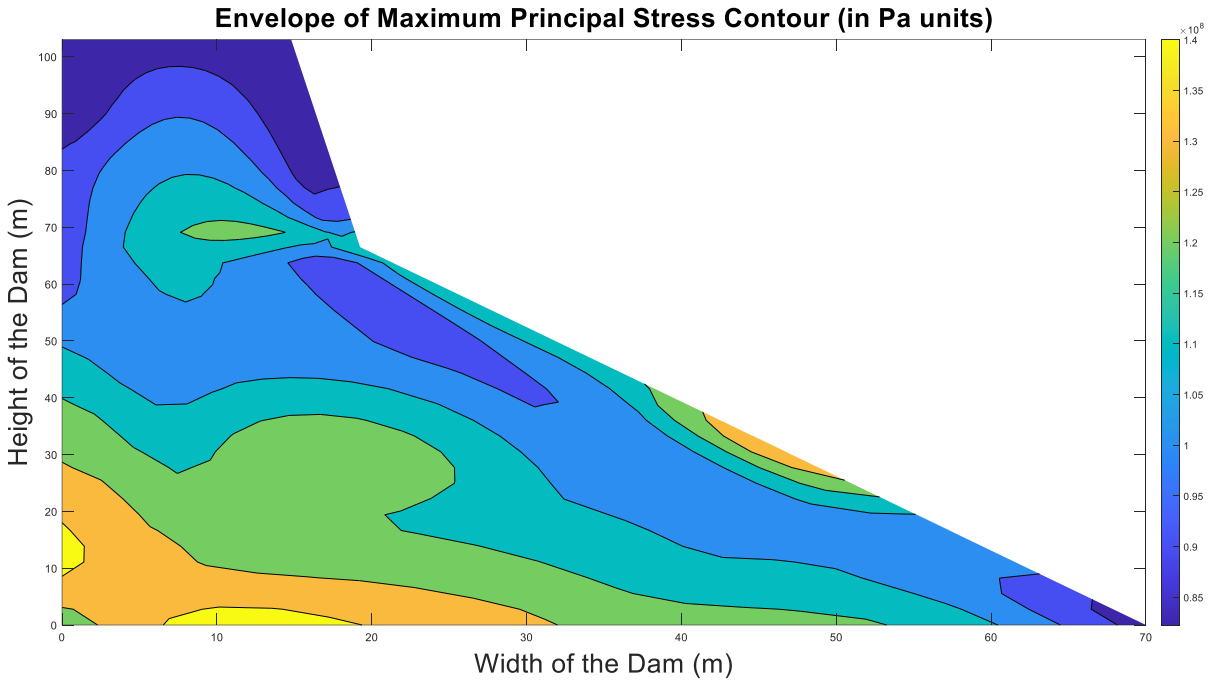

Figure 103: Contour plot of Maximum Principal Stress for dynamic analysis with maximum AAR strain as 75 percent of maximum possible AAR strain (in Pa units)

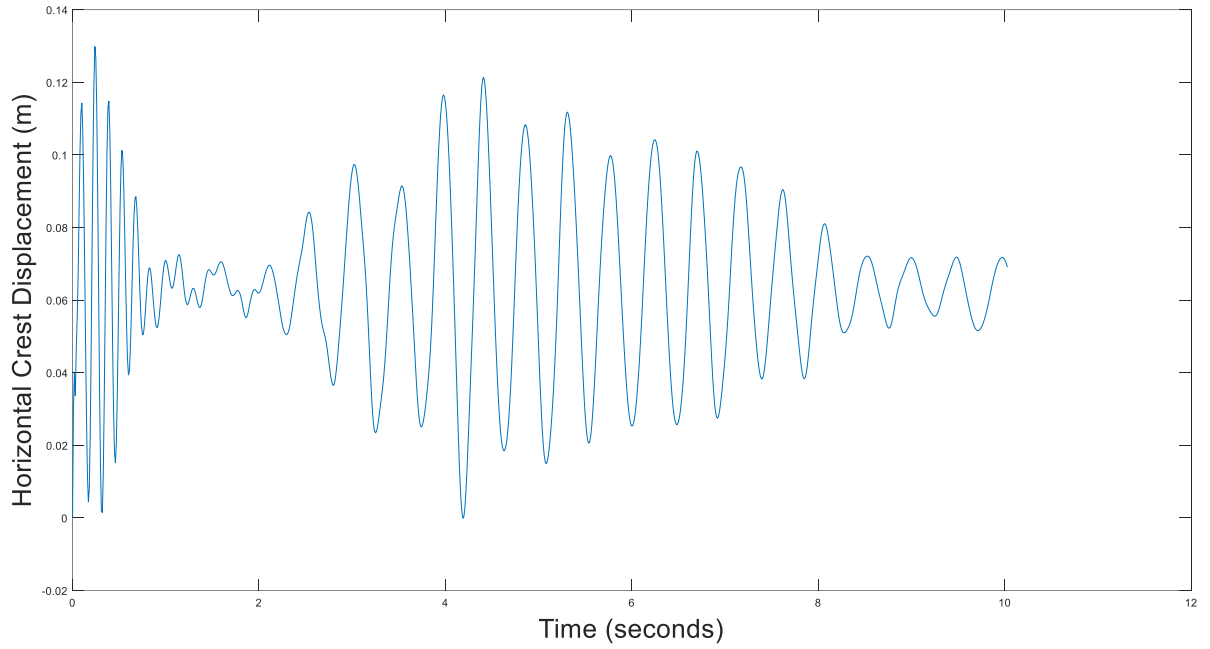

Figure 104: Time history of horizontal crest displacement for dynamic analysis with maximum AAR strain as 100 percent of maximum possible AAR strain

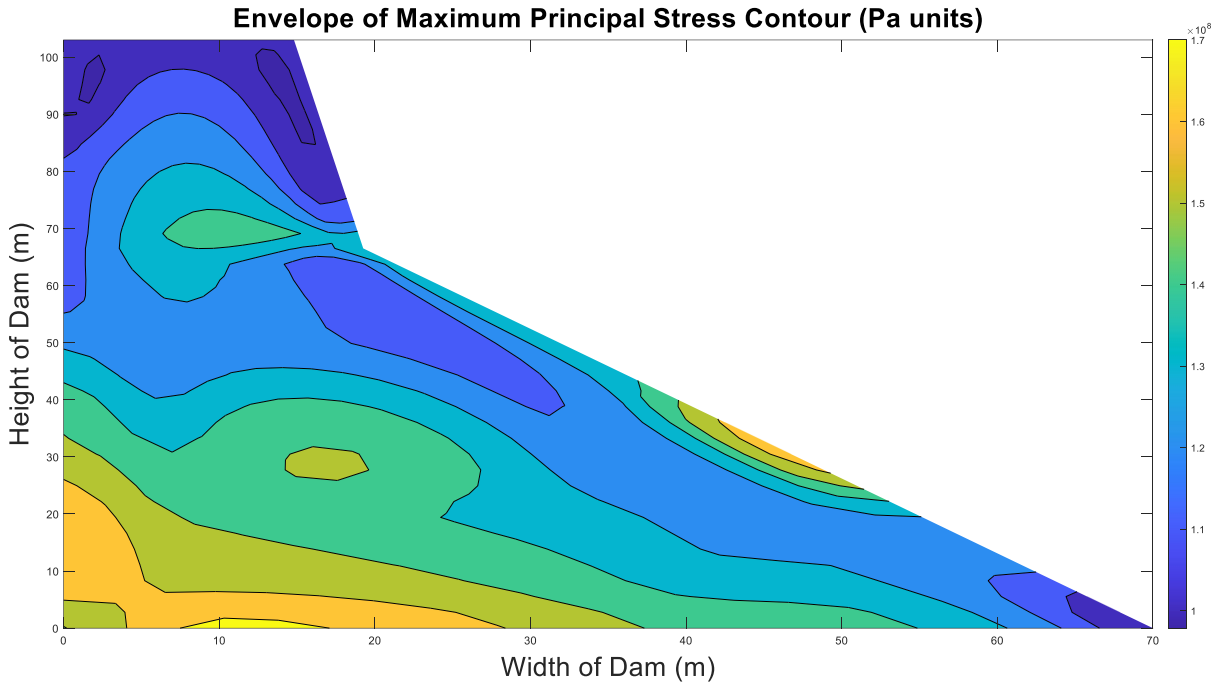

Figure 105: Contour plot of Maximum Principal Stress for dynamic analysis with maximum AAR strain as 100 percent of maximum possible AAR strain (in Pa units)

VI. Discussions, conclusions and summary

Figures 87 and 88 depict the contours illustrating the maximum and minimum principal stresses during static analysis without Alkali-Aggregate Reaction (AAR), while Figures 89 and 90 display the same scenarios with the full impact of AAR considered. Noticeably, stress values are markedly elevated in the presence of AAR. For dynamic analysis, Figure 91 exhibits the temporal evolution of horizontal crest displacement without AAR, whereas Figure 92 illustrates the corresponding scenario with full AAR effects. It is evident that in the presence of AAR, the structural deformation is considerable, with a discernible shift in the displacement baseline from zero, suggesting potential cracks and permanent damage that may warrant investigation through nonlinear analysis. Comparison of principal stresses between scenarios without and with full AAR effects is presented in Figures 93, 94, and 95, 96. Significantly higher stress levels are observed in the AAR case, indicating that the dam's failure could be precipitated by the onset of full AAR effects.

Figures 98 to 105 depict the results of dynamic analysis for the stagewise progression of AAR strain and considering a variation of AAR strain across the dam body as a function of temperature variation of the dam body. These situations depict more practical scenarios of AAR simulation of the dam body compared to the previous case where the whole dam is considered to be uniformly

affected by the maximum AAR strain. Also, the stagewise analysis helps to understand the possible failure pattern of the dam as the AAR strain effect increases over time. Figure 98 shows the maximum displacement to be 55mm at the 25 percent maximum strain level which increases to 73 mm, 96mm and 125 mm respectively for the strain levels of 50, 75 and 100 percent respectively (Figures 100, 102 and 104 respectively). Similar plots for the envelope of maximum principal stress contours are shown in Figures 99, 101, 103 and 105.

In this chapter, a simplified thermo-mechanical approach has been presented to model the effects of alkali-aggregate reactions on large concrete structures like concrete gravity dams. The alkali-aggregate reaction is a complex chemical phenomenon that occurs in concrete structures leading to large cracks and rendering the structure impossible for use without severe retrofitting measures. In dams, this phenomenon has been observed to be often causing failure. While the present literature suggests various complex chemical models based on experimental results to model the alkali-aggregate reactions in structures, those models require complex, rigorous experimental and analytical techniques. Also, as the phenomenon is time and temperature-dependent, there are certain difficulties in simulating the exact field conditions in the laboratory-based experimental setup. The authors have recognized these facts and presented a simple thermo-mechanical analysis approach to determine the effects of alkali-aggregate reactions on dam structures. The authors have used a pseudo-temperature approach to estimate the AAR strains, based on the simple fact that AAR causes mechanical expansion which is also caused by the increase in temperature.

In this chapter, the results show that the considered dam is severely affected by the AAR effects as compared to the results of analysis with no AAR effects. For static as well as dynamic analysis, the stresses in the dam body show that AAR can lead to the failure of the structure. In the dynamic analysis, it is observed that the dam has deformed significantly due to the effects of AAR and maximum displacements and stresses are detrimental and failure of the dam is caused. In this chapter, at first, two stages of analysis are considered- an initial stage without the onset of AAR effects and a final stage when the full AAR effects have set in. In a more detailed study, stepwise analysis is considered to note the progression of AAR effects on the dam body over time. Also, the variation of AAR over the dam body is considered as a function of the temperature.

CHAPTER 8: SUMMARY, CONCLUSIONS AND SCOPE OF FUTURE WORK

I. Summary

This thesis provides an alternative finite element-based modeling technique for numerical analysis of large structures like concrete gravity dams. By the literature review, it is concluded that the most commonly used methods of dynamic analysis and damage detection based on changes in modal parameters have certain inherent shortcomings. Also, the finite element method as an analysis tool has the requirement of very fine mesh size in problems of dynamics and thus, computationally inefficient in terms of space and time. This thesis presents FEM-based alternative computational methods for dynamic analysis of two-dimensional structures. The methods reviewed here include the two most common SFEM methods found in literature- frequency or Fast Fourier Transform (FFT) based spectral finite element (FDSFEM) and time domain based spectral finite element method (TDSFEM). From the discussion, the TDSFEM is considered more suitable than the FDSFEM for application to dynamic analysis of structures with any arbitrary geometry and boundary conditions. A set of MATLAB based programs were developed to demonstrate the computational efficiency of the TDSFEM for dynamic analysis of large structures (validation studies have been performed using a simply supported beam and the Pine Flat concrete gravity dam (U.S.A)). For the present study, a benchmark structure has been considered i.e., the Koyna Dam (India) and its geometric and material properties used to validate the results with available literature (Chopra & Chakrabarti (1973), Bhattacharjee & Leger (1993), Tidke et al (2022)). However, the developed codes could be adopted for any two-dimensional structure.

The significant reduction of computation time in the TDSFEM (due to diagonalization obtained by using the GLL integration points) compared to the conventional FEM demonstrates that this method could be successfully implemented for dynamic analysis of large structures with a similar level of accuracy as demonstrated in the results of modal analysis and dynamic time history analysis. The performance of TDSFEM considering higher order elements is particularly beneficial as the accuracy is same as conventional FEM with significant reduction of computational time. Thus, the results of the study demonstrate the suitability of considering higher

order TDSFEM elements as a viable alternative to the conventional FEM for the dynamic analysis of large structures.

The foundation has been modeled using infinite elements using both FEM and proposed TDSFEM-based technique. The use of infinite elements using TDSFEM for foundation modeling is an advancement in this domain. The modeling of dam-foundation-reservoir system as a whole has also been taken up leading to the saving in computational time (as the size of matrix solved is even greater than the dam with fixed base case).

Damage identification and localization has been performed using modal parameters and it has been observed that modal strain energy is the most effective modal parameter for accurate determination of presence of damage in a structure and its location.

Non-linear analysis of Koyna Dam has been performed considered material nonlinear behavior as an extension of the linear analysis. The proposed TDSFEM-based formulation has been further improved by including material nonlinearity suitable to concrete structures. While linear analysis is an important step which helps in understanding the structural behavior, the result of nonlinear analysis is deemed more realistic behavior of the structure. As the nonlinear analysis is numerically more rigorous, the saving in computation time is even more advantageous which has been demonstrated.

As a part of the verification study, a concrete beam from literature was modelled and analyzed for static loads, modal analysis of a dam was performed, and nonlinear static analysis of a concrete deep beam was conducted. The failure modes of FRP reinforced concrete deep beams have been numerically simulated using pseudo static analysis performed using the time domain based spectral finite element method. These results have been validated against experimental investigations previously conducted at the Structural Engineering Laboratory of Concordia University. This is a novel attempt to model FRP reinforced concrete deep beams using the time domain based spectral finite element method.

A benchmark concrete gravity dam, namely the Koyna Dam has been used as a case study to demonstrate the methods developed in this thesis. Both linear and nonlinear dynamic analysis was performed using the recorded ground motion at the dam site. In order to model the deterioration

effects of concrete gravity dams caused by AAR, a simplified thermo-mechanical approach has been developed. Results show the possible failure zones of a dam affected by AAR.

II. Conclusions

The main findings of the study can be summarized as:

1) The conventional FEM requires considerable computation time for dynamic analysis of large structures. TDSFEM is found to be comparatively more efficient, and it consumes much less amount of time for the analysis, and provides reasonable accuracy, especially when higher order elements are used. In the case of linear dynamic analysis, time of computation is reduced by 60 percent in case of TDFSEM in comparison to conventional FEM. It needs to be pointed out here that all the computations in this study are performed using an ordinary personal computer with an Intel Core i5 8^{th} Gen @1.87GHz CPU and 4GB memory.
2) Both the modal analysis and time history analysis results show a similar level of computational efficiency of TDSFEM over the conventional FEM,
3) The computational efficiency of TDSFEM is also demonstrated when the whole dam-foundation-reservoir model is considered for dynamic analysis. Due to the global matrices' sizes getting bigger in this case, the advantage of computational time saving is even better realized.
4) The vibration-based damage identification and localization shows that modal strain energy is a better indicator of damage location than the modal parameters like modal displacement and modal curvature.
5) The results of dynamic analysis using material non-linear behavior show a better representation of the performance of the structure when subjected to seismic ground motion and the actual stress levels of the dam and failure zones are identified even better than linear dynamic analysis. In case of non-linear analysis, the system of equations need iterations to be performed while solving, thus the time of computation becomes even more critical and TDSFEM provides saving in computation time in each step.
6) The results of dynamic analysis using material non-linear behavior show the potential permanent lateral displacement of the dam body subjected to seismic ground motion.

7) The saving in computation time using TDSFEM for non-linear dynamic analysis in comparison FEM is even higher as the procedure requires iterative solution techniques at each step in solving the matrix equations of motion.
8) Alkali-Aggregate reaction is a severe issue in the case of concrete structure and causes severe material degradation. A simplified thermos-mechanical analysis using TDSFEM to model the effects of AAR shows that the dam undergoes severe deformations and is susceptible to complete failure under the combined impact of seismic ground motion and AAR effects.

III. Scope for future research

The scope of future work includes system identification, damage detection, uncertainty quantification of large structures using the TDSFEM. It needs to be pointed out here that the adopted methodology in this work can also be extended to 3D structures with complex geometry. In the case of three-dimensional modeling of dams, the computational efficiency achieved by TDSFEM methodology could lead to enormous saving of computation time. In this thesis, the reservoir has been modeled using the simplified method while this can be further modeled using acoustic elements for better prediction of the dam behavior. Non-linear analysis has been performed in this thesis using the concrete damage plasticity model, which is a widely used nonlinear material model for concrete nonlinear behavior, however, it cannot capture the crack mechanics and crack propagation in structures. Thus, more advanced crack propagation modeling techniques could be implemented with the TDSFEM framework for better prediction of crack generation in structures subjected to dynamic loading. In this thesis, the whole work has been done using developed codes in MATLAB for the time domain based spectral finite element method, as it is not available in commercial software packages. In future, element subroutines can be developed in powerful commercial software packages and time domain spectral finite element can be incorporated into their modules. This would enable the range of operations which are available in the software packages to be implemented using TDSFEM and its numerical efficiency could be fully utilized for a varied range of analysis. The simplified methodology developed for AAR analysis in the case of dams can be extended to more complicated analysis using TDSFEM. In that, the other material deterioration effects like ageing can also be considered. Also, geometric and contact nonlinearity could be considered along with material nonlinearity. While the above aspects are out of the scope of the present work, they will be considered in the future.

REFERENCES

A. C. I. Committee, “Guide to durable concrete,” American Concrete Institute, 2001.

Abaqus Example Problems Guide, Abaqus online documentation 6.14, Simulia, Dassault Systèmes, Vélizy-Villacoublay, France Web source: http://abaqus.software.polimi.it/v6.14/books/exa/default.htm.

Bagchi, A., Humar, J. and Noman, A. 2007, “Development of a Finite Element System for Vibration Based Damage Identification in Structures”, *Journal of Applied Sciences,* **7**(17): 2404-2413.

Bagchi, S., Roy, T. B., & Bagchi, A. (2019, June). Multiple damage localization of gravity dam: Strain energy-based approach using random data. In *Proceedings, Annu. Conf.-Can. Soc. Civ. Eng*.

Bagchi, Saikat & Roy, Timir & Bagchi, Ashutosh. (2019). Multiple damage localization of gravity dam: strain energy-based approach using random data.

Balla, Taraka MR, S. Suriya Prakash, and Amirtham Rajagopal. "Role of size on the compression behaviour of hybrid FRP strengthened square RC columns–Experimental and finite element studies." *Composite Structures* 303 (2023): 116314.

Bhattacharjee, S.S. and Léger, P. (1993), Seismic cracking and energy dissipation in concrete gravity dams. *Earthquake Engineering and Structural Dynamics.*, 22: 991-1007. https://doi.org/10.1002/eqe.4290221106

Bhatti, M. A. (2005). Fundamental finite element analysis and applications: with Mathematica and Matlab computations.

Boudaa, S., Khalfallah, S., & Hamioud, S. (2019). Dynamic analysis of soil structure interaction by the spectral element method. *Innovative Infrastructure Solutions*, 4, 1-8.

Bukenya, P., P. Moyo, H. Beushausen, and C. Oosthuizen. 2014. “Health monitoring of concrete dams: a literature review.” *Journal of Civil Structural Health Monitoring*, 4(4):235-244.

Çağlar, N. M., & Şafak, E. (2019). Application of spectral element method for dynamic analysis of plane frame structures. *Earthquake Spectra*, 35(3), 1213-1233.

Cawley, P., & Adams, R. D. (1979). The location of defects in structures from measurements of natural frequencies. The Journal of Strain Analysis for Engineering Design, 14(2), 49-57.

Cervera, M., J. Oliver, and O. Manzoli, "A Rate-Dependent Isotropic Damage Model for the Seismic Analysis of Concrete Dams," *Earthquake Engineering and Structural Dynamics*, vol. 25, pp. 987–1010, 1996

Cheng, L., Yang, J., Zheng, D., Li, B. and Ren, J. 2015. The health monitoring method of concrete dams based on ambient vibration testing and kernel principle analysis. *Shock and Vibration*, *Hindawi Publishing Corporation*, 1-11, Article ID: 342358.

Chopra AK, Chakrabarti P. Earthquake response of concrete gravity dams including hydrodynamic foundation interaction effects, UCB/EERC–80/01Report, University of California, Berkeley, USA, 1980.

Chopra, A. K., & Chakrabarti, P. (1973). The Koyna earthquake and the damage to Koyna dam. *Bulletin of the Seismological Society of America*, *63*(2), 381-397.

Chróścielewski, J., Rucka, M., Wilde, K., & Witkowski, W. (2009). Formulation of spectral truss element for guided waves damage detection in spatial steel trusses. *Archives of Civil Engineering*, 55(1), 43-63.

Comi, C., Fedele, R., & Perego, U. (2009). A chemo-thermo-damage model for the analysis of concrete dams affected by alkali-silica reaction. *Mechanics of materials*, *41*(3), 210-230.

Cormen, T. H., Leiserson, C. E., Rivest, R. L., & Stein, C. (2001). Introduction to algorithms second edition. *The Knuth-Morris-Pratt Algorithm*.

D. Systèmes, "Abaqus analysis user's guide, version 6.14." Dassault Systèmes, 2014. [Online]. Available: http://130.149.89.49:2080/v6.14/

de Larrard, T., & Duprat, F. (2015, May). Structural damage prediction of an AAR affected dam. In *CIGOS (Congrès International de Géotechnique-Ouvrages-Structures)*.

Doebling, S. W., Farrar, C. R., & Prime, M. B. (1998). A summary review of vibration-based damage identification methods. Shock and vibration digest, 30(2), 91-105.

Doyle, J. F. and Farris, T. N. (1990), "A spectrally formulated finite element for flexural wave propagation in beams", *Int. J. of Analytical and Experimental Modal Analysis*, 99-107.

Doyle, J.F. (1997) Wave Propagation in Structures: Spectral Analysis Using Fast Discrete Fourier Transforms, 2nd edn, Springer-Verlag, New York.

Droz, P., Vallotton, O., Menouillard, T., & Leroy, R. (2013). Slot cutting an AAR-affected dam: case study of the Salanfe dam. *Hydropower and Dams*, 4.

Fan, W., & Qiao, P. (2011). Vibration-based damage identification methods: a review and comparative study. Structural health monitoring, 10(1), 83-111.

Feltrin, G., Galli, M. and Bachmann, H. (1992). "Influence of Cracking on the Earthquake Response of Concrete Gravity Dams with Reservoir", *Proceedings of the Tenth World Conference on Earthquake Engineering, Madrid, Spain, Vol. 8, pp. 4627–4632.*

Garabedian, A., Bagchi, A., Joshi, A. and Dong, J. (2006b), "Developing an Intelligent System for Modelling the Dam Behaviour Based on Statistical Pattern Matching of Sensory Data", *ASCE/ICCCBE-XI Conference, Montreal, May.*

Garabedian, A., Bagchi, Joshi, A., Dong, J., Harffort, D., Scott, D. and Thai, T.M. (2006a), "Monitoring the Dam Behaviour using Innovative Approaches based on Linear and Nonlinear Techniques", *Annual Conference of Canadian Dam Association (CDA 2006), Quebec City, September.*

Ghanaat, Yusof. "Failure Modes Approach to Safety Evaluation of Dams." 13th World Conference on Earthquake Engineering Vancouver, B.C., Canada, no. Paper No. 1115 (August 1, 2004): 15

Ginsberg, J.H. (2001) An Introduction to Random Vibrations, Spectral and Wavelet Analysis, Addison Wesley Longman Ltd, Essex.

Gopalakrishnan, S., Martin, M. and Doyle, J.F., 1992. A matrix methodology for spectral analysis of wave propagation in multiple connected Timoshenko beams. *Journal of Sound and Vibration*, *158*(1), pp.11-24.

Grassl, P. "On a damage-plasticity approach to model concrete failure". *Engineering and Computational Mechanics*. Volume 162, Issue 4, pp. 221-231, 2009.

Hafeez, M. B., & Krawczuk, M. (2023). A Review: Applications of the Spectral Finite Element Method. *Archives of Computational Methods in Engineering, 30(5), 3453-3465.*

Hamioud, S. (2021). Dynamic Analysis of Soil-Structure Interaction Using the Spectral Element Method (Doctoral dissertation).

He, S., & Ng, C. T. (2017). Guided wave-based identification of multiple cracks in beams using a Bayesian approach. *Mechanical Systems and Signal Processing, 84, 324-345.*

Hildebrandt, F.B. Introduction to Numerical Analysis, McGraw-Hill Book Company Inc., 1956

Hughes, T.J.R. The Finite Element Method: Linear Static and Dynamics Finite Element Analysis, Dover Publications, Inc., New York, 2000

Humar, J. Bagchi, A. and Xu, H. 2006, "Performance analysis of vibration based techniques for structural damage identification", *Structural Health Monitoring –International Journal*, **5**(3):215-227

Humar, J. L., Bagchi, A., & Xia, H. (1998). Frequency domain analysis of soil-structure interaction. *Computers & Structures*, *66*(2-3), 337-351.

Humar, J.L. (2001) Dynamics of Structures, A.A. Balkema Publishers, Lisse.

ICOLD, "World Register of Dams." Accessed: Sep. 29, 2023. [Online]. Available: https://www.icold-cigb.org/GB/world_register/general_synthesis.asp

In *International Conference on Experimental Vibration Analysis for Civil Engineering Structures* (pp. 623-631). Cham: Springer Nature Switzerland.

Jin, G., Ma, X., Liu, Z., & Xuan, L. (2017). Dynamic analysis of general rotationally symmetric built-up structures using a modified fourier spectral element approach. *Journal of Vibration and Acoustics*, 139(2), 021012.

Kim, T., & Lee, U. (2017). Dynamic analysis of a multi-span beam subjected to a moving force using the frequency domain spectral element method. *Computers & Structures*, *192*, 181-195.

Kolousek, V. (1941) Anwendung des gesetzes der virtuellen verschiebungen und des reziprozitatssatzes in der stabwerksdynamic. Ingenieur Archiv, 12, 363–370.

Komatitsch, D., & Tromp, J. (1999). Introduction to the spectral element method for three-dimensional seismic wave propagation. *Geophysical journal international*, *139*(3), 806-822.

Komatitsch, D., & Tromp, J. (2002). Spectral-element simulations of global seismic wave propagation—I. Validation. *Geophysical Journal International*, *149*(2), 390-412.

Komatitsch, D., Erlebacher, G., Göddeke, D., & Michéa, D. (2010). High-order finite-element seismic wave propagation modeling with MPI on a large GPU cluster. *Journal of computational physics*, *229*(20), 7692-7714.

Krawczuk, M. (2002). Application of spectral beam finite element with a crack and iterative search technique for damage detection. *Finite Elements in Analysis and Design*, 38(6), 537-548

Kudela, P., & Ostachowicz, W. (2009, August). 3D time-domain spectral elements for stress waves modelling. In *Journal of Physics: Conference Series* (Vol. 181, No. 1, p. 012091). IOP Publishing.

Kudela, P., Żak, A., Krawczuk, M., & Ostachowicz, W. (2007). Modelling of wave propagation in composite plates using the time domain spectral element method. *Journal of Sound and Vibration*, 302(4-5), 728-745.

L. Holman, "Does this Dam Have a Future? Taking a Closer Look at the Mactaquac Dam," NiCHE. Accessed: Mar. 06, 2024. [Online]. Available: https://niche-canada.org/2016/01/25/does-this-dam-have-a-future-taking-a-closer-look-at-the-mactaquac-dam/

Latosh, A., Rashid, A.R. and Bagchi, A., (2018). "Non-Linear Analysis of Concrete Deep Beams Reinforced with FRP", 3rd International Conference on Civil, Structural and Transportation Engineering (ICCSTE'18), Niagara Falls, Canada – June 10 – 12, 2018, Paper ID-150

Latosh, Fawzi. "Structural behaviour of conventional and FRP-reinforced concrete deep beams." PhD diss., Concordia University, 2014.

Lee, J., and G. L. Fenves, "A Plastic-Damage Concrete Model for Earthquake Analysis of Dams," *Earthquake Engineering and Structural Dynamics*, vol. 27, pp. 937–956, 1998.

Lee, J., & Fenves, G. L. (1998). Plastic-damage model for cyclic loading of concrete structures. Journal of engineering mechanics, 124(8), 892-900.

Lee, J., & Lee, U. (1996). Spectral element analysis of the structure under dynamic distributed loads. *In 37th Structure, Structural Dynamics and Materials Conference (p. 1494).*

Lee, U. (2000). Vibration analysis of one-dimensional structures using the spectral transfer matrix method. *Engineering structures*, 22(6), 681-690.

Lee, U. (2009). *Spectral element method in structural dynamics*. John Wiley & Sons.

Léger, P. Reducing the Earthquake Induced Damage and Risk in Monumental Structures: Experience at Ecole. Natural Hazards in Dynamics of Structures, Springer, 285-309 (2007).

Leung, A.Y.T. (1993) Dynamic Stiffness and Substructures, Springer-Verlag, London.

Lubliner, J., Oliver, J., Oller, S. and Onate, E., 1989. A plastic-damage model for concrete. *International Journal of solids and structures*, 25(3), pp.299-326.

Malleswara Rao, Balla Taraka, and S. Suriya Prakash. "Shape effects on the behavior of hybrid FRP–strengthened rectangular RC columns under axial compression." *Journal of Composites for Construction* 25, no. 5 (2021): 04021042.

Matlab, 2021 "Math. Graphics. Programming", Mathworks Inc., https://www.mathworks.com/products/matlab.html, last cited April 5, 2021

Mitra, M., & Gopalakrishnan, S. (2005). Spectrally formulated wavelet finite element for wave propagation and impact force identification in connected 1-D waveguides. *International journal of solids and structures*, 42(16-17), 4695-4721.

Mohammadpour, S. (2017). Numerical Simulation for the Mechanical Behaviors of a Concrete Dam with Consideration of Alkali-Aggregate Reaction.

Narayanan, G.V. and Beskos, D.E. (1978) Use of dynamic influence coefficients in forced vibration problems with the aid of fast fourier transform. Computers & Structures, 9 (2), 145–150.

Nayak, A. N., R. B. Swain, G. N. Prajapati, and S. Swetapadma Palanichamy. "Strengthening of square RC columns using externally bonded FRP sheets." In *Proc. of the Second Intl. Conf. on Advances In Civil, Structural and Mechanical Engineering-CSM*, pp. 21-25. 2014.

Newland, D.E. (1993) An Introduction to Random Vibrations, Spectral and Wavelet Analysis, 3rd edn, Addison Wesley Longman Ltd, Essex.

Ng, C. T., Veidt, M., Lam, H. F. (2009): “Guided wave damage characterization of beams using probabilistic optimization”, *Engineering Structures*, 31 (12), 2842-2850

Ostachowicz, W., Kudela, P., Krawczuk, M., & Zak, A. (2011). Guided waves in structures for SHM: the time-domain spectral element method. John Wiley & Sons.

Palacz, M. (2018). Spectral methods for modelling of wave propagation in structures in terms of damage detection—a review. *Applied Sciences*, 8(7), 1124.

Palacz, M., & Krawczuk, M. (2002). Analysis of longitudinal wave propagation in a cracked rod by the spectral element method. Computers & structures, 80(24), 1809-1816.

Palacz, M., Krawczuk, M., & Ostachowicz, W. (2005). Detection of additional mass in rods: Experimental and numerical investigation. *Archive of Applied Mechanics*, 74(11-12), 820-826

Palacz, Magdalena. "Spectral methods for modelling of wave propagation in structures in terms of damage detection—a review." *Applied Sciences* 8, no. 7 (2018): 1124.

Pan, J. W., Jin, F., Xu, Y. J., Zhang, C. H., & Feng, Y. T. (2012). Seismic Damage-Cracking Analysis of Concrete Dams Affected by Alkali-Aggregate Reaction. In *Proceedings of the 15th World Conference in Earthquake Engineering, Lisbona, Portugal*.

Pan, J., Feng, Y., Xu, Y., Jin, F., Zhang, C., & Zhang, B. (2013). Chemo-damage modeling and cracking analysis of AAR-affected concrete dams. *Science China Technological Sciences*, *56*, 1449-1457.

Pan, J., Xu, Y., Jin, F., & Zhang, C. (2014). A unified approach for long-term behavior and seismic response of AAR-affected concrete dams. *Soil Dynamics and Earthquake Engineering*, *63*, 193-202.

Pandey, A. K., & Biswas, M. (1994). Damage detection in structures using changes in flexibility. Journal of sound and vibration, 169(1), 3-17.

Pandey, A. K., Biswas, M., & Samman, M. M. (1991). Damage detection from changes in curvature mode shapes. Journal of sound and vibration, 145(2), 321-332.

Park, I., & Lee, U. (2012). Dynamic analysis of smart composite beams by using the frequency-domain spectral element method. *Journal of Mechanical Science and Technology*, *26*, 2511-2521.

Patera, A. T. (1984). A spectral element method for fluid dynamics: laminar flow in a channel expansion. *Journal of computational Physics*, *54*(3), 468-488.

Patera, Anthony T. "A spectral element method for fluid dynamics: laminar flow in a channel expansion." *Journal of computational Physics* 54, no. 3 (1984): 468-488.

Prajapati, G. N., AALOK AD PANDEY, and T. B. Reddy. "Finite element simulation of shear Strengthened RC beams externally reinforced with FRP." (2017): 357-370.

Przemieniecki, J.S. (1968) Theory of Matrix Structural Analysis, McGraw-Hill Inc., New York.

Rea D, Liaw CY, Chopra AK (1972) Dynamic properties of pine flat dam. Report No. UCB/EERC-72/7

Rizzi, S.A. and Doyle, J.F. (1992) A spectral element approach to wave motion in layered solids. Journal of Vibration and Acoustics, 114 (4), 569–577.

Rotter, H. M., Tschegg, E. K., Nadu, M., & Schieber, M. (1998). Determination of the specific fracture energy of AAR-affected concrete using the wedge-splitting method. *Magazine of Concrete Research*, *50*(3), 257-262.

Rucka, M. (2010). Experimental and numerical studies of guided wave damage detection in bars with structural discontinuities. *Archive of Applied Mechanics*, 80(12), 1371-1390.

Rucka, M. (2011). Modelling of in-plane wave propagation in a plate using spectral element method and Kane–Mindlin theory with application to damage detection. *Archive of Applied Mechanics*, 81(12), 1877-1888.

Salamon, J. W., Wood, C., Hariri-Ardebili, M. A., Malm, R., & Faggiani, G. (2021). Seismic analysis of pine flat concrete dam: formulation and synthesis of results. *In Numerical Analysis of Dams: Proceedings of the 15th ICOLD International Benchmark Workshop 15 (pp. 3-97). Springer International Publishing.*

Sanchez, L. F. M., Fournier, B., Jolin, M., Mitchell, D., & Bastien, J. (2017). Overall assessment of Alkali-Aggregate Reaction (AAR) in concretes presenting different strengths and incorporating a wide range of reactive aggregate types and natures. *Cement and concrete research*, *93*, 17-31.

Saouma, V., & Perotti, L. (2006). Constitutive model for alkali-aggregate reactions. *ACI materials journal*, *103*(3), 194.

Sarkar, A. and Bagchi, A., 2023, August. Stress Analysis of Concrete Gravity Dams Using Time Domain Spectral Finite Element Method Under the Action of Seismic Ground Motion. In *International Conference on Experimental Vibration Analysis for Civil Engineering Structures* (pp. 623-631). Cham: Springer Nature Switzerland.

Sarkar, A., Bagchi, S., & Bagchi, A. (2022, August). Damage Localization of Concrete Gravity Dams based on Modal Strain Energy using Time Domain Spectral Finite Element Method. In *11th International Conference on Structural Health Monitoring of Intelligent Infrastructure, SHMII-11, Montreal, Canada, 2022*

Sarkar, A., Ghodke, S., & Bagchi, A. (2024, January). Performance of 2D-spectral finite element method in dynamic analysis of concrete gravity dams. In *Structures* (Vol. 59, p. 105770). Elsevier.

Sarvestan, V., Mirdamadi, H. R., & Ghayour, M. (2017). Vibration analysis of cracked Timoshenko beam under moving load with constant velocity and acceleration by spectral finite element method. *International Journal of Mechanical Sciences, 122, 318-330.*

Sellier, A., Bourdarot, E., Multon, S., Cyr, M., & Grimal, E. (2009). Combination of structural monitoring and laboratory tests for assessment of alkali-aggregate reaction swelling: application to gate structure dam. *Materials Journal*, *106*(3), 281-290.

Semblat, J. F., & Brioist, J. J. (2009). Efficiency of higher order finite elements for the analysis of seismic wave propagation. arXiv preprint arXiv:0901.3715.

Shayan, A., & Grimstad, J. (2006). Deterioration of concrete in a hydroelectric concrete gravity dam and its characterisation. *Cement and Concrete Research*, *36*(2), 371-383.

Simo, J.C. and Taylor, R., 1986. A return mapping algorithm for plane stress elastoplasticity. *International Journal for numerical methods in engineering*, 22(3), pp.649-670.

Smith, W. D. (1975). The application of finite element analysis to body wave propagation problems. *Geophysical Journal International*, *42*(2), 747-768.

Sooch, G.S. and Bagchi, A., 2012, "Effect of seismic wave scattering on the response of dam-reservoir-foundation systems", *Proc. Of 15th World Conference on Earthquake Eng.,* Lisbon, Portugal.

Sooch, G.S. and Bagchi, A., 2014, "A New Iterative Procedure for Deconvolution of Seismic Ground Motion in Dam-Reservoir-Foundation Systems", *J of Applied Mathematics*, Article ID 287605, 10 pages, DOI: http://dx.doi.org/10.1155/2014/287605.

Thomas, M. D. A., & Folliard, K. J. (2007). Concrete aggregates and the durability of concrete. *Durab. Concr. Cem. Compos*, *10*, 247-281.

Tidke, A. R., Adhikary, S., & Noroozinejad Farsangi, E. (2022). Influence of earthquake excitations on concrete gravity dams founded on homogeneous and layered foundation. *Innovative Infrastructure Solutions*, 7(6), 338.

Tromp, J., Komatitsch, D., & Liu, Q. (2008). Spectral-element and adjoint methods in seismology. *Communications in Computational Physics*, *3*(1), 1-32.

Unger, J. F., Eckardt, S., & Kooenke, C. (2011). A mesoscale model for concrete to simulate mechanical failure. *Computers & Concrete*, *8*(4), 401-423.

Wang, J., Li, H., & Xing, H. (2022). A lumped mass Chebyshev spectral element method and its application to structural dynamic problems. *Earthquake Engineering and Engineering Vibration*, *21*(3), 843-859.

Westergaard, H. M., "Water Pressures on Dams during Earthquakes," *Transactions of the American Society of Civil Engineers*, vol. 98, pp. 418–433, 1933.

Witkowski, W., Rucka, M., Chróścielewski, J., & Wilde, K. (2012). On some properties of 2D spectral finite elements in problems of wave propagation. Finite Elements in Analysis and Design, 55, 31-41.

Witkowski, W., Rucka, M., Wilde, K., & Chróścielewski, J. (2009). Wave propagation analysis in spatial frames using spectral Timoshenko beam elements in the context of damage detection. *Archives of Civil Engineering*, 55(3), 367-402.

Witkowski, Wojciech, Magdalena Rucka, Jacek Chróścielewski, and Krzysztof Wilde. "On some properties of 2D spectral finite elements in problems of wave propagation." *Finite Elements in Analysis and Design* 55 (2012): 31-41.

Wittrick, W.H. and Williams, F.W. (1971) A general algorithm for computing natural frequencies of elastic structures. Quarterly Journal of Mechanics and Applied Mathematics, 24 (3), 263–284.

Wood, J. (2001). Winning the battles on AAR [Alkali aggregate reaction in dams]. *International Water Power and Dam Construction*, *53*.

Wu, Zhi-Jing, Feng-Ming Li, and Yi-Ze Wang. "Study on vibration characteristics in periodic plate structures using the spectral element method." *Acta Mechanica* 224, no. 5 (2013): 1089-1101.

Yoshikazu, Y. Seismic performance evaluation of concrete gravity dams, Paper No. 1068. 13th World Conference on Earthquake Engineering (2004).

Żak, A. (2009). A novel formulation of a spectral plate element for wave propagation in isotropic structures. *Finite Elements in Analysis and Design*, 45(10), 650-658.

APPENDIX 1: RELATED CONTRIBUTIONS

Journal articles

1) **Sarkar, A.**, Ghodke, S., & Bagchi, A. [2024, January]. Performance of 2D-spectral finite element method in dynamic analysis of concrete gravity dams. *Structures* (Vol. 59, p. 105770). Elsevier.
2) **Sarkar, A.** and Bagchi A. [2024] "Seismic analysis of concrete gravity dams using time domain spectral finite element considering material nonlinearity", (**submitted to journal-under review**).
3) **Sarkar, A.,** Latosh F. & and Bagchi A. [2024] "Analysis of FRP reinforced concrete deep beams using time domain based spectral finite element method", (**submitted to journal-under review**).
4) Murthy, S., **Sarkar A**., Bagchi S**.,** Patra B. and Bagchi A. [2023] "Effect of ground motion scaling methods on seismic assessment of buildings" (**submitted to journal-under review**).

Conference articles

1) **Sarkar, A** and Bagchi A. [2024, June] "Non-linear seismic analysis of concrete gravity dams using time domain spectral finite element method", 18th World Conference on Earthquake Engineering, Milan, Italy (**accepted**)
2) **Sarkar, A.,** Patra B. and Bagchi A. [2024, June] "A simplified thermo-mechanical model for damage assessment in concrete gravity dams due to Alkali-Aggregate-Reaction (AAR)", Canadian Society of Civil Engineering (CSCE) Annual Conference, Niagara Falls, Ontario. (**accepted**)
3) **Sarkar, A.**, Latosh, F. & Bagchi A. [2024, January] "A novel time domain spectral finite element method for analysis for FRP-reinforced concrete deep beams", Indian Concrete Institute, *International Symposium on Innovative World of Concrete*, IWC 2024, on Concrete Construction, Present and Future, Kolkata, India.
4) **Sarkar, A.,** & Bagchi, A. [2023, August]. Stress Analysis of Concrete Gravity Dams Using Time Domain Spectral Finite Element Method Under the Action of Seismic Ground Motion. *International Conference on Experimental Vibration Analysis for Civil Engineering Structures* (pp. 623-631). Cham: Springer Nature Switzerland.
5) **Sarkar A.,** Patra B., Ghodke S., and Bagchi A. [2023, September] "Monitoring the deformation pattern of an instrumented concrete arch dam", *14th International Workshop on Structural Health Monitoring*, IWSHM 2023 Conference-September 2023, Stanford University, USA.
6) **Sarkar A**., Bagchi S**.** and Bagchi A. [2022, September] **"**Damage Localization of Concrete Gravity Dams based on Modal Strain Energy using Time Domain Spectral Finite Element Method**"**, *SHMII-11:11th International Conference on Structural Health Monitoring of Intelligent Infrastructure, Concordia University*, Montreal, Quebec, Canada.
7) Bagchi S., **Sarkar A.** and Bagchi A. [2020, January] "Efficient arrangement of friction damped bracing system (FDBS) for multi-storey steel frame", *Recent*

Advances in Computational Mechanics and Simulations, Proceedings of the 7th ICCMS, Springer, Berlin, Germany.

8) **Sarkar A.** and Bagchi A. [2019, December] "Application of Conditional Mean Spectrum for Ground Motion Scaling", *7th International Conference on Computational Mechanics and Simulation*, IIT Mandi, India.

Other

1) **Sarkar, A.** and Bagchi A. [2023, November] "A novel spectral finite element method for evaluating the seismic performance of concrete gravity dams", Poster Presentation at "Programme colloque annuel du CEISCE (Study Center interuniversity structures under load extremes) 2023 - 17 Nov. - Université Concordia"

APPENDIX 2: MATLAB CODES

I. Creation of geometry

```
L2=19.25;
L3=70;
m2=24;
N=20;
H2=66.5;
m1=14;
L1=14.8;
H1=36.5;
%D=0.25; m=16; n=128;
eln=(m1+m2)*N;
nodes=(m1+m2+1)*(N+1);
node=[];
rdof=[1 2 3 4 5 6 7 8 9 10 11 12 13 14 15 16 17 18 19 20 21 22 23 24 25 26 27 28 29 30 31↙
32 33 34 35 36 37 38 39 40 41 42];
dof=[];
for a1=1:2*nodes
    dof(a1)=a1;
end
for b1=1:length(rdof)
    dof(dof==rdof(b1))=[];
end

 ndof=length(dof);
 el=[];
 node1=[];
 node2=[];
 node3=[];
 node4=[];
 xcoord=[];
 ycoord=[];
 for i=1:(m2+1)
     L(i)=L3-(L3-L2)*(i-1)/m2;
     for j=(i-1)*(N+1)+1:i*(N+1)
         node(j)=j;
         if rem(j,N+1)==0
             x=N+1;
         else
             x=rem(j,N+1);
         end
         xcoord(j)=(L(i)/N)*(x-1);
         if j>floor(j/(N+1))*(N+1)
         y=floor(j/(N+1))+1;
         else
         y=floor(j/(N+1));
         end
         ycoord(j)=(H2/m2)*(y-1);
     end
```

```
end
for i=(m2+2):(m1+m2+1)
    L(i)=L2-(L2-L1)/m1-(L2-L1)*(i-m2-2)/m1;
    for j=(i-1)*(N+1)+1:i*(N+1)
        node(j)=j;
        if rem(j,N+1)==0
            x=N+1;
        else
            x=rem(j,N+1);
        end
        xcoord(j)=(L(i)/N)*(x-1);
        if j>floor(j/(N+1))*(N+1)
        y=floor(j/(N+1))+1-(m2+1);
        else
        y=floor(j/(N+1))-(m2+1);
        end
        ycoord(j)=H2+(H1/m1)*(y);
    end
end
for i=1:(m1+m2)
    for j=(i-1)*N+1:i*N
        el(j)=j;
        node1(j)=el(j)+(i-1);
        node2(j)=el(j)+i;
        node3(j)=el(j)+i+N+1;
        node4(j)=el(j)+i+N;
    end
end
```

II. Creation of element matrices

```
for p=1:eln
    dof1(p)=2*node1(p)-1;
    dof2(p)=2*node1(p);
    dof3(p)=2*node2(p)-1;
    dof4(p)=2*node2(p);
    dof5(p)=2*node3(p)-1;
    dof6(p)=2*node3(p);
    dof7(p)=2*node4(p)-1;
    dof8(p)=2*node4(p);
% element local stiffness matrix
% inputs needed are E matrix, B matrix, integration points and weights
% let us now consider random value of Young's Modulus and Poisson's Ratio,
% E=2, u=0.5
    zhi=[];eta=[];
    zhi(1)=-1;
    zhi(2)=1;
    zhi(3)=1;
    zhi(4)=-1;
    eta(1)=-1;
    eta(2)=-1;
    eta(3)=1;
    eta(4)=1;
   E=31027000000;
   u=0.2;
   Emat=(E/(1-u*u))*[1 u 0; u 1 0; 0 0 0.5*(1-u)];
   k{p}=zeros(8,8);
   mass{p}=zeros(8,8);
% calculation of Jacobian for an element
% Defining the shape functions first
   syms X Y e n;
   N1=0.25*(1-e)*(1-n);
   N4=0.25*(1-e)*(1+n);
   N3=0.25*(1+e)*(1+n);
   N2=0.25*(1+e)*(1-n);


    X=N1*xcoord(node1(p))+N2*xcoord(node2(p))+N3*xcoord(node3(p))+N4*xcoord(node4(p));
    Y=N1*ycoord(node1(p))+N2*ycoord(node2(p))+N3*ycoord(node3(p))+N4*ycoord(node4(p));
    J=[diff(X,e) diff(X,n); diff(Y,e) diff(Y,n)];
    dj=det(J);
    J11=diff(X,e);
    J12=diff(X,n);
    J21=diff(Y,e);
    J22=diff(Y,n);
    Jinv11=(1/dj)*J22;
    Jinv12=-(1/dj)*J12;
    Jinv21=-(1/dj)*J21;
    Jinv22=(1/dj)*J22;
    ksipx=Jinv11;
    etapx=Jinv12;
    ksipy=Jinv21;
    etapy=Jinv22;
      for i=1:4
        e=zhi(i);
        n=eta(i);
        B=[];
        B(1,1)=-0.25*(1-eta(i))*simplify(subs(ksipx))-0.25*(1-zhi(i))*simplify(subs↙
(etapx));
        B(1,2)=0;
        B(1,7)=-0.25*(1+eta(i))*simplify(subs(ksipx))+0.25*(1-zhi(i))*simplify(subs↙
(etapx));
        B(1,4)=0;
        B(1,5)=0.25*(1+eta(i))*simplify(subs(ksipx))+0.25*(1+zhi(i))*simplify(subs↙
(etapx));
        B(1,6)=0;
        B(1,3)=0.25*(1-eta(i))*simplify(subs(ksipx))-0.25*(1+zhi(i))*simplify(subs↙
(etapx));
        B(1,8)=0;
        B(2,1)=0;
        B(2,2)=-0.25*(1-zhi(i))*simplify(subs(etapy))-0.25*(1-eta(i))*simplify(subs↙
(ksipy));
        B(2,3)=0;
        B(2,8)=0.25*(1-zhi(i))*simplify(subs(etapy))-0.25*(1+eta(i))*simplify(subs↙
(ksipy));
        B(2,5)=0;
        B(2,6)=0.25*(1+zhi(i))*simplify(subs(etapy))+0.25*(1+eta(i))*simplify(subs↙
(ksipy));
        B(2,7)=0;
        B(2,4)=-0.25*(1+zhi(i))*simplify(subs(etapy))+0.25*(1-eta(i))*simplify(subs↙
(ksipy));
        B(3,1)=B(2,2);
        B(3,2)=B(1,1);
        B(3,3)=B(2,4);
        B(3,4)=B(1,3);
        B(3,5)=B(2,6);
        B(3,6)=B(1,5);
        B(3,7)=B(2,8);
```

```
    B(3,8)=B(1,7);
    k{p}=k{p}+B''*Emat*B*simplify(subs(dj));
    SF=[];
    SF(1,1)=0.25*(1-eta(i))*(1-zhi(i));
    SF(1,2)=0;
    SF(1,7)=0.25*(1-zhi(i))*(1+eta(i));
    SF(1,4)=0;
    SF(1,5)=0.25*(1+zhi(i))*(1+eta(i));
    SF(1,6)=0;
    SF(1,3)=0.25*(1+zhi(i))*(1-eta(i));
    SF(1,8)=0;
    SF(2,1)=0;
    SF(2,2)=0.25*(1-eta(i))*(1-zhi(i));
    SF(2,3)=0;
    SF(2,8)=0.25*(1-zhi(i))*(1+eta(i));
    SF(2,5)=0;
    SF(2,6)=0.25*(1+zhi(i))*(1+eta(i));
    SF(2,7)=0;
    SF(2,4)=0.25*(1+zhi(i))*(1-eta(i));
    mass{p}=mass{p}+SF''*SF*simplify(subs(dj));
 end
kelement{p}=double(k{p});
melement{p}=double(mass{p})*density;


if ycoord(node4(p)) <= Hw && rem(p,N)==1
    elemheight(p)=ycoord(node4(p))-ycoord(node1(p));
    ycoordcentroid(p)=0.5*(ycoord(node4(p))+ycoord(node1(p)));
    rho(p)=0.875*waterdensity*sqrt(Hw*(Hw-ycoord(node1(p))));
    addedmass(p)=rho(p)*elemheight(p);
    melement{p}(1,1)=melement{p}(1,1)+addedmass(p);
    %melement{p}(7,7)=melement{p}(7,7)+addedmass(p);
end
```

III. Application of static water pressure

```
% adding static water pressure force
Forcemat=zeros(2*nodes,1);
if Hw>H2
    waterheight=zeros(m1+m2+1,1);
    waterforce=zeros(m1+m2+1,1);
for i=1:(m2+1)
        waterheight(i)=(i-1)*(H2/m2);
        waterforce(i)=waterdensity*9.81*(Hw-waterheight(i));
        Forcemat((i-1)*2*(N+1)+1)=Forcemat((i-1)*2*(N+1)+1)+waterforce(i);
end
for i=(m2+2):(m1+m2+1)
    waterheight(i)=H2+(i-(m2+1))*(H1/m1);
    if waterheight(i)<Hw
       waterforce(i)=waterdensity*9.81*(Hw-waterheight(i));
        Forcemat((i-1)*2*(N+1)+1)=Forcemat((i-1)*2*(N+1)+1)+waterforce(i);
    else
       waterforce(i)=0;
       Forcemat((i-1)*2*(N+1)+1)=Forcemat((i-1)*2*(N+1)+1)+waterforce(i);
    end
```

```
end
end
if Hw<H2
    waterheight=zeros(m1+m2+1,1);
    waterforce=zeros(m1+m2+1,1);
for i=1:(m2+1)
        waterheight(i)=(i-1)*(H2/m2);
        if waterheight(i)<H2
        waterforce(i)=waterdensity*9.81*(Hw-waterheight(i));
        Forcemat((i-1)*2*(N+1)+1)=Forcemat((i-1)*2*(N+1)+1)+waterforce(i);
        else
            waterforce(i)=0;
            Forcemat((i-1)*2*(N+1)+1)=Forcemat((i-1)*2*(N+1)+1)+waterforce(i);
        end
end
end
```

IV. Time history analysis

```
% solving displacements for all time steps
ti = 0 ;     % initial time step
tf = 10.04 ;   % final time step
dt = 0.01 ;   % size of the time step
nt = fix((tf-ti)/dt);      % number of time steps
% initializing the displacement, velocity and acceleration matrices
depl = zeros(ndof,nt) ;
vel = zeros(ndof,nt) ;
accl = zeros(ndof,nt);
Reff = zeros(ndof,nt) ;
%accl(:,1) = [0;10];
% Solve for initial accelerations
accl(:,1) = inv(mass_reduced)*(Force_reduced(:,1)-damping_reduced*vel(:,1)-s_reduced*depl↙
(:,1));
% Parameters for Newmark time integration
alpha = 0.25 ;delta = 0.5 ;
% Calculating integration constants
a0 = 1/(alpha*dt^2) ; a1 = delta/(alpha*dt) ; a2 = 1/(alpha*dt) ;
a3 = (1/(2*alpha))-1 ; a4 = (delta/alpha)-1 ;a5 = (dt/2)*(delta/alpha-2) ;
a6 = dt*(1-delta) ; a7 = delta*dt ;
% calculating effectvie stiffness matrix
keff = s_reduced+a0*mass_reduced+a1*damping_reduced ;


%
% time step starts
for it = 1:nt
 Reff(:,it) = Force_reduced(:,it)+mass_reduced*(a0*depl(:,it)+a2*vel(:,it)+a3*accl(:,↙
it))....
              +damping_reduced*(a1*depl(:,it)+a4*vel(:,it)+a5*accl(:,it));
% solving for displacements at time (it+dt)
             depl(:,it+1)= keff\Reff(:,it);
% calculating velocities and accelerations at time (it+dt)
             accl(:,it+1) = a0*(depl(:,it+1)-depl(:,it))-a2*vel(:,it)....
             -a3*accl(:,it) ;
             vel(:,it+1) = vel(:,it)+a6*accl(:,it)+a7*accl(:,it+1);
end
% calculation of displacement complete for all time steps
```

V. Calculation of principal stress values

```
% calculation of stress values for all elements and then principal stresses
DISPTOTAL=[];
DISPTOTAL=zeros(2*nodes,ntimesteps);
for i=1:ndof
    for j=1:ntimesteps
    DISPTOTAL(i+length(rdof),j)=DISPTOTAL(i+length(rdof),j)+depl(i,j);
    end
end
for p=1:eln
    zhi=[];eta=[];
        zhi(1)=-1;
        zhi(2)=1;
        zhi(3)=1;
        zhi(4)=-1;
        eta(1)=-1;
        eta(2)=-1;
        eta(3)=1;
        eta(4)=1;
        syms X Y e n;
        N1=0.25*(1-e)*(1-n);
        N4=0.25*(1-e)*(1+n);
        N3=0.25*(1+e)*(1+n);
        N2=0.25*(1+e)*(1-n);
        X=N1*xcoord(node1(p))+N2*xcoord(node2(p))+N3*xcoord(node3(p))+N4*xcoord(node4↙
(p));
        Y=N1*ycoord(node1(p))+N2*ycoord(node2(p))+N3*ycoord(node3(p))+N4*ycoord(node4↙
(p));
        J=[diff(X,e) diff(X,n); diff(Y,e) diff(Y,n)];
        dj=det(J);
        J11=diff(X,e);
        J12=diff(X,n);
        J21=diff(Y,e);
        J22=diff(Y,n);
        Jinv11=(1/dj)*J22;
        Jinv12=-(1/dj)*J12;
        Jinv21=-(1/dj)*J21;
```

```
        Jinv22=(1/dj)*J22;
        ksipx=Jinv11;
        etapx=Jinv12;
        ksipy=Jinv21;
        etapy=Jinv22;
       e=zhi(1);
       n=eta(1);
       B1=[];
       B1(1,1)=-0.25*(1-eta(1))*simplify(subs(ksipx))-0.25*(1-zhi(1))*simplify(subs↙
(etapx));
       B1(1,2)=0;
       B1(1,7)=-0.25*(1+eta(1))*simplify(subs(ksipx))+0.25*(1-zhi(1))*simplify(subs↙
(etapx));
       B1(1,4)=0;
       B1(1,5)=0.25*(1+eta(1))*simplify(subs(ksipx))+0.25*(1+zhi(1))*simplify(subs↙
(etapx));
       B1(1,6)=0;
       B1(1,3)=0.25*(1-eta(1))*simplify(subs(ksipx))-0.25*(1+zhi(1))*simplify(subs↙
(etapx));
       B1(1,8)=0;
       B1(2,1)=0;
       B1(2,2)=-0.25*(1-zhi(1))*simplify(subs(etapy))-0.25*(1-eta(1))*simplify(subs↙
(ksipy));
       B1(2,3)=0;
       B1(2,8)=0.25*(1-zhi(1))*simplify(subs(etapy))-0.25*(1+eta(1))*simplify(subs↙
(ksipy));
       B1(2,5)=0;
       B1(2,6)=-0.25*(1+zhi(1))*simplify(subs(etapy))+0.25*(1+eta(1))*simplify(subs↙
(ksipy));
       B1(2,7)=0;
       B1(2,4)=-0.25*(1+zhi(1))*simplify(subs(etapy))+0.25*(1-eta(1))*simplify(subs↙
(ksipy));
       B1(3,1)=B1(2,2);
       B1(3,2)=B1(1,1);
       B1(3,3)=B1(2,4);
       B1(3,4)=B1(1,3);
       B1(3,5)=B1(2,6);
       B1(3,6)=B1(1,5);
       B1(3,7)=B1(2,8);
       B1(3,8)=B1(1,7);


       e=zhi(2);
       n=eta(2);
       B2=[];
       B2(1,1)=-0.25*(1-eta(2))*simplify(subs(ksipx))-0.25*(1-zhi(2))*simplify(subs↙
(etapx));
       B2(1,2)=0;
       B2(1,7)=-0.25*(1+eta(2))*simplify(subs(ksipx))+0.25*(1-zhi(2))*simplify(subs↙
(etapx));
       B2(1,4)=0;
       B2(1,5)=0.25*(1+eta(2))*simplify(subs(ksipx))+0.25*(1+zhi(2))*simplify(subs↙
```

```
(etapx));
        B2(1,6)=0;
        B2(1,3)=0.25*(1-eta(2))*simplify(subs(ksipx))-0.25*(1+zhi(2))*simplify(subs↙
(etapx));
        B2(1,8)=0;
        B2(2,1)=0;
        B2(2,2)=-0.25*(1-zhi(2))*simplify(subs(etapy))-0.25*(1-eta(2))*simplify(subs↙
(ksipy));
        B2(2,3)=0;
        B2(2,8)=0.25*(1-zhi(2))*simplify(subs(etapy))-0.25*(1+eta(2))*simplify(subs↙
(ksipy));
        B2(2,5)=0;
        B2(2,6)=0.25*(1+zhi(2))*simplify(subs(etapy))+0.25*(1+eta(2))*simplify(subs↙
(ksipy));
        B2(2,7)=0;
        B2(2,4)=-0.25*(1+zhi(2))*simplify(subs(etapy))+0.25*(1-eta(2))*simplify(subs↙
(ksipy));
        B2(3,1)=B2(2,2);
        B2(3,2)=B2(1,1);
        B2(3,3)=B2(2,4);
        B2(3,4)=B2(1,3);
        B2(3,5)=B2(2,6);
        B2(3,6)=B2(1,5);
        B2(3,7)=B2(2,8);
        B2(3,8)=B2(1,7);

        e=zhi(3);
        n=eta(3);
        B3=[];
        B3(1,1)=-0.25*(1-eta(3))*simplify(subs(ksipx))-0.25*(1-zhi(3))*simplify(subs↙
(etapx));
        B3(1,2)=0;
        B3(1,7)=-0.25*(1+eta(3))*simplify(subs(ksipx))+0.25*(1-zhi(3))*simplify(subs↙
(etapx));
        B3(1,4)=0;
        B3(1,5)=0.25*(1+eta(3))*simplify(subs(ksipx))+0.25*(1+zhi(3))*simplify(subs↙
(etapx));
        B3(1,6)=0;
        B3(1,3)=0.25*(1-eta(3))*simplify(subs(ksipx))-0.25*(1+zhi(3))*simplify(subs↙
(etapx));
        B3(1,8)=0;
        B3(2,1)=0;
        B3(2,2)=-0.25*(1-zhi(3))*simplify(subs(etapy))-0.25*(1-eta(3))*simplify(subs↙
(ksipy));
        B3(2,3)=0;
        B3(2,8)=-0.25*(1-zhi(3))*simplify(subs(etapy))-0.25*(1+eta(3))*simplify(subs↙
(ksipy));
        B3(2,5)=0;
        B3(2,6)=0.25*(1+zhi(3))*simplify(subs(etapy))+0.25*(1+eta(3))*simplify(subs↙
(ksipy));
        B3(2,7)=0;
```

```
        B3(2,4)=-0.25*(1+zhi(3))*simplify(subs(etapy))+0.25*(1-eta(3))*simplify(subs↙
(ksipy));
        B3(3,1)=B3(2,2);
        B3(3,2)=B3(1,1);
        B3(3,3)=B3(2,4);
        B3(3,4)=B3(1,3);
        B3(3,5)=B3(2,6);
        B3(3,6)=B3(1,5);
        B3(3,7)=B3(2,8);
        B3(3,8)=B3(1,7);

        e=zhi(4);
        n=eta(4);
        B4=[];
        B4(1,1)=-0.25*(1-eta(4))*simplify(subs(ksipx))-0.25*(1-zhi(4))*simplify(subs↙
(etapx));
        B4(1,2)=0;
        B4(1,7)=-0.25*(1+eta(4))*simplify(subs(ksipx))+0.25*(1-zhi(4))*simplify(subs↙
(etapx));
        B4(1,4)=0;
        B4(1,5)=0.25*(1+eta(4))*simplify(subs(ksipx))+0.25*(1+zhi(4))*simplify(subs↙
(etapx));
        B4(1,6)=0;
        B4(1,3)=0.25*(1-eta(4))*simplify(subs(ksipx))-0.25*(1+zhi(4))*simplify(subs↙
(etapx));
        B4(1,8)=0;
        B4(2,1)=0;
        B4(2,2)=-0.25*(1-zhi(4))*simplify(subs(etapy))-0.25*(1-eta(4))*simplify(subs↙
(ksipy));
        B4(2,3)=0;
        B4(2,8)=0.25*(1-zhi(4))*simplify(subs(etapy))-0.25*(1+eta(4))*simplify(subs↙
(ksipy));
        B4(2,5)=0;
        B4(2,6)=0.25*(1+zhi(4))*simplify(subs(etapy))+0.25*(1+eta(4))*simplify(subs↙
(ksipy));
        B4(2,7)=0;
        B4(2,4)=-0.25*(1+zhi(4))*simplify(subs(etapy))+0.25*(1-eta(4))*simplify(subs↙
(ksipy));
        B4(3,1)=B4(2,2);
        B4(3,2)=B4(1,1);
        B4(3,3)=B4(2,4);
        B4(3,4)=B4(1,3);
        B4(3,5)=B4(2,6);
        B4(3,6)=B4(1,5);
        B4(3,7)=B4(2,8);
        B4(3,8)=B4(1,7);

        matdis{p}=zeros(8,ntimesteps);
        strainmattotall{p}=zeros(3,ntimesteps);
        stressmattotall{p}=zeros(3,ntimesteps);
```

```
        strainmattotal2{p}=zeros(3,ntimesteps);
        stressmattotal2{p}=zeros(3,ntimesteps);

        strainmattotal3{p}=zeros(3,ntimesteps);
        stressmattotal3{p}=zeros(3,ntimesteps);

        strainmattotal4{p}=zeros(3,ntimesteps);
        stressmattotal4{p}=zeros(3,ntimesteps);

        strainmattotal{p}=zeros(3,ntimesteps);
        stressmattotal{p}=zeros(3,ntimesteps);

    for j=1:ntimesteps
        dispelement=[DISPTOTAL(dof1(p),j) DISPTOTAL(dof2(p),j) DISPTOTAL(dof3(p),j) ↙
DISPTOTAL(dof4(p),j) DISPTOTAL(dof5(p),j) DISPTOTAL(dof6(p),j) DISPTOTAL(dof7(p),j) ↙
DISPTOTAL(dof8(p),j)]';
        matdis{p}(:,j)=matdis{p}(:,j)+dispelement;

        strainmatrixelement1=B1*matdis{p}(:,j);
        strainmatrixelement2=B2*matdis{p}(:,j);
        strainmatrixelement3=B3*matdis{p}(:,j);
        strainmatrixelement4=B4*matdis{p}(:,j);

        strainmattotal1{p}(:,j)=strainmattotal1{p}(:,j)+strainmatrixelement1;
        stressmattotal1{p}(:,j)=stressmattotal1{p}(:,j)+Emat*strainmattotal1{p}(:,j);

        strainmattotal2{p}(:,j)=strainmattotal2{p}(:,j)+strainmatrixelement2;
        stressmattotal2{p}(:,j)=stressmattotal2{p}(:,j)+Emat*strainmattotal2{p}(:,j);

        strainmattotal3{p}(:,j)=strainmattotal3{p}(:,j)+strainmatrixelement3;
        stressmattotal3{p}(:,j)=stressmattotal3{p}(:,j)+Emat*strainmattotal3{p}(:,j);

        strainmattotal4{p}(:,j)=strainmattotal4{p}(:,j)+strainmatrixelement4;
        stressmattotal4{p}(:,j)=stressmattotal4{p}(:,j)+Emat*strainmattotal4{p}(:,j);

        strainmattotal{p}(:,j)=0.25*(strainmattotal1{p}(:,j)+strainmattotal2{p}(:,j) ↙
+strainmattotal3{p}(:,j)+strainmattotal4{p}(:,j));
        stressmattotal{p}(:,j)=0.25*(stressmattotal1{p}(:,j)+stressmattotal2{p}(:,j) ↙
+stressmattotal3{p}(:,j)+stressmattotal4{p}(:,j));

        maxprincipalstress(p,j)=0.5*(stressmattotal{p}(1,j)+stressmattotal{p}(2,j))+sqrt ↙
(0.25*(stressmattotal{p}(1,j)-stressmattotal{p}(2,j))^2+(stressmattotal{p}(3,j))^2);
        minprincipalstress(p,j)=0.5*(stressmattotal{p}(1,j)+stressmattotal{p}(2,j))-sqrt ↙
(0.25*(stressmattotal{p}(1,j)-stressmattotal{p}(2,j))^2+(stressmattotal{p}(3,j))^2);
    end
    envelopemaxprincipalstress(p)=max(maxprincipalstress(p,:));
    envelopeminprincipalstress(p)=min(minprincipalstress(p,:));
end
% calculation complete
```

VI. Plot of principal stress values

```
for i=1:(m1+m2+1)*(N+1)
    maxprincipalstressnode(i)=0;
    count(i)=0;
    for j=1:eln
        if i==node1(j) || i==node2(j) || i==node3(j) || i==node4(j)
            count(i)=count(i)+1;
            maxprincipalstressnode(i)=maxprincipalstressnode(i)↙
+envelopemaxprincipalstress(j);
        else
            count(i)=count(i);
            maxprincipalstressnode(i)=maxprincipalstressnode(i);
        end
    end
    maxprincipalstressnode(i)=maxprincipalstressnode(i)/count(i);
end
xvalues=reshape(xcoord,N+1,m1+m2+1);
yvalues=reshape(ycoord,N+1,m1+m2+1);
maxprincipalstressnodal=reshape(maxprincipalstressnode,N+1,m1+m2+1);
contourf(xvalues,yvalues,maxprincipalstressnodal)
```

```
for i=1:(m1+m2+1)*(N+1)
    minprincipalstressnode(i)=0;
    count(i)=0;
    for j=1:eln
        if i==node1(j) || i==node2(j) || i==node3(j) || i==node4(j)
            count(i)=count(i)+1;
            minprincipalstressnode(i)=minprincipalstressnode(i)↙
+envelopeminprincipalstress(j);
        else
            count(i)=count(i);
            minprincipalstressnode(i)=minprincipalstressnode(i);
        end
    end
    minprincipalstressnode(i)=minprincipalstressnode(i)/count(i);
end
xvalues=reshape(xcoord,N+1,m1+m2+1);
yvalues=reshape(ycoord,N+1,m1+m2+1);
minprincipalstressnodal=reshape(minprincipalstressnode,N+1,m1+m2+1);
contourf(xvalues,yvalues,minprincipalstressnodal)
```